University of Strathclyde
Department of Chemical and Process Engineering

Primary and Secondary Crystal Nucleation of Pharmaceutics

Maria Lucia Briuglia

A thesis submitted for the degree of Doctor of Philosophy

Supervisors: Prof Jan Sefcik and Prof. Joop H.ter Horst

September 2017

This thesis is the result of the author's original research. It has been composed by the author and has not been previously submitted for examination whoch has led to the award of a degree.

Abstract

Control of the crystallisation process is essential in the consistent and reliable production of many particulate materials in the pharmaceutical and chemical industries. Crystal Nucleation defines the crystal size distribution of the obtained crystal population affecting downstream operations. The literature agrees on crystal nucleation division as primary and secondary nucleation depending on the conditions of the used supersaturated solution. Primary nucleation occurs in a clear supersaturated solution, while secondary nucleation is induced by at least one parent crystal present in the solution. Despite the large amount of research conducted on this field, several challenges for primary and secondary nucleation fundamental understanding are still identifiable.

The aim of this thesis is to develop meticulous and accurate methods to measure primary and secondary nucleation in order to systematically study nucleation mechanisms relevant to industrial scales.

This thesis is constituted of two main parts: one part studies primary nucleation and develops a method for control and measure primary nucleation rate within the metastable zone width (Chapter 2) using different volumes and hydrodynamics (Chapter 3). The second part concerns studies of secondary nucleation under well-controlled conditions providing a systematic method to measure secondary nucleation rates (Chapter 4), which can be integrated in industrial workflows (Chapter 5) and applied to study the chiral outcomes (Chapter 6).

The developed methods decouple primary and secondary nucleation events improving crystallisation processes understanding. The reliability and reproducibility of the novel proposed methods offer an appropriate process control strategy to address existing challenges on crystal nucleation.

Chapter 1: Introduction

Chapter 2: Crystal Nuclation within the Metastable zone

Chapter 3: Comparing Methods for Induction Time Probability Distribution Measurements

Chapter 4: Measuring Secondary Nucleation through Single Crystal Seeding

Chapter 5: A general method for secondary nucleation rates under industrial conditions

Chapter 6: Primary and Secondary Nucleation Kinetics of Chiral Crystals

Chapter 7: Conclusions

Chapter 1

Introduction

Crystallisation is one of the most applied industrial processes for separation and purification of day-to-day life products such as table salt, sugar, active pharmaceutical ingredients, fertlizers, etc. Crystallisation is an intricate purification process that produces a final crystalline product through crystal nucleation, crystal growth and agglomeration[1].

With increasing use of continuous crystallization processes in pharmaceutical industry, it is increasingly important to control and predict nucleation. Nucleation is the formation of new and small crystalline entities in a liquid phase and it can be classified based on the presence or the absence of the crystalline material in solution[2]. If nucleation occurs in the absence of crystalline material of its own kind, it is referred to as primary nucleation. If this happens in a clear supersaturated solution in absence of foreign surface this is known as homogeneous nucleation. Otherwise, primary nucleation proceeds on the surface of foreign particles or on the surface of the equipment, which is called heterogeneous nucleation. If new crystals appear in a suspension it is classified as secondary nucleation. Thus, secondary nucleation is responsible for the birth of crystals in a supersaturated solution in which parent crystal of the same substance are present, which serve as catalyst for the formation of further crystals[3,4].

In Continuous Stirred Tank Crystallizer (CSTR) type processes, secondary nucleation is the crucial step to arrive at a preferred CSD. It is important to quantify secondary nucleation rate dependence of supersaturation in order to understand the dynamic of the crystal nucleation. Secondary nucleation, also, influences the yield of crystallizer via the surface area of crystals available for growth. A high secondary nucleation rate dependence on supersaturation indicates that it will be difficult to grow large crystals regardless of the equipment[5]. In continuous processes insufficient secondary nucleation can have catastrophic effects because supersaturation may rise due to the lack of crystal growth surface. The system will then reach a metastable zone of activated nucleation that will largely affect the state of successive process, such as crystal growth [6].

The MSZW is the temperature difference between the saturation temperature and the temperature at which crystals are detected upon applying a constant cooling rate[7]. The MSZW is not a fixed

thermodynamic property. In fact, it is a complex and not fully understood function of the cooling, nucleation, and growth rates, of the process conditions, such as the stirring speed, and of the used detection technique[8].

Generally, in cooling crystallisation, the temperature is reduced until the metastable limit is reached and it is possible to detect formed crystals.The driving force to obtain nucleation within the MSZW is represented by the degree of supersaturation (S), which can be expressed as the difference between the solute concentration in the solution and the saturation concentration at the given temperature[9]. When $S > 1$, the solution is supersaturated and nucleation can occur.

This chapter aims at determining the challenges, which must be addressed in order to achieve a fundamental and systematic understanding of nucleation events. First, a literature review was conducted analysing the state of art achieved so far on primary and secondary nucleation understanding. Then, several research questions were formulated and a research plan was organized dividing the thesis in two main parts. One part studies primary nucleation and develops a method for control and measure primary nucleation rate within the metastable zone width. The second part concerns studies of secondary nucleation under well-controlled conditions providing a systematic method to measure secondary nucleation rates, which can be integrated in industrial workflows.

1.1. Literature review on primary and secondary nucleations

1.1.1 Primary Nucleation

Crystals form when supersaturation is generated and the energy barrier for nucleation is overcomed. There are two main currents of thought to describe the dynamics of cluster formation during the nucleation process[10]. They are represented by the classical nucleation theory and the second is the non-classical theory based on two-steps mechanisms (figure 1).

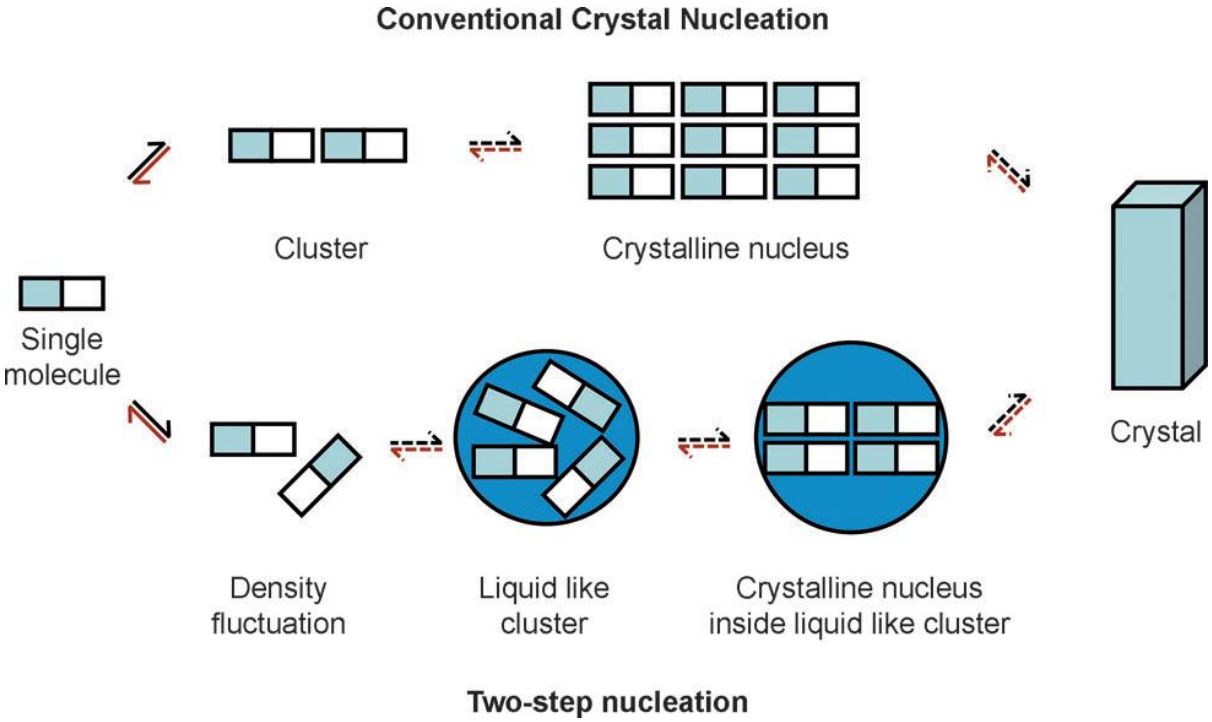

Figure 1: The two possible routes for crystal nucleation from a supersaturated solution. The top route, indicated as conventional crystal nucleation or classical nucleation theory, indicates how the crystalline nucleus reflects the molecular packing of the final crystal. The bottom route represents the two-step nucleation where there is an intermediate stage with liquid like cluster before the final crystal is formed.

The school of classical nucleation theory (CNT) leads to the formation of clusters, which reflect the same structure of the mature crystal. In a supersaturated solution, according to the CNT, the molecular packing reflects all possible polymorphs of the solute[11]. The second crystal nucleation pathways in figure 1 is the two-steps mechanism. Initially, the formed clusters are liquid-like and the crystals appear over time.

Classical Nucleation Theory (CNT)

The crystal nucleation rate *J* is the number of crystalline particles that form from a supersaturated solution per unit of volume and time. The supersaturation ratio S is a measure of the distance from equilibrium experienced by the supersaturated system. According to CNT, the crystal nucleation rate can generally be expressed by the following equation[2]:

$$J = A \exp(-\frac{B}{ln^2 S})$$

A and B are usually considered to be constants, and the exponent $B/\ln^2 S = W/kT$ is the nucleation work that represents the energy barrier for nucleation. Nucleation rate *J* and *S* are not directly proportional: small changes in supersaturation can induce changes of several orders of magnitude in the nucleation rate (Figure 2).

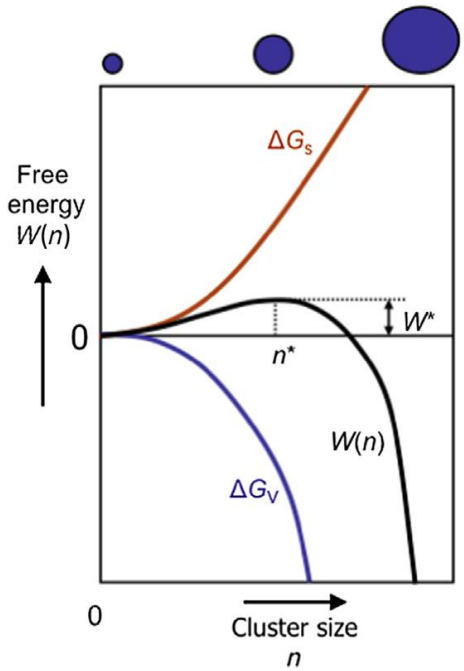

Figure 2: Relation between free energy and cluster size at a constant supersaturation. At the nucleus size n* the free energy of formation is maximum, which is the nucleation work W*.

Two-steps nucleation

According to the two-step nucleation model, the density fluctuations is followed by structural fluctuations [12,13]. A droplet of dense liquid is formed initially in the supersaturated solution which is

followed by nucleation of a crystal showing periodicity within the droplet. This means that two energy barriers must be crossed before nucleation occurs.

1.1.1.1. Measuring Primary Nucleation

Despite the vast amount of research in characherization of nucleation, this essential step of crystallisation is still a challenge because nuclei cannot be detected in situ until they reach the critical size. The nuclei have to grow into crystals of detectable sizes after which characterization is possible[14]. On of the first works on primary nucleation measurements was conducted by Christiansen and Nielsen in 1951[15]. They measured the induction times for barium sulfate precipitation in a glass, which consisted of a mixing chamber, two inflow channels for two components and one outflow channel for the mixture. After mixing of the two components the induction time was noted. In this work, precipitation was considered as crystallisation. The required time for detecting crystallisation at the desired supersaturation was defined as induction time. Induction time measurements were later performed by other researchers through rapid cooling of undersaturated solutions at different temperatures reaching a desired supersaturation under stirring confitions and nothing the time needed for crystals to appear [16, 17].

Another method applied to determine nucleation rate is represented by MSZW measurements. Nyvlt was the first author, which showed results with this procedure[18]. He measured MSZW for 25 model systems and determined their nucleation rates. He assumed that the effect of growth on supersaturation depletion can be neglected and the nucleation rate is equal to the rate of supersaturation generation.

1.1.2. Secondary Nucleation

One of the most frequently used classifications of the possible crystal nucleation mechanisms that a researcher can find in literature is shown in figure 3. Different terms such as initial breeding and contact nucleation had been coined to describe particular secondary nucleation mechanisms.

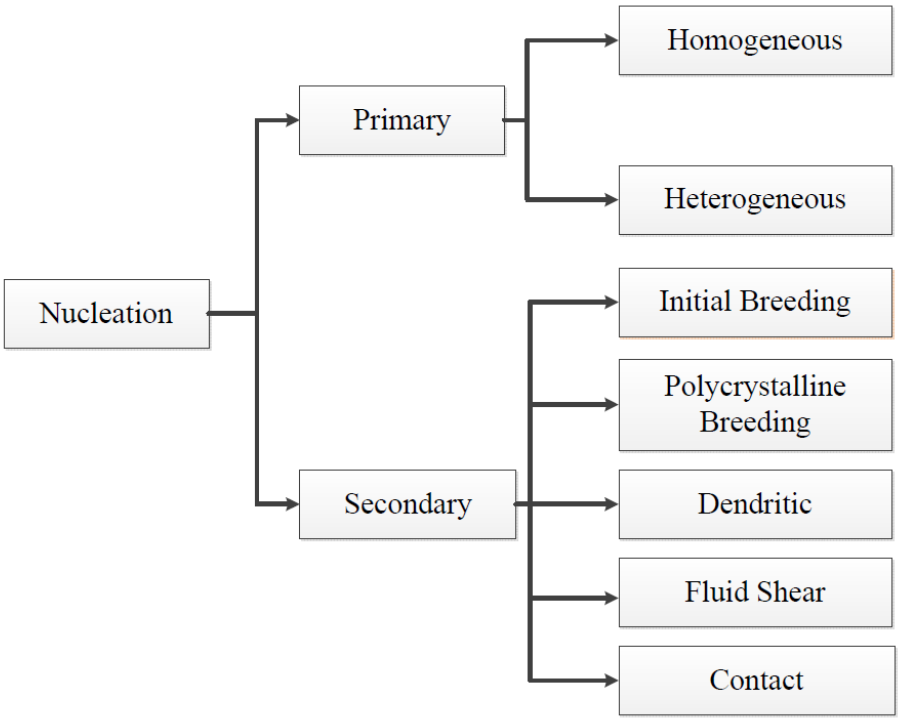

Figure 3: Crystal nucleation is classified in literature as primary and secondary nucleation events. Primary nucleation can be divided as homegeous and heterogeneous depending on the number of particles present. Secondary nucleation mechanisms are initial breeding, polycrystalline breeding, dendritic, fluid shear and contact.

Initial breeding

Initial breeding is the mechanism by which secondary nucleation is promoted due to micro-crystalline fragments being washed off the seed crystal surfaces and becoming viable growing crystals in the mother liquor[19]. It is considered as spontaneous dislodgement of crystallites already present on the crystal before its introduction in the solution[20]. However, the small fragments could also form in proximity of the parent crystal surface. Initial breeding was firstly observed by Strickland-Constable et al.[21] after the introduction of a large dry single crystal in a supersaturated solution secondary nuclei were detected. This mechanism can be identified as a fluid shear mechanism.

Attrition

Attrition creates fracture generating a change in crystal surface, which can be the source of a breakage for secondary nuclei. The capacity to generate fractures depends on the impact energy between crystal-crystal, crystal-walls, and crystal-impeller[22]. Attrition is a collision mechanism.

Fragmentation

It was defined by Asakuma [23] that fragmentation is the breakage of agglomerates due to a collision induced by an impeller or by a hydrodynamic force. Due to energy absorption, a small fragment breaks off a crystal. The fragment could be in a considerably disordered state, with many dislocations and mismatch surfaces [2]. The literature does not clarify yet the difference between attrition and fragmentation, making fragmentation also a collision mechanism.

Polycrystalline breeding

Polycrystalline breeding is the spontaneous breaking away of visible pieces from the crystal mass[24] and it is generally induced by either collisions and or shear mechanisms. This breakage refers to the fragmentation of irregular polycrystalline aggregates[2] but the differences in polycrystalline breeding respect to attrition are not clear.

Dendritic breeding

When supersaturation is high enough to induce dendritic growth on the seed crystals, fluid shear forces can break of these dendritic features from the surface and new crystals are formed. One characteristic of this effect is the irregular surface of the new crystals induced by the uniformity and the intensity of the fluid shear [4].

Despite the literature reports all these possible mechanisms for secondary nucleation induction, we suggest a more general division of secondary nucleation by the origin of the secondary nuclei providing a more useful research plan point of view. All literature mechanisms are either collision-based (solid-solid contact) or fluid shear-based (solid-liquid contact) and terms as initial breeding, polycrystalline breeding and attrition can be considered as possible effects when secondary nucleation occurs (Table 1).

Table 1: Mechansisms and effects of secondary nucleation

Mechanisms	Interface	Effects
Collisions	Solid-solid	Attrition Fragmentation Polycrystalline breedinf
Fluid shear	Solid-liquid	Fragmentation Dendritic breeding Initial breeding Polycrystalline breeding

1.1.2.1. Collision Mechanism

Ting and McCabe[25] were the first to report the effect of mechanical action on secondary nucleation process for batch cooling crystallization experiments. The breakage of needle-like outgrowths by contacting a crystal of magnesium sulphate was reported by Mason et al. [26]. It was noted that at lower supersaturations in the "good growth region" (metastable zone) due to collisions of crystals with presumably a stirrer or other crystals new nuclei were formed. The phenomenon of collision was further characterized by Lal et al.[27] providing the classification of three types of idealized contact:

1) Collision of crystals with impeller

2) Collision between crystals

3) Collision of crystals with walls of the crystallizer

Collision breeding induced by high stirring speeds cause macroabrasion of crystals results in fragment that serve as nucleation sites. The rate of nucleation by collision breeding mechanism is a function of the crystal hardness, the concentration of the suspension and the retention time[6]. Following the theory of initial breeding or dust breeding, tiny crystallites are formed on the crystal surface during the growth of seed crystals or due to fragmentation during storage. When introduced in the solution crystallites act as nucleation sites [25]. These crystallites are larger than the critical nucleus size and the rate of nucleation is independent of the supersaturation of the solution or the

stirring rate. Needle- like or dendritic crystals are formed at high levels of supersaturation. These crystals fragment in the solution and serve as nucleation sites.

1.1.2.2. Fluid shear Mechanism

This mechanism was proposed from Power et al. [28] considering dendritic growth occurs at the crystal surface at high supersaturation level. In his experiment, a "sufficient violent shearing force" produced a cloud of nuclei from a "fluidized layer" of molecules on the interface, acting as a "buffer reservoir layer" of fluidized material. Power reports microscopic observations of needles and monoclinic crystals as a result of the secondary nucleation of sucrose at elevated values of the supersaturation. Clontz and McCabe[29] followed Power suggestion considering that fluid shear might play a role in the formation of nuclei from a "zone of partially organized solute clusters, microscopic dendrites, and unstable agglomerates", but they reported no nucleation observed when a magnesium sulphate crystal was placed in a supersaturated solution near an agitator. Sung et al. [30] argued that the non- nucleation by fluid shear in Clontz and McCabe experiment was a result of the dissolution of the nuclei at the low values of the supersaturation in accordance to Strinckland-Constable[21] theory. In order to prove fluid-shear nucleation, a crystal of magnesium sulphate was placed in a supersaturation solution with a correct distance from the cylindrical rotor and at a higher value of supersaturation. Wang et al. [31] investigated the fluid shear nucleation of citric acid in a Couette flow crystallizer. The number of nuclei was dependent by sub-cooling of solution, saturation temperature and agitation speed in the couette. In secondary nucleation, there must be a mechanism responsible for the removal of new nuclei from the parent crystal. One of the possible removal mechanisms can be the action of the fluid shear, which easily occurs when on the surface of the parent crystal there are protruding parts such as needles, dendrites or polycrystallinities. An important aspect to consider in fluid shear mechanism is the presence of impurities in the solution because dissolving impurities in the solution growth rates is inhibited. Some of the impurities are incorporated into the crystal surface.

Quality aspect of secondary nuclei

It is possible to summarize the reported literature focusing on the morphology of the potential secondary nuclei formed due to collision and fluid shear mechanisms describing four particular parameters. The descriptors of interest are particle size, particle shape, polymorphic forms and purity. It must be noted that unfortunately the conducted studies on fluid shear mechanism so far appear poor of information in the characterization of the product outcomes (Table 2)

Table 2: Literature review on secondary nuclei quality.
*Abbreviation in Table 2: SNM (Single Nucleus Mechanism); SN (Secondary Nucleation); P.FORM (Polymorphic Form)

	COLLISION MECHANISM				**FlUID SHEAR MECHANISM**			
	Authors	Year	Aims	Conclusions	Authors	Year	Aims	Conclusions
Size	Evans [32]	1974	Effects of hardness and geometries of contact materials	Coating the crystallizer nucleation rate is reduced	Shamlou[33]	1989	Turbulent agitation gives breaking energy	Fractures by hydrodynamic effects
	Sun [34]	2009	Comparison between breakage and attrition	Increasing seed mass and stirring speed, induction speed is reduced				
	Frawley[4]	2012	Critical seed concentration to ensure nucleation	SN is dependent upon seed loading and size fraction				
Shape	Reyhanu[35]	1999	Morphology of parent and new crystals	Shape of new nuclei is determined by the nature of the parent nuclei				
P.Form	Ferrari[36]	2004	Nucleation of a stable polymorph from an unstable polymorph	The surface of one polymorph acts as a template for the nucleation of another form				
Purity	Kulkarni[37]	2014	Studying the outcome of a polymorph crystallizaion	Using SNM would lead to 100% pure polymorphic fraction				

1.1.2.3. Measuring secondary nucleation

Secondary nuclei from solid-solid contact

Coulter Counter: Larson and co-workers [38] introduced a nucleator where a macrocrystal was

steadily tapped in a well-stirred supersaturated medium and the secondary nuclei born from the parent crystal were measured by a Coulter Counter. From size distribution, the nucleation rate per crystal contact was determined studying the influence of supersaturation, residence time, contact energy, and frequency of contact.

Dynamic mini-nucleator: Through a mini-nucleator, which was similar to MSMPR crystallizer, Randolph and co-workers [39] used an electronic counter to measure birth of nuclei directly. Conventional sieving techniques used cannot discriminate mechanistic details of secondary nucleation, while dynamic mini-nucleator can detect suitable correlations to understand the mechanisms of secondary nucleation [40].

Secondary nuclei from fluid shear

Couette flow crystallizer: The number of nuclei produced due to fluid shear was observed as a function of solution subcooling in a Couette flow crystallizer where the fluid shear forces was generated by rotating the inner cylinder of the Couette flow [9]. Using "homemade" crystallizer: Secondary embryonic species produced by fluid shear from a single crystal were detected developing a special crystallizer.

1.1.3. Factors that influence nucleation

Rotation speed, geometries and position of impeller

Secondary nucleation occurs when the impact energy in collision of a crystal with a crystallizer (impeller or walls) or other crystals is above a critical value. The geometry and the position of the impeller have some effect on secondary nucleation rate. The impeller- bottom distance affected both crystal-impeller and crystal-bottom collisions [43]. Increasing axial velocity decreases impact velocity in collisions of crystals with pitched blade impeller. Decrease in impact velocity decreases secondary nucleation rate [44].

Fluid Dynamics

Sung et al. [30] and a more recent investigation by Liang et al.[45], suggested that crystallizer fluid dynamic has an important role on nucleation. Turbulent fluid-dynamic provides an attrition process inducing fragment generation from the parent crystals through the fluid-induced stress acting upon the surface[28]. It is widely accepted [46] that different layout crystallizers (stirrer tank vessel compared to a continuous crystallizer such as a moving fluid batch oscillatory baffled) generates discrepancies in mixing and flow patterns influencing the nucleation.

Effects of hardness and geometries of the contact materials

Especially in collision mechanism the micro-hardness properties must be considered. Asakuma et al.[18,47] investigated the amount of attrition and fragmentation that strongly affect the crystal size distribution, crystal shape reducing the crystal quality and yielding a worn crystal. It was found that a harder material is more effective in enhancing the nucleation rates so the elastic modulus and fracture strength at the micro-level types for various types of crystal were measured[48].

Impurity

Additives are able to influence crystal nucleation since their presence can enhance or inhibit the solubility of a substance changing the required level of supersaturation to achieve secondary nucleation.

1.2. Single Nucleus Mechanism (SNM)

Considering the number of seeded crystal in the solution, it is possible to count the new generated secondary nuclei. One of the most recently approach in secondary nucleation understanding is the single nuclei mechanism (SNM) according to which all secondary nuclei originate from the same parent single crystal [49]. This mechanism generally occurs when the crystal develops dendrite-like outgrowths on its surfaces that only occur at high supersaturations or in melt crystallization. The seeded single nucleus in the supersaturated solution grows into a parent crystal and after reaching

an appropriate size at which the parent crystal can undergo attrition crystal fragments start appearing generating secondary nucleation. One secondary nucleation event is enough to generate detectable crystal volume in negligible amount of time . If really all secondary nuclei originate from one crystal form, it will give access to secondary nucleation rate allowing the determination of secondary nuclei per unit of time.This mechanism has industrial and scientific implications; industrially, the single nucleus mechanism implies that one crystal is the origin of all crystals in the final suspensions; scientifically, the occurrence of the SNM indicates fluctuations in the Metastable Zone Width (MSZW)[50]. Kubota et al.[51] and Soare et al.[52], investigated in a cooling crystallization process the crystal growth behaviour as a function of the amount of crystal in a seed suspension. Soare et al. used two different type of airlift crystallizer to investigate the crystal growth rate in a system where attrition and breakage are tried to be minimized. A straight line indicates the ideal growth line at which the number of crystals in the batch is equal to the number of seed crystals.

1.3. Challenges for Primary and Secondary Fundamental Understanding

1.3.1. Challenges in controlling Primary Nucleation

Primary nucleation is a stochastic process. This means that the time required for each molecular cluster in a supersaturated solution to reach critical size and be detected would be different[53]. Recently, a statical approach to study the random nature of nucleation has been developed and largely applied using probability distribution of induction time. This method detects and examines the variation of nucleation kinetic in an agitated supersaturated solution at a constant temperature.

In the light of this, MSZW is also a stochastic property and not deterministic as it is conventionally considered. It is necessary to address the gap in understanding primary nucleation within the MSZW and to sequence the events, which lead to detection of crystals. MSZW is an inexact concept and a function of, e.g., cooling rate. So, while being within a MSZW, still nucleation can occur. However, relation between MSZW and induction times is unclear.

1.3.2 Challenges in determing Secondary Nucleation

Secondary nucleation has been and still is not well understood and therefore is difficult to predict and control. A major difficulty in its investigation towards better understanding is the verification of a secondary nucleation event on micro or nano scale in a supersaturated and mixed environment because no direct observation of the process is possible. Furthermore, several secondary nucleation mechanisms are identified which all could be dominant under specific process conditions and equipment. They could even operate at the same time making the interpretation difficult. Numerous experiments at various conditions are needed to characterize secondary nucleation and its effect on product quality. Scale up of secondary nucleation processes in order to design industrial crystallisation processes is still difficult. It is therefore not possible to incorporate secondary nucleation in a rigorous process model for process design or for good process and product quality control. According to the Single Nucleus Mechanism (SNM), primary and secondary nucleations are two subsequent events. The single nucleus formed through primary nucleation reaches a certain appreable size and then, through attrition and/or fluid shear, induces the formation of secondary nuclei. When spontaneous nucleation occurs, primary and secondary nucleation cannot be decoupled and the study of nucleation combined the two rates. It is necessary to develop a systematic method to assess secondary nucleation and distinguish it from primary nucleation events.

1.4. Research Plan

The research described in this thesis is organised in order to answer in each chapter at a different research question leading to a fundamental understanding of primary and secondary nucleation events and developing methods to systematically study nucleation also at industrial scales.

1.4.1. Primary Nucleation Understanding

Chapter 2: Crystal Nucleation within the metastable zone

Research question: Is nucleation possible within the MSZW? Stopping the cooling within the metastable zone, is it possible to calculate the nucleation rate?

Objective: Determing Crystal Nucleation rates at isothermal condition within the MSW

Approach:

First, the MSZ widths at different cooling rates were determined for Isonicotinamide in 1 ml ethanol solutions using different stirrer layout. This was followed by induction time measurements at isothermal conditions within the MSZ varying the cooling rate to achieve the desired constant temperature. Subsequently, the crystal nucleation rates were determined from the obtained induction time probability distributions as a function of the applied cooling times. Finally, a relation between the cooling time and the crystal nucleation rate was established.

Chapter 3: Comparing methods for induction time probability distribution measurements

Research question: How do volume, hydrodynamics and solution interface affect the primary nucleation rate?

Objective: Comparing obtained experimental nucleation rates from 1ml stirred solution and microfluidic systems.

Approach:

Recently a method, based on the determination of probability distributions of induction times under equal supersaturated conditions in 1ml stirred solutions was developed by Jiang and ter Horst[52]. An alternative approach to determine nucleation kinetics from such variations makes use of microfluidics. It is a fast and easy method studying the nucleation in nanoliter droplets. A large

number of experiments with independent nucleation events are provided within droplets of equal chemical composition[54]. In principle both methods, under the same experimental conditions, should result in the same kinetic behaviour. However, to our knowledge, this has never been tested in practise. The optimal conditions to ensure nucleation of isonicotinamide in ethanol within the droplets and in 1 ml stirred solution were established. Then, using both methods, isothermal induction times were measured at different supersaturation ratios. Finally, nucleation rate parameters from both methods were determined and compared.

1.4.2. Secondary Nucleation Understanding

Chapter 4: Measuring Secondary Nucleation through Single Crystal Seeding

Research question: What is the best procedure for seeding experiments in order to systematically study secondary nucleation?

Objective: Understanding secondary nucleation using a single crystal to generate a crystal population.

Approach:

The procedure comprises of the seeding of a carefully selected single crystal in a well-controlled supersaturated solution, under conditions at which spontaneous nucleation only occurs after substantial amounts of time. Seeding a batch crystallizer with a known number of crystals and counting at the end of the process how many secondary nuclei have been formed, it will provide a mathematical method to determine if secondary nucleation occurred. When the number of crystals remains constant, it means that no secondary nucleation takes place. The number of particles generated in the supersaturated solution after seeding will be measured as a function of seed crystal size and supersaturation. After calibration of the measurement method the increasing number of crystals in time after seeding allows for the determination of the secondary nucleation rate. The assessment method for the secondary nucleation rate can be used for a better nucleation events

understanding and to develop a workflow for secondary nucleation determination.

Chapter 5: A general method for secondary nucleation rates under industrial conditions

Research question: Is it possible to control the process of secondary nucleation in crystallisation on industrial scales?

Objective: Determine and understand the effect of crystallization volume and crystal loading on the secondary nucleation rate.

Approach:

On a small ml scale, a single seed crystal is added to a clear, supersaturated and agitated solution at constant temperature whilst the number of crystals subsequently formed is monitored. The measurement of the increasing number of particles generated in the solution after seeding, allows secondary nucleation rate determination. The new seeding method will be applied on larger scales of crystallisers (100 and 700 ml) using different seeds loading (0.5% and 1% w/w). The crystals will be monitored using in-situ measurements such as FBRM. If the results are successful the novel seeding procedure can be incorporate in process design to enable rapid development of industrial crystallisation processes for secondary nucleation threshold.

Chapter 6: Primary and Secondary Nucleation Kinetics of Chiral Crystals

Research question: Can crystallization outcomes such as product chirality be controlled by single crystal seeding?

Objective: Control the chiral outcomes and the kinetic control outcomes after seeding a single crystal in a supersaturated solution under well-controlled isothermal conditions in V=3 ml.

Approach:

To control the chiral outcome of crystal nucleation processes, the seeding procedure developed in Chapter 4 is applied for different combination of $NaClO_3$ and $NaBrO_3$. With homogeneous seeding: a solution of $NaClO_3$ will lead to crystallization of A-$NaClO_3$ when A-$NaClO_3$ is used as the seed crystal. Alternatively, the outcome can also be controlled through heterogeneous seeding. For example, crystallization of A-$NaClO_3$ can be triggered by using A-$NaBrO_3$ [55]. Similarly, crystallization of A-$NaBrO_3$ can be triggered by A-$NaClO_3$ [56]. But how do unseeded and the different forms of seeded nucleation processes compare in terms of kinetics? In unseeded experiments we often obtained just one of the two chiral forms indicating that a single nucleus mechanism is in place. In seeded experiments, the outcome can be controlled by the seed crystal, whether homogeneous or heterogeneous seeding is applied. Although the chiral outcome of homogeneous and heterogeneous seeding is the same, the kinetics are different.

1.5. References

1) Nyvlt, J., 1984. Nucleation and Growth Rate in Mass Crystallization. Prog. Crystal Growth and Charact. 9, 335-370.

2) Mullin, J.W. Crystallization, 4 ed., Butterworth-Heinemann, Oxford, 1997

3) Myerson, A.S. Handbook of Industrial Crystallization. Second ed., Butterworth-Heinemann: Woburn, 2002.

4) Frawley, P.J., Mitchell, N.A., O´Ciardha, C.T., Hutton, K.W. 2012. The effects of supersaturation, temperature, agitation and seed surface area on the secondary nucleation of paracetamol in ethanol solutions. Chemical Engineering Science. 75, 183–197.

5) Verdurand, E., Bebon, C., Colson, C, Klein, J.P, Blandin, A.F, Bossountrot, J.M., 2005. Secondary nucleation and growth of organic crystals in industrial crystallization , Journal of Crystal Growth. 275, e1363–e1367.

6) Meadhra, R.O, Kramer, H.J.M, Van Rosmalen, G.M., 1996. Model for Secondary nucleation in a suspension crystalliser, AIChE, 42, 972-982.

7) Kadam, S.S., Kramer, H.J.M., Horst, J.H., 2011. Combination of a Single Primary nucleation event and secondary nucleation in crystallization processes. Crystal Growth and Design. 11, 1271-1277.

8) Kashchiev, D.; van Rosmalen, G. M. 2003. Review: Nucleation in solutions revisited. Crystal Research and Technology. 38, 7-8, 555-574.

9) Tavare, N.S. In Industrial Crystallization-Process Simulation Analysis and Design. Plenum Publishing Corporation. New York, 1995.

10) Davey, J.,Schroeder S.L.M.,ter Horst, J.H. 2013. Nucleation of Organic Crystals-A molecular perspective. Angew. Chem. Int. Ed. 52, 2166 – 2179

11) Weissbuch, I., Lahav, M., Leiserowitz, L. 2003. Cryst. Growth Des. 3, 125 – 150.

12) Talanquer, V.; Oxtoby, D. W. 1998. Crystal nucleation in the presence of a metastable critical point. The Journal of Chemical Physics. 109, 1, 223-227.

13) Wolde, P. R. t.; Frenkel, D.1997. Enhancement of Protein Crystal Nucleation by Critical Density Fluctuations. Science. 277, 5334, 1975-1978.

14) Garside, J. M., A.; Nyvlt, J., Growth and Nucleation Rates. 2nd ed.; Institution of Chemical Engineers. Rugby, UK, 2002.

15) Christiansen, J. A., Nielsen, A. E. 1951. On the Kinetics of Formation of Precipitates of Sparingly Soluble Salts. Acta. Chem. Scand. 05, 673-674.

16) Schöll, J.; Vicum, L.; Müller, M.; Mazzotti, M. 2006. Precipitation of L-Glutamic Acid: Determination of Nucleation Kinetics. Chemical Engineering & Technology. 29, 2, 257-264.

17) Qu, H.; Louhi-Kultanen, M.; Kallas, J. 2006. In-line image analysis on the effects of additives in batch cooling crystallization. Journal of Crystal Growth. 289, 1, 286- 294.

18) Nývlt, J.1968. Kinetics of nucleation in solutions. Journal of Crystal Growth. 3-4, 377-383.

19) Gora, L., Thompson, R.W., 1995. Investigations of secondary nucleation by initial breeding in clear solution zeolite NaA systems. Zeolites. 15, 526-534.

20) Shimizu, K. Tsukamoto, J. Horita, T. Tadaki.1984. Origin of secondary nucleation as revealed

by isotopic labelling J. Crystal Growth 69,623.

21) Strickland-Constable,1972. The Breeding of Crystal Nuclei - A Review of the Subject, AlChE Symp. 121, 68, l.

22) Rajesh, N.P., V. Kannan, V., Raghavan, P.S., Ramasamy, P., Lan, C.W. 2002. Optical and microhardness studies of KDP crystals grown from aqueous solutions with organic additives. Materials Letters. 52, 326–328.

23) Asakuma, Y., Honda, T., Maeda, K., Miki, H., Fukui, K., 2008. Fragmentation behaviour of aggregated crystal in suspension crystallization processes. Powder Technology. 181, 266– 272.

24) Mason, B.J. The physics of Clouds. Clarendon: Oxford, 1957.

25) Ting, H.H., McCabe, W.L. 1934. Supersaturation and crystal formation in seeded solutions. Ind Eng Chem. 26, 1201.

26) Mason, B.J. The physics of Clouds. Clarendon: Oxford, 1957.

27) Lal, D.P., Mason, R.E.A., Strickland-Constable, R.F. 1969. Collision breeding of crystal nuclei. Journal of Crystal Growth. 1, 1-8.

28) Powers, H.E.C. 1963. Nucleation and early crystal growth. The industrial chemist. 39, 351- 353.

29) Clontz, N.A., McCabe, W.L. 1971. Collision nucleation, Chem. Eng. Progr. Symp. Ser. 110 67.

30) Sung, C.Y., Estrin, J., Youngquist, G.R. 1973. Secondary nucleation of Magnesium Sulfate by fluid shear. AIChe. 19, 957-962.

31) Wang, M.L., Huang, H.T. 1981. Secondary nucleation of Citric Acid due to fluid forces in a Couette Flow Crystallizer. AIChe. 27, 312- 315.

32) Evans, T.W, Margolis, G., Sarofim, A.F. 1974. Mechanisms of Secondary Nucleation in Agitated Crystallizers. AIChe. 20, 950-958.

33) Shamlou, P.A., Jones, A.G., Djamarani, K. 1990. Hydrodynamics of secondary nucleation in suspension crystallization. Chemical Engineering Science. 45, 1405-1416.

34) Sun, Y., Song, X., Wang, J., Luo, Y., Yu, J. 2009. Seeded Induction Period and Secondary Nucleation of Lithium Carbonate. The Chinese Journal of Process Engineering. 9, 652-660.

35) Reyhani, M.M., Freij, S., Parkinson G.M. 1999. In situ atomic force microscopy investigation of the growth of secondary nuclei produced by contact of different growth faces of potash alum crystals under supersaturated conditions. Journal of Crystal Growth 198/199,258–263.

36) Ferrari, E., Davey, R.J. 2004. Solution-Mediated transformation of α to β L- Glutamic Acid: Rate enhancement due to secondary nucleation. Crystal Growth and Design. 4, 1061-1068.

37) Kulkarni, S.A., Meekes, H., ter Horst, J.H. 2014. Polymorphism control through a single nucleation event. Crystal Growth and Design. 14, 1493-1499.

38) Larson, M.A., Bendig, L.L. 1974. Nuclei Generation from Repetitive Contacting. ERI- 74152, Iowa State Univ., Ames.

39) Randolph, A.D., Cise, M.D. 1972. Nucleation Kinetics of the Potassium Sulfate-Water System. AIChE. 18, 806.

40) Sikdar, S.K., Randolph, A.D. 1975. Secondary nucleation of two fast growth systems in a mixed suspension crystallizer: magnesium sulfate and citric acid water systems. AIChe. 22, 110-117.

43) Liiri, M., Koiranen, T., Aittamaa, J., 2002. Secondary nucleation due to crystal-impeller and crystal-vessel collisions by population balances in CFD-modelling. Journal of Crystal Growth. 237–239, 2188–2193.

44) Kee, K.C., Rielly, C.D., 2000. Proceedings of the 10th European Conference on Mixing. The Netherlands, Elsevier, Amsterdam, 231–238.

45) Liang, Q., Borthwick, A.G.L., Stelling, G., 2004. Simulation of Dam and Dyke-break Hydrodynamics on Dynamically Adaptive Quadtree Grids. International Journal for Numerical Methods in Fluids, 46: 127-162.

46) Callahan, C.J., Ni, X.W., 2012. Probing into nucleation mechanisms of cooling crystallization of sodium chlorate in a stirred tank crystallizer and an Oscillatory Baffled Crystallizer. Crystal Growth and Design. 12, 2525-2532.

47) Asakuma, Y., Tetahima, T., Maeda, K., Hideo, M., Fukeu, D., 2006. Attrition behaviour by

micro-hardness parameters in suspension-crystallization processes. Powder Technology. 171, 75–80.

48) Gahn, C., Mersmann, A., 1999. Brittle fracture in crystallization processes. Part A and Part B. Attrition and abrasion of brittle solids. Chemical Engineering Science. 54, 1273-1282.

49) Kadam, S.S., Kramer, H.J.M., Horst, J.H., 2011. Combination of a Single Primary nucleation event and secondary nucleation in crystallization processes. Crystal Growth and Design. 11, 1271-1277.

50) Kadam, S. S., Kulkarni, S. A., Ribera, R. C., Stankiewicz, A. I., ter Horst, J. H., Kramer, H. J. M., 2012. A New View on the Metastable Zone Width during Cooling Crystallization. Chem. Eng. Sci. 72, 10-19.

51) Kubota, N., Kigashiyama,K., Sugeno, H., Shimizu, K. 1986. Waiting time distribution and supercooling temperatures for contact nucleation of ammonium sulphate from single seed crystal. Journal of Crystal Growth. 76,75-82.

52) Soare, A., Lakerveld, R., van Royen, J., Zocchi, G., Stanckiewicz, A.I., Kramer, H.J.M. 2012. Minimization of attrition and breakage in an Airlift Crystallizer. Industrial & Engineering Chemistry Research. 51, 10895-10909.

53) Jiang, S., ter Horst, J.H. 2010. Crystal Nucleation Rate from Probability Distribution of Induction Times. Crystal Growth & Design, Vol. 11, No. 1.

54) Ildefonso, M., Candoni, N., Veesler, S. 2011. Using microfluidics for fast, accurate measurement of lysozyme nucleation kinetics. Cryst. Growth Des. 11, 5, 1527-1530.

55) Kondepudi, D.K., Kaufman, R. J., Singh, N. 1990. Chiral symmetry breaking in sodium chlorate crystallisation. Science. 250, 975-976.

56) Buhse, T., Durand, D., Kondepudi, D., Laudadio, J., Spilker, S. 2000. Phys. Rev. Lett. 84, 4405-4408.

Chapter 2

Crystal Nucleation within the Metastable Zone

2.1. Introduction

The control of crystal form, size, shape and purity is crucial in particle manufacturing because these properties can affect the physical and chemical characteristics of the product as well as downstream operations[1]. Industrial suspension crystallisation is a particle formation process often relying on intricate seeding procedures to circumvent the crystal nucleation step[2], which is still not well enough understood for reliable crystal nucleation control and prediction[3].

A frequently applied experimental method for investigating the crystal nucleation behaviour is based on the metastable zone width (MSZW)[4,5,6] which represents a measure of the tendency of solutions to crystallise[7]. One side of the metastable zone is characterised by the saturation temperature T_s of the measured solution, while the other side follows from the temperature $T_n<T_s$ (the metastable zone limit) at which crystals are first detected in a clear solution upon cooling with a constant rate[7,8,]. It is well known that the metastable zone limit T_n decreases with increasing cooling rate[9], leading to a larger MSZW. With knowledge about the MSZW, primary nucleation can be induced or even avoided if, for example, seed crystals are added to a supersaturated solution within the metastable zone.

Recently, a second method, based on induction time probability distributions, which detects and examines the variation in nucleation kinetics of crystal nucleation measurements, was developed[10]. The experiments were performed in an agitated supersaturated solution at a constant temperature and the time from the creation of constant supersaturation until the detection of crystals, the induction time, was measured. The induction times showed a wide variation, captured in an induction time probability distribution. The variation was attributed to the stochastic nature of crystal nucleation and indicates that a single nucleus mechanism (SNM) is occurring[11]. According to the SNM, only a single crystal is born through primary nucleation in the clear solution, which eventually grows out to a particular size resulting in secondary nucleation to create the suspension

of crystals. Assuming the SNM enables the determination of the crystal nucleation rate from the probability distribution at the supersaturation used to determine the distribution.

Although MSZWs and induction times are widely used in studies of crystal nucleation, their interconnection is unclear. Often, the variations in MSZWs, which also can be used to determine nucleation rates8, are not reported. On the other hand, for the induction time measurements, the influence of the time to reach a constant temperature has not been investigated. The objective of this study is to understand MSZW and induction time results and their interconnection through crystal nucleation. The model system used is Isonicotinamide (INA) in the solvent ethanol. First, we studied the variation in MSZWs at different cooling rates. Then, we investigated the induction time variations within the MSZW using different times to reach constant temperature. Subsequently, we determined the crystal nucleation rates from the obtained induction time probability distributions as a function of these cooling times. Finally, we establish a relation between the cooling time and the crystal nucleation rate.

2.2. Method

INA and Ethanol, with a purity of ≥ 99% and 99.8% respectively, were obtained from Sigma-Aldrich. Solubility, metastable zone width and induction time measurements were carried out in a 1 mL multiple reactor set up (Crystal16, Technobis Crystallization Systems B.V.). A recalibration of the Crystal-16 temperature was performed because of a small constant temperature difference between the actual and set temperature of the wells.

2.2.1. Solubility Measurements

Known amounts of INA and 1 mL of ethanol were subsequently added to a 1.5 mL glass vial generating differently concentrated samples. The vials were placed in the Crystal-16 and heated to T=60°C to dissolve the crystals. The solution was cooled using a cooling rates of 0.3°C/min to T=-10°C during which crystallization occurs. The solution was subsequently heated with a heating rate

of 0.3°C/min to T=60°C and the transmission of light through the sample was recorded. The temperature at which the transmission reached 100% was taken as the saturation temperature (T_s) of the measured composition. Two subsequent measurements of the same sample were performed. The samples were stirred with a controlled stirring speed of 700 rpm, using a PTFE coated magnetic stirring bar (VWR, micro 0.7x0.2 mm). A fit of the Van't Hoff equation to the solubility data facilitated the interpolation of the solubility and the determination of supersaturation.

2.2.2. Metastable zone width Measurements

20 ml of stock solution, with a composition of 78 mg per ml of solvent, was prepared by dissolving INA in ethanol at 45°C. A syringe, pre-warmed to avoid crystallisation during sample preparation, was used to dispense 1 mL of clear solution into 16 1.5 mL glass vials containing a magnetic stirrer bar (VWR, micro 0.7x0.2 mm) and 16 1.5 mL glass vials with a hook top stirrer (Hastelloy and Peek, Crystal 16 Overhead Stirring Assembly). The vials were tightly closed with a lid and sealed with para-film to avoid solvent evaporation and then placed in the Crystal-16 setup at a stirring speed of 700 rpm for bottom stirrer and 900 rpm for top stirrer. These stirrer speeds were found to give a good suspension of the formed crystals. Four different cooling rates (r = 5, 1, 0.2 and 0.04^o C/min) were used to measure the MSZW variation. The temperature at which the transmission of light dropped below 100% was taken as the cloud point temperature T_n, the temperature at which the clear solution turned into a suspension. Four vials of the prepared 16 were used for each cooling rate and three subsequent cycles were performed for MSZW determination, resulting in 12 cloud point temperatures for each cooling rate.

2.2.3. Induction time Measurements

The same sample preparation method as that for the MSZW measurements was used for the induction time measurements. Each sample was cooled to a temperature T_i using a specific cooling rate (r = 5, 1, 0.2 and 0.04^o C/min) after which the constant temperature T_i was maintained. For each cooling rate a new stock solution was prepared. The moment the solution reached the

temperature T_i, was taken as time zero for the induction time measurements. At a certain time t_i, the transmission of light through the sample dropped below 100% indicating the presence of crystals. The difference between the time t_i and time zero was taken as induction time. Induction time measurements were performed at T_i = 19.0, 19.5, 20.0, 20.5, 21.0, 21.5 and 22.0ºC for cooling rate r = 5ºC/min, T_i = 19.0, 19.5, 20, 20.5 and 21ºC for cooling rate r = 1 and 0.2°C/min; T_i = 20.0, 20.5, 21.0, 21.5 and 22.0ºC for cooling rate r = 0.04ºC/min. Visual observations for possible fouling and crowning on the vial surfaces were conducted in order to avoid any false induction time measurements. Fouling and crowning were never observed, as in a previous study[11]. Some induction time measurements were performed by cooling the solution very fast (5°C/min) to a constant temperature within the MSZW, subjecting the sample to a holding time at that constant temperature and then again cool very fast to the lower constant temperature at which the induction time was measured.

2.3. Results

2.3.1. Solubility

Figure 1 shows the average values of the determined solubilities of INA in ethanol. The obtained results present a good consistency since the error bars are smaller than symbol. The solubility curve shows good agreement with literature data[11]. Although INA is a polymorphic compound[12,13], multiple crystallization experiments under various conditions showed that only INA form II crystallized from ethanol[14]. This was confirmed in this study by XRPD analysis.

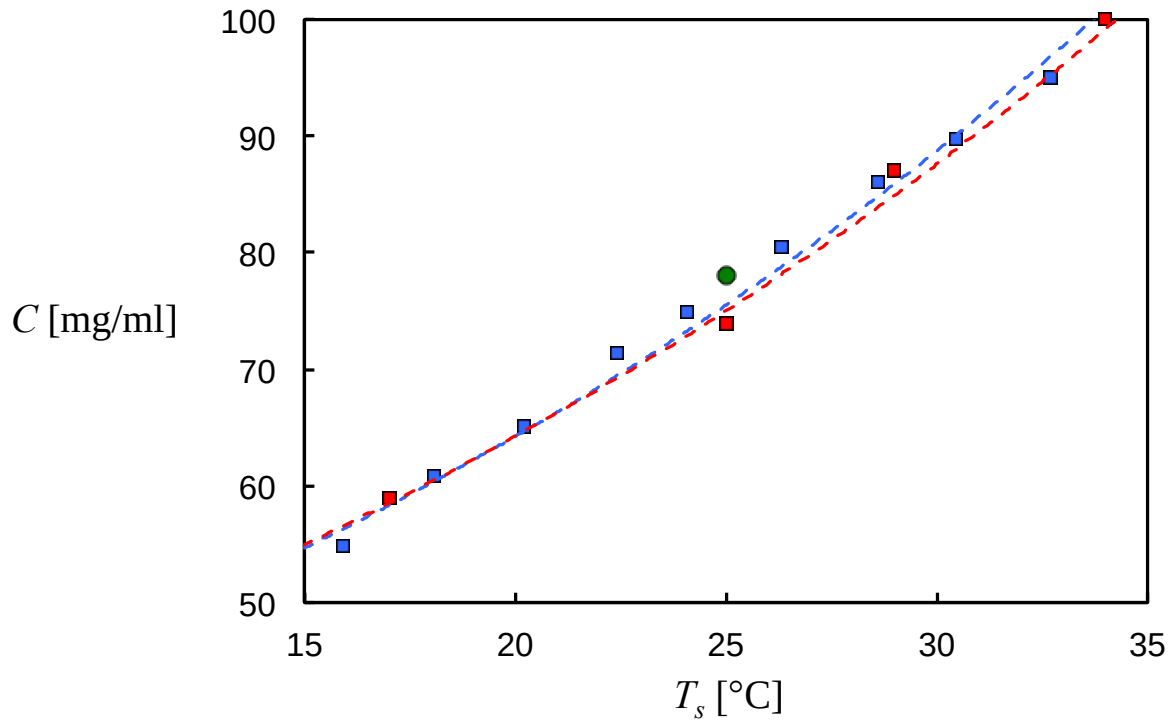

Figure 1: Saturation temperatures T_s of INA in Ethanol at different concentrations C (mg per ml of solvent). The blue symbols show the experimental data and the red squares are values from elsewhere[11]. The green dot represents the chosen concentration for this research (C=78 mg/mL and T_s=25°C). Each blue square represents the average value of the three measured saturation temperatures. The lines are a fit of the Van't Hoff equation to the experimental data in order to link the solubility measurements to the thermodinamic changes of the system.

2.3.2. Metastable zone width Measurements

A solution composition of 78.0 mg/ml INA in ethanol having a saturation temperature of T_s=25.0°C was chosen for the MSZW measurements. Figure 2 shows the measured cloud point temperatures for the four cooling rates and the two different stirrer types used. The blue line indicates the saturation temperature.

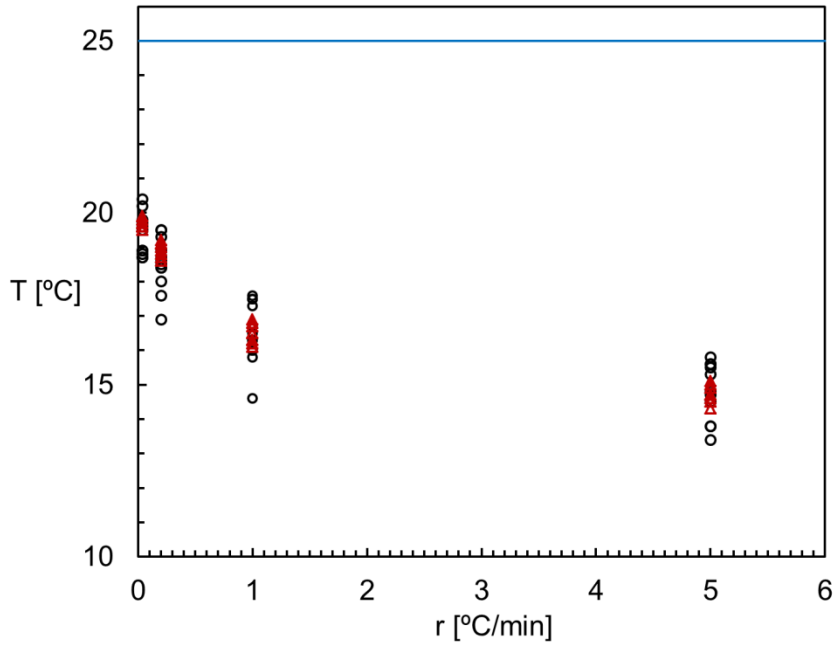

Figure 2: MSZWs using bottom stirrer (red) and top stirrer (black) for INA solution in ethanol with a concentration of 78 mg/ml using cooling rates r = 5, 1, 0.2 and 0.04º C/min in 1 mL solution T_s=25°C. The dots and the triangles represent the cloud points for top and bottom stirrers respectively, while the blue line shows the saturation temperature. The metastable zone is the region between saturation temperature and cloud points.

At a cooling rate of 5º C/min, the cloud point temperatures vary from 14.3ºC to 15.1ºC for the bottom stirrer experiments. This results in a MSZW of 10.3±0.4°C for this cooling rate. For the top stirrer experiments at the same cooling rate the MSZW is the same. However, the variation in the cloud point temperature from 13.4ºC to 15.8ºC is larger. Probably, this difference is due to the position of the stirrer in the vial. The magnetic stirrer bar touches the bottom of the vial triggering more secondary nucleation compared to the overhead stirrer, which is suspended in the middle of the vial.

The temperature fluctuations determined for all the used cooling rates and the resulted MSZWs values are reported in Table 1:

Table 1: Cloud point temperatures and MSZWs for 78 mg/ml of isonicotinamide in ethanol using bottom and top stirrer and cooling rates r = 5, 1, 0.2 and 0.04º C/min.

	Bottom Stirrer			**Top Stirrer**		
r [ºC/min]	T variation [ºC]		MSZW [ºC]	T variation [ºC]		MSZW [ºC]
	T_{min}	T_{max}		T_{min}	T_{max}	
5	14.3	15.1	10.3±0.4	13.4	15.8	10.4±1.2
1	16.1	16.9	8.5±0.4	14.6	17.6	8.3±2.1
0.2	18.6	19.2	6.1±0.3	16.9	19.5	6.2±1.4
0.04	19.5	19.9	5.3±0.2	18.7	20.4	5.5±0.9

The average MSZW for both stirrer types is the same and it is smaller at lower cooling rate r applied. In all cooling rate cases, the variation in the cloud points is quite small and does not exceed 0.8°C.

Figure 3 shows the distribution of the cloud point temperatures within the cooling profile, enabling the view of the time variation for each series of MSZW measurements at a specific cooling rate. The coloured lines indicate the time dependent solution temperature governed by the used cooling rate starting at the point t = 0 and T = 25.0ºC, at which the solution is at its saturation temperature. A more negative slope of the coloured lines coincides with a faster cooling rate. All cooling lines end at the lowest cloud point temperature measured. As the blue lines show, a faster cooling rate provides the opportunity to reach a lower cloud point temperature, leading to a larger MSZW. A reduction of cooling rate from 5ºC/min to 0.04ºC/min induces an evident smaller metastable zone from 10.3±0.4 to 5.3±0.2°C. However, the time lapse until crystal detection increases with decreasing cooling rate. While at a cooling rate of 5°C/min the crystals are detected between 2.22 and 3.12 minutes, at a cooling rate of 0.04 detection takes place between 127.52 and 137.46 minutes. This reflects that the system at lower cooling rate has longer time to respond to the increasing supersaturation.

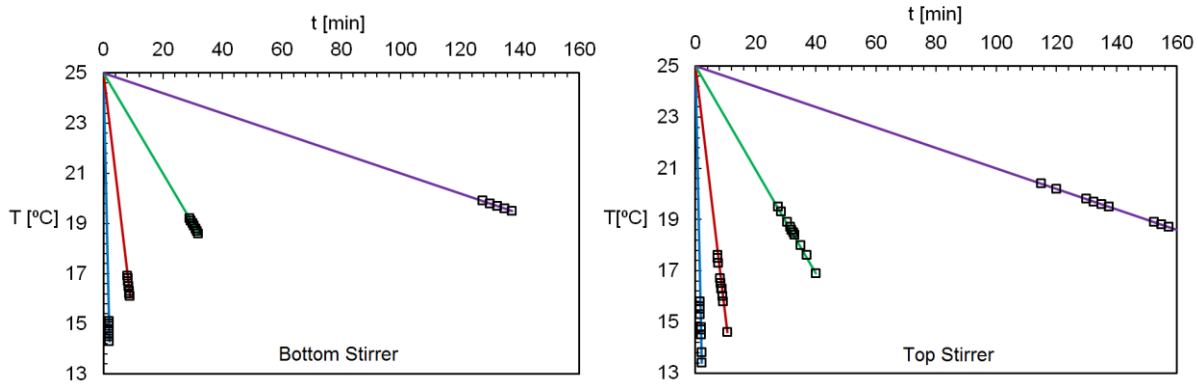

Figure 3: Cooling profile and measured cloud point temperatures as a function of time for INA solution in ethanol with a concentration of 78 mg/ml using bottom stirrer (left) and top stirrer (right) using cooling rates r = 5ºC/min (blue lines), 1ºC/min (red lines), 0.2ºC/min (green lines) and 0.04ºC/min (purple lines) in 1 mL solution with a saturation temperature of 25ºC. Each square represents a cloud point temperature measurement. In total 12 experiments for each cooling rate were performed.

MSZW calculated under different conditions was found to be a function of the cooling rate. A higher cooling rate leaves the system less time to respond to the supersaturation because of the rapid changes in temperatures. There is a lower chance that crystals are detected due to the diminished time for nucleation and growth providing a larger metastable zone. Induction time measurements within the MSZW have been performed using the method of Janse and de Jong[15], adjusted to account for induction time variations. A single measurement series is constructed by measuring the induction time in 16 vials containing a solution of 78.0 mg of INA in 1 ml of ethanol at a specific temperature $T_i < T_s$ within the MSZ. A precisely controlled cooling rate r is used to reach the temperature T_i. Once the temperature T_i was reached, the temperature remained constant ensuring a controlled supersaturation S, providing isothermal conditions for induction time measurements.

2.3.3. Induction Time Measurements

Figure 4 shows the induction time data for a single series of measurements using a cooling rate r = 1°C/min to reach the constant measurement temperature T_i=20°C. The green horizontal line indicates the isothermal period, which starts when the system reaches the desired temperature T_i and finishes after all 16 vials are nucleated. Each point indicates one induction time measurement and

the random order of the experiment number in the right graph of figure 4 underlines the stochastic nature of nucleation[8,10,11,16,17]. The smallest induction time t_i measured is 31.38 minutes and the largest 174.23 minutes. Half of the samples crystallized out within 25 minutes while the remained took roughly four times longer. Several sets of induction time measurements were performed varying constant temperature T_i and the cooling rate r to reach this temperature T_i.

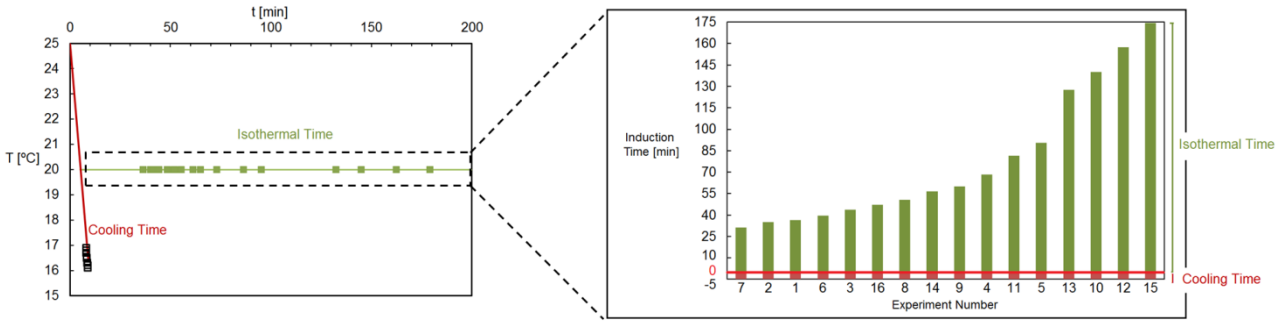

Figure 4: 16 induction time measurements within the MSZW at T_i= 20.0ºC for a supersaturated solution of 78.0 mg/ml in ethanol using a bottom stirrer (left: green line and points). The constant temperature T_i was reached using a cooling rate of r = 1°C/min. The cloud point temperatures for the MSZW measurement using the same concentration and cooling rate are shown for comparison (left: red line, empty black squares). The bar graph on the right shows the induction times measured ordered to size. The experiment number shows the random order of nucleation. The moment the solution reached temperature T_i was taken as time zero for the induction time measurements shown as green bars. The negative times (red bars) represent the time needed to reach T_i= 20.0ºC starting from T_s=25.0ºC using a cooling rate of 1ºC/min.

Figure 5b shows the full data set of t_i at 5 constant temperatures T_i using a cooling rate r =1ºC/min to reach the temperature T_i at which the induction time was measured. At the low T_i in some samples the crystallization commences quite soon after reaching the target temperature. At higher T_i the smallest induction time is larger and the distribution wider. The line of the linear cooling and the shortest induction time at all T_i create a V-shape. This V-shape indicates that at higher T_i it takes longer to detect crystals. The region inside the V-shape indicates suitable conditions for seeding, similar to what was earlier reported by Janse and de Jong [15].

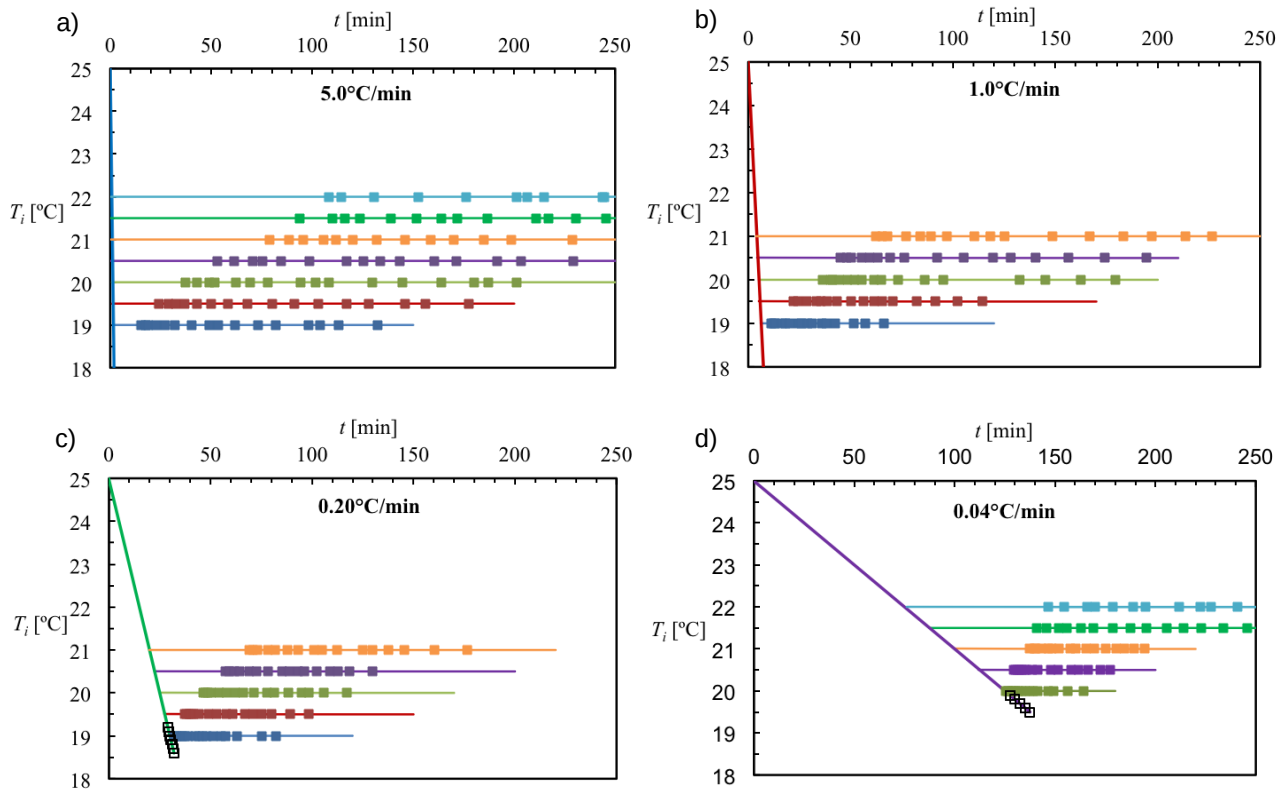

Figure 5: Multiple sets of induction times for INA in ethanol using a magnetic stirrer bar as bottom stirrer and using different cooling rates to reach the desired temperature T_i. a) r = 5ºC/min; b) r = 1ºC/min; c) r = 0.2ºC/min; d) r = 0.04ºC/min. Blue: T_i= 19ºC, S= 1.27; red: T_i= 19.5ºC, S= 1.23; green: T_i= 20ºC, S= 1.21; violet: T_i= 20.5ºC, = 1.19, orange T_i= 21ºC, S= 1.17; emerald in part a and d: T_i= 21.5ºC, S= 1.15 and light blue in part a and d T_i= 22.0ºC, S= 1.13. The cloud points under r = 5°C/min and r = 1ºC/min are not represented in figure 5a and 5b because they occur at lower temperature in respect to the displayed scale.

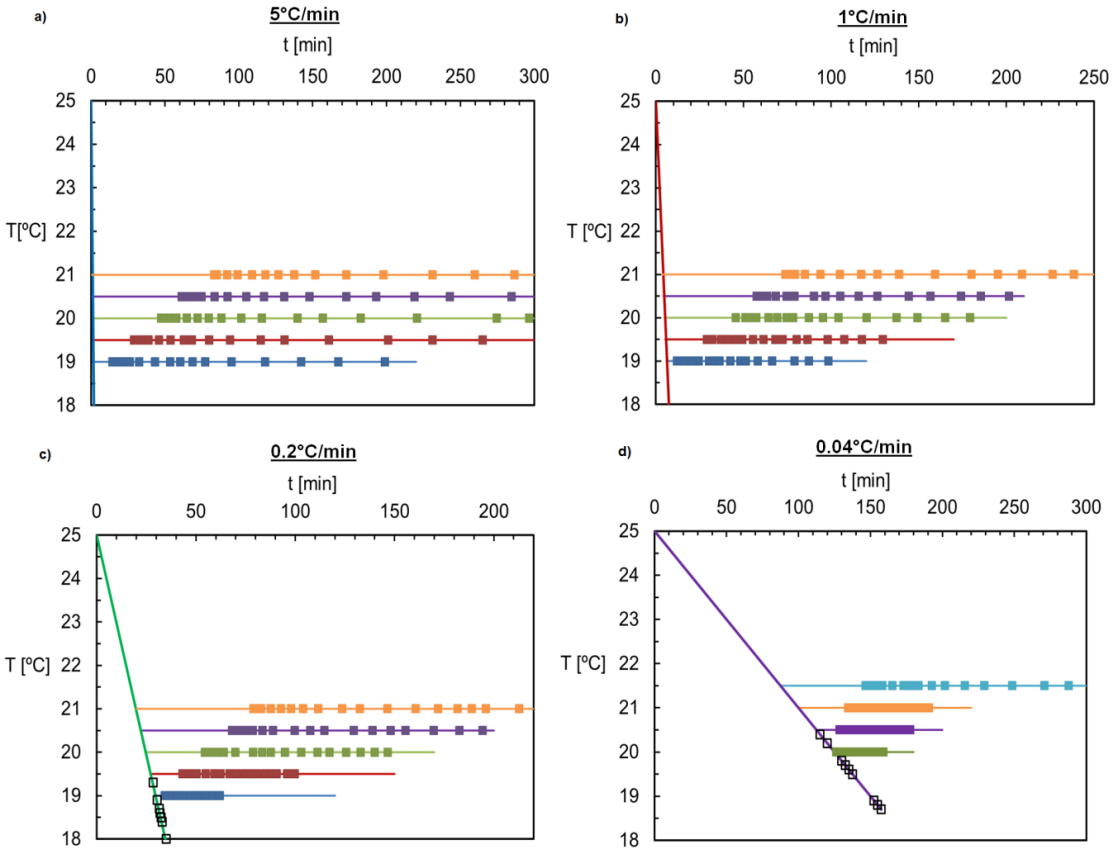

Figure 6: Multiple sets of induction times for INA in ethanol using a top stirrer and using different cooling rates to reach the desired supersaturation at temperature T_i. a) r = 5ºC/min; b) r = 1ºC/min; c) r = 0.2ºC/min; d) r = 0.04ºC/min. Blue represents T_i= 19ºC and S= 1.27; red shows T_i= 19.5ºC and S= 1.23; green indicates T_i= 20ºC and S= 1.21; violet illustrates T_i= 20.5ºC and S= 1.19, orange characterizes T_i= 21ºC and S= 1.17; light blue in part d expresses T_i= 21.5ºC and S= 1.15.

Similar results were carried out also for r = 0.2, 0.04ºC/min for top stirrer experiments (figure 6c and 6d). The bottom stirrer (figure 5) and top stirrer experiments (figure 6) for all investigated temperatures at different cooling rates, do not present a wide difference in terms of t_i. However, a slight delay for top stirrer was noted and results in a longer average induction time with more variation. At a temperature T_i=20ºC and therefore a supersaturation ratio of 1.21, in a larger MSZ (figure 5-a and 6-a) the average t_i = 37 minutes for bottom stirrer and the average t_i = 47 minutes for top stirrer experiments. When the MSZW becomes smaller (figure 5-d and 6-d) at the same supersaturation level, t_i for bottom and top stirrer are t_i=1 minute and t_i=2 minutes respectively.

2.3.4. Nucleation Within the Metastable Zone

The induction time data sets are all acquired at specific temperature T_i using a specific cooling rate r to reach this temperature T_i. The concentration of INA in ethanol was chosen equal for all samples at 78.0 mg/ml. The induction time probability $P(t)$ is the experimental probability of measuring a certain induction time t or smaller and it is defined using the following equation:

$$P(t) = \frac{M^+(t)}{M} \qquad (1)$$

Where $M^+(t)$ is the number of the experiments in which nucleation is detected at time t and M=16 is the total number of experiments in a set of induction time measurements. All data sets therefore can be represented as cumulative induction time probability distributions[11]. The experimental induction time probability distributions at 7 different temperatures are plotted in figure 7. The cooling rate to reach the desired temperature in all these sets of induction time measurements is r =5°C/min. The figure 7 shows that at a lower temperature (e.g., dark blue line), the probability $P(t)$ approaches value 1 in a shorter time, indicating a higher nucleation rate. If the temperature is regularly increased, a reduced nucleation rate is detected.

If we assume that the nucleation rate follows the single nucleus mechanism[8] and is time independent, as nucleation occurs at constant supersaturation, temperature and volume, it is possible to estimate the nucleation rate J by fitting the experimental induction time probabilities to the induction time probability distribution function $P(t)$ using the nucleation rate and growth time as fitting parameters[11]:

$$P(t) = 1 - \mathrm{e}^{[-JV(t-t_g)]} \qquad (2)$$

Where V is the solution volume, t is the induction time and t_g is the growth time, which starts when the system reaches a constant temperature and not when the analysed sample enters the metastable zone. The growth time describes the time needed for nuclei to be detected and it is a combination of growth rate and secondary nucleation kinetics[10]. In figure 7, the experimental induction times (unfilled squares) and the obtained fits (solid lines) at each analysed temperatures, constantly show

a lack of good fit at hight P(t) underling that the solid line always underestimates the experimental data. This problem can be adjusted with future extensions of the used method with major attention on the inteval of confidence providing the range of error for the measured nucleation rate.

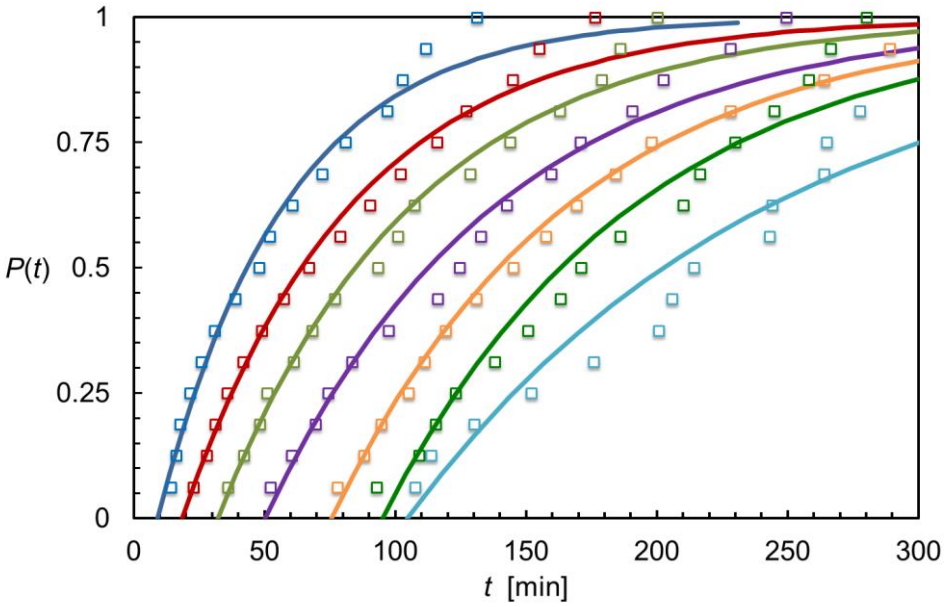

Figure 7: Obtained experimental induction time probabilities for INA in ethanol and cooling rate r = 5ºC/min to reach constant temperature T_i= 19.0°C (blue), T_i=19.5°C (red), T_i=20.0°C (green), T_i=20.5°C (violet), T_i=21.0°C (orange), T_i=21.5°C (emerald) and T_i=22.0ºC (light blue). The solid lines are the fits of the induction time probability distribution function (eq. 2) with the experimental data.

The determined nucleation rate J and growth time t_g are presented in table 2 and table 3 for bottom stirrer and top stirrer respectively. Both tables show that an increase of temperature leads to a decrease of the driving force for both nucleation and growth and therefore nucleation rate J reduces and the growth time t_g increases.

Table 2: Nucleation Rate (J) and Growth time (t_g) calculated from the experimental probability distribution P(t) of induction time using **bottom stirrer.**

	***J* [m^{-3} s^{-1}]**				***t*$_g$ [s]**			
	r [°C/min]				*r* [°C/min]			
***T*[°C]**	5	1	0.2	0.04	5	1	0.2	0.04
19.0	340±40	520±60	770±80	-	550±110	230±60	70±30	-
19.5	250±30	440±50	670±90	-	1110±150	910±100	420±80	-
20.0	220±30	380±70	540±60	1420±150	1930±170	1640±140	1100±110	0±10
20.5	190±20	280±40	490±40	900±110	3020±250	2060±210	1980±160	875±80
21.0	180±30	260±30	370±50	620±90	4540±380	3190±280	2740±240	2154±260
21.5	170±30	-	-	270±40	5320±510	-	-	3247±340
22.0	120±20	-	-	180±40	6270±780	-	-	4214±410

Table 3: Nucleation Rate (J) and Growth time (t_g) calculated from the experimental probability distribution P(t) of induction time using **top stirrer.**

	J [m^{-3} s^{-1}]				**t$_g$ [s]**			
	r [°C/min]				*r* [°C/min]			
***T*[°C]**	5	1	0.2	0.04	5	1	0.2	0.04
19.0	268±30	468±40	874±50	-	617±130	481±80	313±60	-
19.5	217±30	384±70	539±50	-	1192±110	1346±110	997±110	-
20.0	190±20	320±50	410±40	1040±130	2010±190	2011±190	1618±150	83±20
20.5	161±40	250±40	340±70	676±100	3200±210	3050±250	2478±210	965±100
21.0	166±20	228±60	283±60	520±60	4700±410	3751±310	3159±280	2324±250
21.5	-	-	-	240±80	-	-	-	3383±310

Interestingly, a slower cooling rate used for reaching the constant temperature T_i of the induction time measurement seems to lead to an apparent higher nucleation rate. At a temperature T_i=20.0°C the apparent nucleation rate increases from J=220 to 1420 $m^{-3}s^{-1}$ decreasing the cooling rate to reach T_i from r = 5 to 0.04°C/min. The results of table 2 (bottom stirrer) are plotted in figure 8 showing how the four applied cooling rates influence the relation between nucleation rate J and different temperatures T. It seems that different cooling rates could converge at value of around T_i=22.0°C. Figure 8 shows in part a the relation of nucleation rate J and the applied supersaturation ratio S as the classical nucleation theory indicates. As clearly the figure presents, there is not a linear relation for the nucleation rates underlining the possibility that the classical nucleation theory

does not represent the real situation in these types of experiments. Therefore, a new plot has been made in figure 8b, where the nucleation rate J is related to the temperature at which the crystal nucleation is detected.

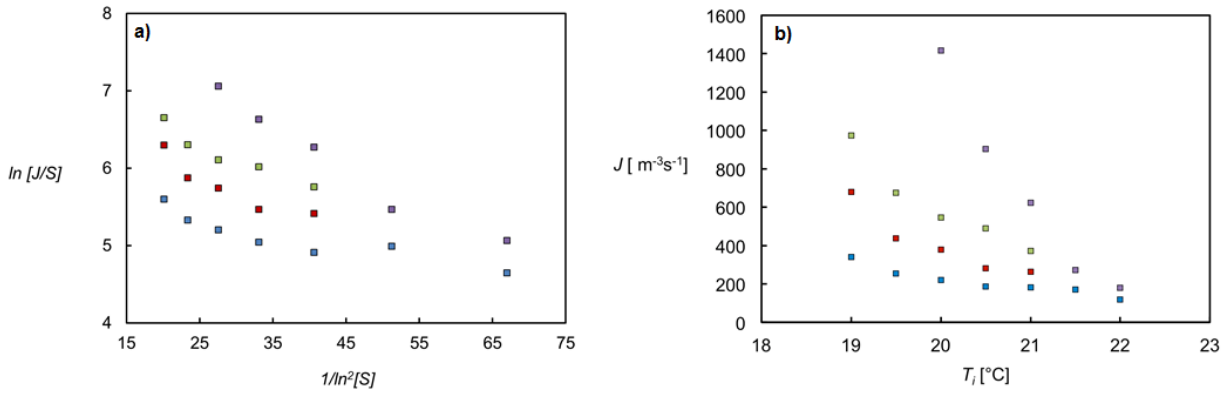

Figure 8: a) Classical Nucleation Theory plot for the nucleation rate experiments at different cooling rates r for INA in ethanol. b) Relation between nucleation rate J and temperatures T_i using different cooling rates r to reach the desired temperature T_i for INA in Ethanol. For both plots, the blue results are for an applied cooling rate r of 5°C/min, the red for 1°C/min, the green for 0.2°C/min and the purple for 0.04°C/min.

Although the induction time measurements are conducted under the same supersaturated conditions the pre-treatment of the solution sample (the cooling rate r used to reach constant temperature T_i for the induction time measurements) has its effect on the measured nucleation rates. In the light of these unusual outcomes, we further investigated this effect. Figure 9 presents different applied temperature profiles we used to test the different temperature treatments before achieving a constant temperature T_i=20.0°C. The showed temperature profiles are 5°C/min (blue), 1°C/min (red), 0.2°C/min (green) and 0.04°C/min (emerald). Three more temperature routes are presented; they are characterized by an added intermediate waiting step during the cooling period at a T_x=22.0°C. This specific temperature was selected because, as it shown in figure 8, J at T_x=22.0°C does not show significant differences when different nucleation rates are applied. A waiting time of 30 minutes at T_x=22.0°C is represented by the purple colour. Different waiting steps of 60 and 90 minutes at T_x=22.0°C are indicated by light blue and orange respectively. The calculated t_g are

represented by the lozenges at the end of each horizontal line. The unfilled symbols have been selected to represent t_g for the temperature routes with a waiting step at T_x=22.0°C.

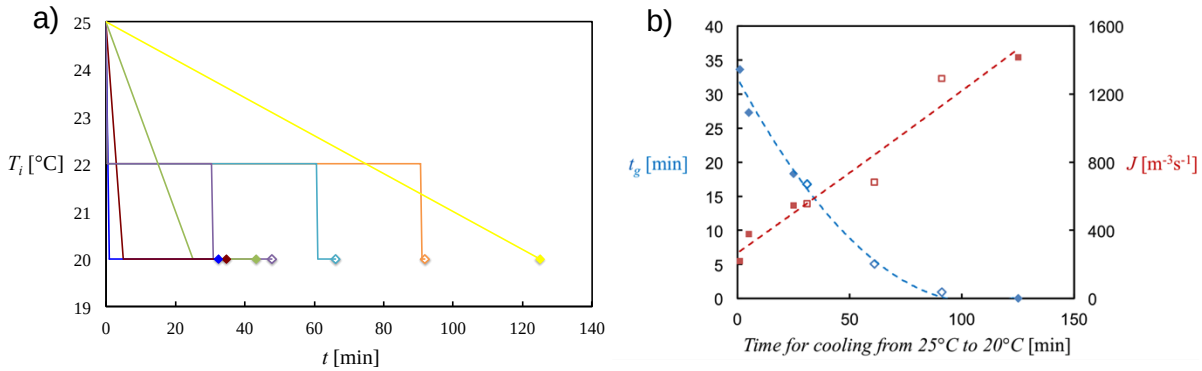

Figure 9: a) Different applied temperature profiles to reach T_i=20.0°C as the target temperature for the induction time measurements. The starting point is the saturation temperature T_s=25.0°C. Blue: 1 minute (5°C/min); red: 5 minutes (1°C/min); green: 25 minutes (0.20°C/min); purple: 32 minutes (5°C/min and waiting step of 30 minutes at T_x=22.0°C); light blue: 62 minutes (5°C/min and waiting step of 60 minutes at T_x=22.0°C); orange: 92 minutes (5°C/min and waiting step of 90 minutes at T_x=22.0°C) and emerald: 125 minutes (0.04°C/min). The horizontal lines show the waiting time at T_i = 20.0°C before the first nucleation event occurs. Each line ends with a differently coloured diamond symbol depending of the cooling applied and represents the calculated t_g for each cooling profile. b) Growth time t_g and nucleation rate J as a function of the time for cooling to the desired temperature T_i=20.0°C for the induction time measurements. The squares symbolize the nucleation rate and the lozenges the growth time. The unfilled symbols represent the results obtained from the temperature holding step at T_x=22.0°C.

Figure 9 (a and b) confirms the unexpected results: although we work at constant supersaturation, the applied temperature route controls the induction time. Figure 9a shows how that a faster cooling profile, without the intermediate step, results in a longer t_g. Adding the waiting period at T_x=22.0°C, t_g will decrease with the increasing of the holding step. t_g is about 1 minute when the system remains constant at T_x=22.0°C for 90 minutes, while is 37 minutes for r =5°C without holding step. Figure 9b presents all t_g and J as results of the the time needed to reach the desired temperature T_i=20.0°C. If the time needed to reach the desired temperature increases, nucleation rate will be higher and growth time will be shorter. The temperature treatment of the solution strongly influences the measured nucleation rate. A solution that spents a longer time at a relatively low supersaturation apparently builds up nucleation potential and therefore is more prone to nucleate than solutions without temperature treatment. Further evidences of effects of temperature on nucleation of a supersaturated solution of Isonicotinamide in ethanol are presented in figure 10. The probability distribution $P(t)$ is calculated for each different solution treatments previously presented (figure 8).

If the solution remains at T_x=22.0°C for 90 minutes (orange experiment), the correspondent P(t) of induction times at T_i=20.0°C needs less time to reach a value of 1 respect the blue experiment, which has a waiting period at T_x=22.0°C of 30 minutes. The distribution results less steeper if the holding time at T_x is reduced. The induction times obtained with a waiting step of 90 minutes at T_x=22.0°C are all less than 20 minutes. Time at which probability starts to rise from zero increases with time of temperature treatment. Width of the distribution increases with time of temperature treatment. Apparently the temperature treatment of the solution before the induction time measurements strongly influences the induction time probability distribution measured at constant temperture.

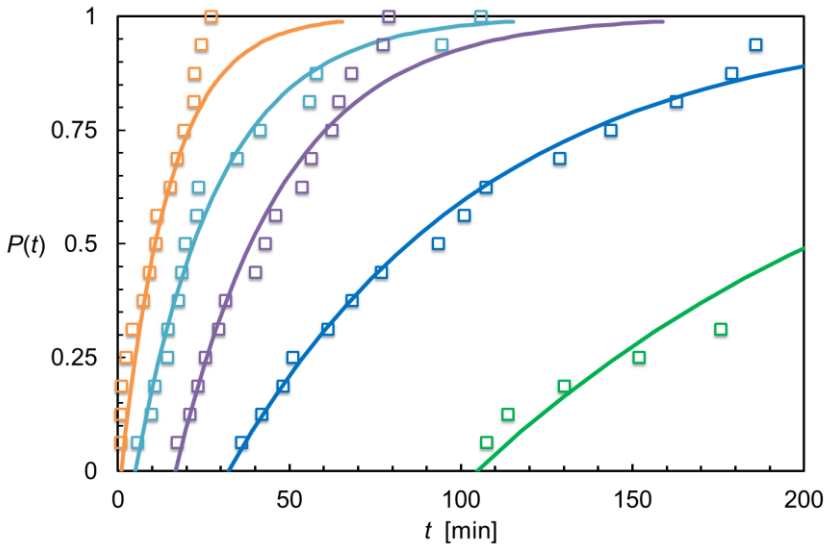

Figure 10: Effect of temperature treatments on probability distribution for a supersaturated solution of INA in ethanol. The green plot represents the probability distribution of 16 induction time at T_i=22.0°C. For this temperature, in this figure, only 5 induction times are presented due to scale reasons. The blue shows the results for a T_i=20.0°C; purple for a T_i=20.0°C but with a waiting time at T_x=22.0°C for 30 minutes; light blue for a T_i=20.0°C but with a waiting time at T_x=22.0°C for 60 minutes and the orange for T_i=20.0°C but with a waiting time at T_x=22.0°C for 90 minutes. All investigated temperatures were reached using a cooling rate of 5°C/min. The solid lines are the fits of the induction time probability distribution function (eq 2) with the experimental data.

2.4. Discussion

2.4.1. Induction Times within the Metastable Zone

Induction times within a metastable zone generated through a fast cooling rate (5°C/min and 1°C/min) provides reliable and reproducible data to estimate nucleation rate and growth time. There

is enough time at isothermal conditions before the first nucleus forms and it can be detected. Meanwhile, within a smaller metastable zone (0.2°C/min and 0.04°C/min) for some temperatures (e.g. 19.0°C and 20.0°C) the induction time is immediate after the cooling time preventing the exact discrimination between nucleation at isothermal conditions and during the cooling. A method is applied that on the one hand results in data that can be applied to accurately determine crystal nucleation rates and on the other hand can be used to study secondary nucleation under well-defined conditions.

2.4.2. Nucleation within the Metastable Zone

The nucleation rate and growth time are influenced by the supersaturated history of the solution: a longer time spend at a relatively low supersaturation in absence of nucleation, increases the nucleation rate and growth time measured at higher supersaturation. Since the consistent reproducibility of the obtained results, it is clear that the unexpected outcomes cannot be considered experimental errors. This research offers insights to look at CNT from a different point of view. What we expected based on the original hypothesis based on CNT is that nucleation rates and growth times should not be affected by the applied temperature profile to reach the desired temperatures because of the role of the supersaturation. However, the results indicate changes in the nucleation rate depending on the pre-treatment of the supersaturated samples. There are two parts within an induction time measurements before crystal detection: the temperature treatment period and the constant supersaturation period. Nucleation takes place in the second part; therefore something happens during sample preparation that influences the nucleation. Having ruled out experimental errors responsible for the observed results, there are a number of possible explanations for this.

Non-Stationary Nucleation. Upon creating a supersaturated solution, clusters form in the solution and develop by attachments and detachments of molecules. A dynamic steady state develops in the supersaturated solution connected to a certain constant cluster distribution[18]. During the

development of this cluster distribution the nucleation rate increases from zero to the stationary nucleation rate value. Usually, in solution nucleation processes this non-stationary nucleation period is assumed to be on the time scale of milliseconds. However, the experimental results described here would suggest a non-stationary nucleation period in the order of hours. In addition, the experimental induction time probability distributions fit well to the distribution function using a constant nucleation rate, indicate a constant nucleation rate in time rather than an increasing one.

Two-step crystal nucleation mechanism. In recent years there was a substantial number of reports on the occurrence of two-step crystal nucleation[19,20,21]. The two-step crystal nucleation mechanism loosens the CNT requirements that cluster size and structures are formed simultaneously: The formation of an unstructured cluster precedes the structure formation and both steps may be associated with an energy barrier. If the first step is slow the formation of the unstructured clusters takes time and therefore the rate of the second step would increase with the duration of the temperature treatment. Therefore, nucleation rate and growth time at a given temperature may not be constant and kinetic parameters may depend on the applied conditions to reach the desired temperature. This behaviour suggests that at lower supersaturation, some clusters form and during the slow cooling, they have time to re-arrange the structure towards crystals.

It would thus appear as if the supersaturated solution remembers how it was cooled to a desired temperature. These results can be compared to previous studies where the history of the supersaturated solution influences nucleation kinetic[22,23].

Finally, it may also be possible that crystals nucleated at different temperatures during cooling will have different growth rates when grown at the same supersaturation and temperature.

2.5. Conclusions

Well-controlled conditions for nucleation studies have been provided through induction time measurements within the MSZ using four cooling rates. Upon faster cooling rate the MSZ shows a larger width because a lower temperature is reached before nucleation can be detected. The

induction time measurements show less variation and faster average when the investigated temperature is closer to the metastable limit. Increasing temperature the induction time becomes longer because supersaturation has been reduced. A combined study of MSZW and induction time measurements provides the determination of kinetic parameter within the MSZ. In this research, a recurrent series of results highlights limits and gaps of CNT. The nucleation rate and the growth time, despite the measurements are performed at constant temperatures, are affected by the cooling rate used to reach the desired temperature within the MSZ. These new information can be very useful for future models to study and predict crystal nucleation in industrial environments. Furthermore, this approach can be a starting point for establishing conditions for seeding procedure. A deep knowledge of conditions for spontaneous nucleation offers the possibility to control crystal formation and provides a suitable working window for future seeding crystallisation.

2.6. References

1) Mullin, J.W. Crystallization, 4th ed.; Butterworth-Heinemann:London, 2001.

2) Ter Horst, J.H., Schmidt, C.; Ulrich, J. Handbook of Crystal Growth. Nishinaga, T. & Rudolph, P. (eds.). 2015 ed. Amsterdam, Vol. II, p. 1317-1349 33 p.

3) Davey, R.J.; Schroeder, S.L.M.; ter Horst, J.H. 2013. Nucleation of Organic Crystals-A Molecular Perspective. Angew. Chem., Int. Ed. 52, 2166−2179.

4) Nyvlt, J.; Rychly, R.; Gottfried, J.; Wurzelova, J.J. 1970. Metastable zone width of some aqueous solutions. Cryst. Growth. 6, 151−162.

5) Ulrich, J.; Strege, C. 2002. Some aspects of the importance of metastable zone width and nucleation in industrial crystallizers. J. Cryst. Growth. 237−239 (Part 3), 2130−2135.

6) Omar, W.; Ulrich, J. 2006. Solid Liquid Equilibrium, Metastable Zone,and Nucleation Parameters of the Oxalic Acid Water System. Cryst.Growth Des. 6, 1927.

7) Nyvlt, J. 1983. Induction period of nucleation and metastable zone width. Collect. Czech. Chem. Commun. 48, 1977.

8) Kadam, S.S.; Kulkarni, S.A.; Coloma Ribera, R.; Stankiewicz, A.I.; ter Horst, J. H.; Kramer, H. J. M. 2012. A new view on the metastable zone width during cooling crystallization. Chem. Eng. Sci. 72, 10−19.

9) Corzo, D.M.C.; Borissova, A.; Hammond, R.B.; Kashchiev, D.; Roberts, K.J.; Ken Lewtas, K.; More, I. 2014. Nucleation mechanism and kinetics from the analysis of polythermal crystallisation data: methyl stearate from kerosene solutions. Cryst.Eng. Comm. 16, 974–991.

10) Jiang, S.; ter Horst, J.H. 2011. Crystal nucleation rates from probability distributions of induction times. Cryst. Growth Des. 11, 256−261.

11) Kulkarni,S.A; Kadam,S.S; Meekes, H.; Stankiewicz, A.I.; ter Horst J.H. 2013.Crystal Nucleation Kinetics from Induction Times and Metastable Zone Widths. Cryst. Growth Des. 13, 2435−2440.

12) Aakeröy, C. B.; Beatty, A. M.; Helfrich, B. A.; Nieuwenhuyzen, M.2003. Do polymorphic compounds make good co-crystallizing agents? A Structural case study that demonstrates the importance of synthon flexibility. Cryst. Growth Des. 3, 159−165.

13) Eccles, K. S.; Deasy, R. E.; Fabian, L.; Braun, D. E.; Maguire, A. R.; Lawrence, S. E. 2011. Expanding the crystal landscape of isonicotinamide: Concomitant polymorphism and co-crystallisation. Cryst Eng Comm. 13, 6923.

14) Li, J.; Bourne, S. A.; Caira, M. R. 2011. New polymorphs of isonicotinamide and nicotinamide. Chem. Commun. (Cambridge, U.K.). 47, 1530−1532.

15) Janse, A.H.; de Jong, E.J. 1978. On the width of the metastable zone. Trans. Inst. Chem. Eng. 56, 187−193.

16) Threlfall, T.L.; De'Ath R.W.; Coles S.J. 2013. Metastable Zone Widths, Conformational Multiplicity, and Seeding. Org. Process Res. Dev. 17, 578−584.

17) Davey, R.J.; Garside, J. From Molecules to Crystallizers: An Introduction to Crystallization; Oxford University Press: Oxford, 2000.

18) Bartels, J.; Schweitzer, F.; Schmelzer, J. 1990. Non-stationary nucleation and cluster growth in

quasi-binary non-ideal solutions. Journal of Non-Crystalline Solids.125, 129-138.

19) Vekilov, P.G. 2010. The two-step mechanism of nucleation of crystals in solution. Nanoscale, 2, 2346–2357.

20) Vivares, D.; Kaler, E.; Lenhoff, A. 2005. Quantitative imaging by confocal scanning fluorescence microscopy of protein crystallization in macromolecular systems. Acta Crystallogr., Sect. D: Biol. Crystallogr. 61, 819–825.

21) Galkin, O.; Chen, K.; Nagel, R.L.; Hirsch, R.E.; Vekilov, P.G. 2002. Liquid-liquid separation in solutions of normal and sickle cell hemoglobin Proc. Natl. Acad. Sci. U. S. A. 99, 8479–8483.

22) Kuhs, M.; Zeglinski, J.; Rasmuson A.C. 2014. Influence of History of Solution in Crystal Nucleation of Fenoxycarb: Kinetics and Mechanisms. Cryst. Growth Des. 14, 905−915.

23) Nordstro, F.L; Svard, M.; Malmberg, B.; Rasmuson, A.C. 2012. Influence of Solution Thermal and Structural History on the Nucleation of m-Hydroxybenzoic Acid Polymorphs. Cryst. Growth Des. 12, 4340-4348.

Chapter 3

Comparing Methods for Induction Time Probability Distribution Measurements

3.1. Introduction

Nucleation is the statistical process of appearance of nanoscopically small clusters of molecules of a new phase in a supersaturated old phase [1,2]. Nucleation is a stochastic process and it can be described by a Poisson distribution [3] and from this relation, kinetic can be derived. Despite nucletion is one of the major events for crystallisation process, it remains poorly understood and difficult to control [4]. Kinetic control of nucleation is a real challenge because it is difficult to obtain reliable data. An accurate determination of nucleation kinetic requires a large sample of independent equivalent nucleation events under equal and well-controlled conditions.

Recently such a method, based on the determination of probability distributions of induction times under equal supersaturated conditions in stirred solutions using Crystal 16 was developed by Jiang and ter Horst [5]. Nucleation rates are determined from cumulative probability distributions of induction times in agitated solutions, closely related to industrial crystallisation conditions.

An alternative approach to determine nucleation kinetics from such variations makes use of microfluidics. In the last decade, microfluidic systems have proven to be reliable experimental tools for studying kinetics of proteins [6,7], salts [8] organic molecules [9,10]. It is a fast and easy method studying the nucleation in nanoliter droplets. A large number of experiments with independent nucleation events are provided within droplets of equal chemical composition. In principle reliable methods, under the same experimental conditions, should result in the same kinetic behaviour. However, to our knowledge, this has never been tested in practise.

The aim of this work is to compare the obtained experimental rates from the two nucleation measurement methods and explain their difference. For the microfluidic method first, the optimal conditions to ensure nucleation of Isonicotinamide in ethanol within the droplets were established and the droplet stability at different temperatures and supersaturation ratios were tested. Then, using both methods, isothermal induction times were measured at different supersaturation ratios. Finally, nucleation rate parameters from both methods were determined and compared.

3.2. Method

3.2.1. 1 ml Stirred Solution

3.2.1.1. Solubility and Metastable Zone Width

The used method to obtain the solubility of Isonicotinamide (INA) in ethanol was presented in section 2.2.1. Metastable zone widths were measured using 20 ml of stock solutions ,with compositions of C=78 mg , 89 mg, 102 mg and 115 mg per ml of solvent. The selected concentrations result in a saturation temperature of T_s= 25, 30, 35 and 40°C respectively. The dissolution of each composition of INA in ethanol was ensured at 20°C above the T_s and therefore at T= 45,50,55 and 60°C. A syringe, pre-warmed to avoid crystallisation during sample preparation, was used to dispense 1 mL of clear solution into 16 1.5 mL glass vials (neck vial, 32x11.6 mm) containing a magnetic stirrer bar (VWR, micro 0.7x0.2 mm). The vials were tightly closed with a lid and sealed with para-film to avoid solvent evaporation and then placed in the Crystal-16 setup at a stirring speed of 700 rpm for bottom stirrer. These stirrer speeds were found to give a good suspension of the formed crystals. A cooling rate of r=5°C/min was used to measure the MSZW variation.

The temperature at which the transmission of light dropped below 100% was taken as the cloud point temperature T_n, the temperature at which the clear solution turned into a suspension. Four vials of the prepared 16 were used for each cooling rate and three subsequent cycles were performed for MSZW determination, resulting in 12 cloud point temperatures for each cooling rate.

3.2.1.2. Induction time Measurements

The same sample preparation method as that for the MSZW measurements was used for the induction time measurements. Each sample was cooled to a temperature T_i using a specific cooling rate r = 5º C/min after which the constant temperature T_i was maintained. The moment the solution reached the temperature T_i, was taken as time zero for the induction time measurements. At a

certain time t_i, the transmission of light through the sample dropped below 100% indicating the presence of crystals. The difference between the time t_i and time zero was taken as induction time. Induction time measurements were performed at T_i = 19.0, 19.5, 20.0, 20.5, 21.0ºC for a composition of 78 mg/ml, T_i = 24.5, 25.0, 25.5, 26.0ºC for a composition of 89 mg/ml; T_i = 29.0, 29.5, 30.0, 30.5°C for a composition of 102 mg/ml; T_i = 34.0, 34.5, 35.0, 35.5°C for a composition of 115 mg/ml. Visual observations for possible fouling and crowning on the vial surfaces were conducted in order to avoid any false induction time measurements.

3.2.2. 65 nl Droplets obtained through Microfluidic

3.2.2.1. Droplets generation

Figure 1 outlines the used setup, developped in CINaM[11], for the droplets generation. 5 ml Hamilton syringes, model 1005 were used to generate the droplets. One syringe with INA solution in ethanol and another syringe with a transparent oil were placed in a temperature-controlled incubator at T =50°C. The solution of INA at the selected temperature was under saturated and the chosen oil was Krytox GPL 106, a fluorinated syntetic oil that is non-reactive, non flammable, safe in chemical and oxygen service, and is long lasting. It is a versatile oil and is compatible with all types of solution and it is usable at high temperatures.

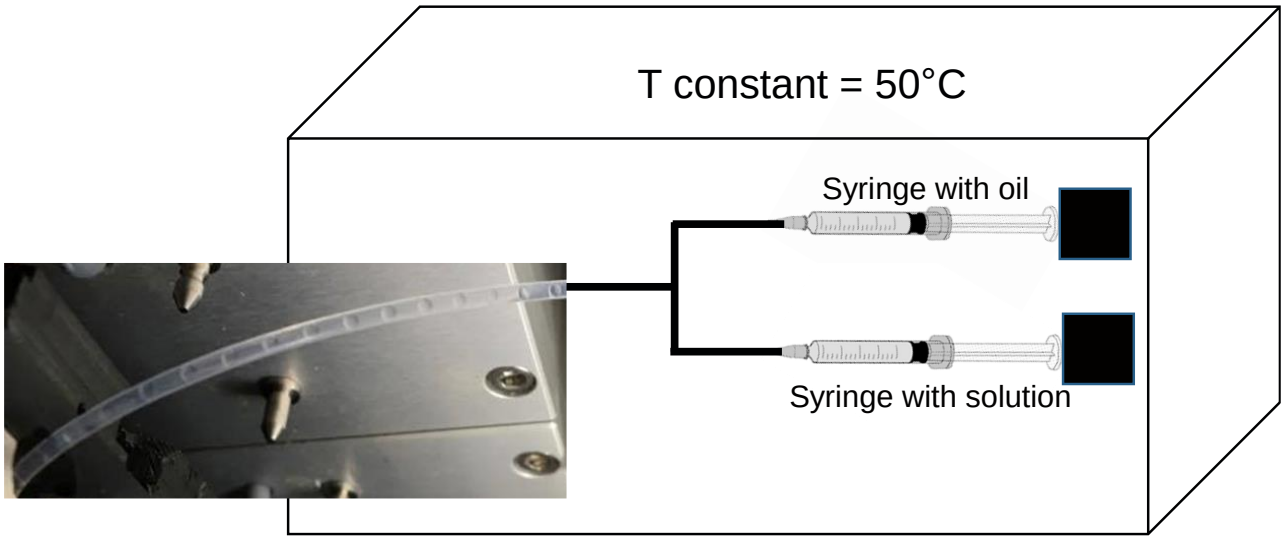

Figure 1: Schematic representation of microfluidic droplets generator. The constant temperature inside the incubetor was set as T=50°C. The two syringes, one for the GPL 106 oil and the other one for the solution, are linked with a T-junction. The content of the syringes is pushed out through indipendent micro-pumps.

The content of the two syringes was mixed through a T-junction forming droplets of solution dispersed in oil. The droplet size was controlled both via the channel size of the plug-factory and via the flow rates. The capillary used for these experiments had a size of 0.5 mm allowing a droplets volume of 65 nl. Different flow ratio conditions were tested to obtain the most stable droplets in terms of size and shape. The resulted flow rate was a ratio 2:1 for oil and solution respectively. Once the droplets were formed we checked that no crystallisation occured during the droplets formation, then the capillaries were placed at the desired temperature (T_i = 20°C, 25°C and 30°C), which needs to be lower than saturation temperature (T_s) in order to ensure generation of supersaturation.

3.2.2.2. Recrystallisation of droplets

The droplets stability was tested running few subsequent cycles of dissolution and recrystallisation for one set of 100 droplets. The generated droplets had a composition of 137 mg/ml and a saturation temperature of T_s=50°C. In order to dissolve any possible crystals formed during the droplets generation, the capillary was placed into the oven at T=60°C for 1 hour. Then

supersaturation was created storing the capillary in a room at T_i=20°C for 2 hours. The same procedure was repeated for five times providing a good data set to understand if the droplets are able to recrystallize.

3.2.2.3. Induction time within supersaturated droplets

Two droplets compositions (C=125 mg/ml and C=137 mg/ml) with saturation temperatures of T_s=45°C and T_s=50°C were selected in order to generate a large amount of droplets allowing induction time measurements. For each composition, 50 droplets were formed and three crystallisation temperature were chosen T_i= 20, 25 and 30°C. Once the droplets were generated through the microfluidic device, they were placed into a special plate linked to a water bath, which controls the desired crystallisation temperature. The plate where the capillaries are placed, is located under an automatic microscope, which moves around the plate with a frequence of 1 minute and 30 seconds to complete the full screening of the plate. The microscope, after proper focus, allows the analysis of the induction time within each droplet at the desired constant temperature. Using this method, the crystal formation within the droplets is monitored constantly and the analysed samples are under the same conditions.

3.3. Results

3.3.1. 1 ml Stirred vessel

3.3.1.1. Induction time measurements

16 samples of four different compositions (C= 78, 89, 102 and 115 mg/ml) were selected to study induction time measurements within the MSZW in 1 ml stirred solution. Figure 2 presents the results for the induction time data for all different concentrations using a cooling rate of r =5°C/min. Figure 2a indicates the results for 78 mg/ml of INA in ethanol. This composition has a saturation temperature of T_s=25°C and it corresponds to the origin of the two axis. The vertical red

line represents the cooling rate, which is r =5°C/min and it stops at each desired temperature T_i providing constant temperature maintenance. The horizontal lines indicate the isothermal period, which starts when the system reaches the desired temperature T_i and finishes after all 16 samples are nucleated. At the low T_i, in this case T_i=19°C, the crystallization commences quite soon after reaching the target temperature. At higher T_i the smallest induction time is larger and the distribution wider.

All the different compositions (figure 2b, 2c and 2d) show similar results and the common message: the line of the linear cooling and the shortest induction time at all T_i create a V-shape. As it was presented and commented in chapter 2, this V-shape indicates that at higher T_i it takes longer to detect crystals and the region inside the V-shape indicates suitable conditions for seeding[12].

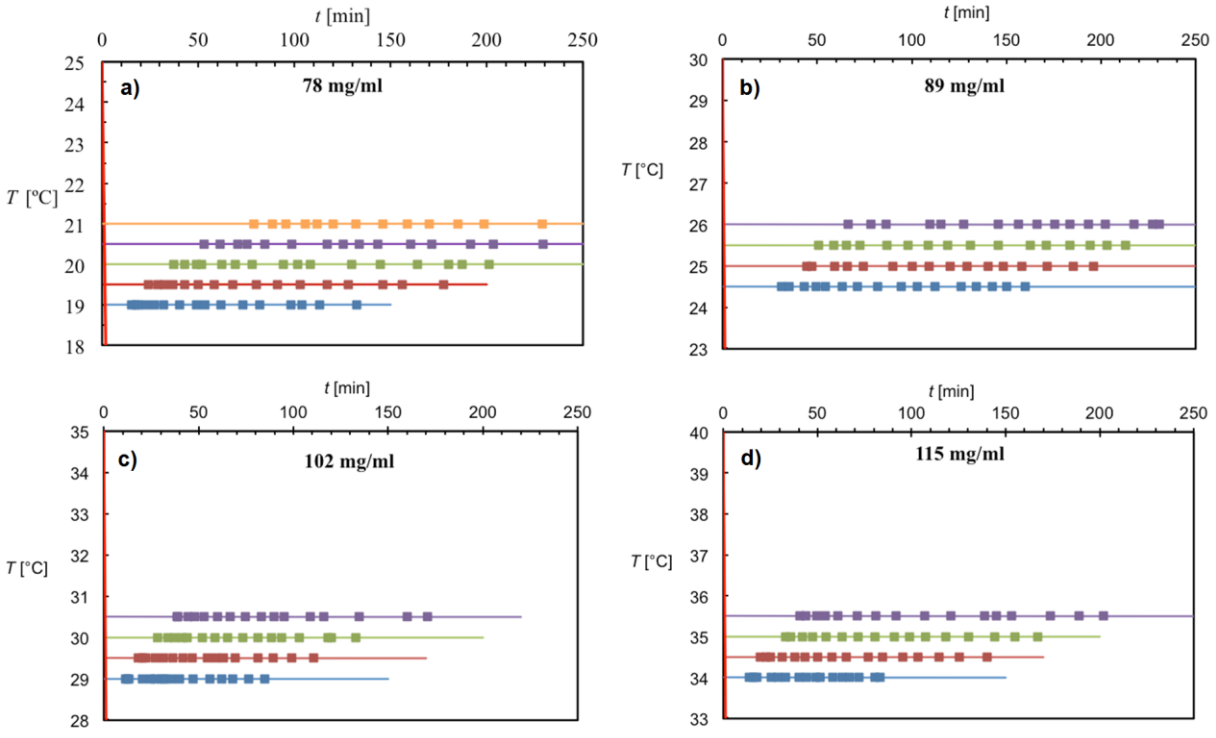

Figure 2: Induction time measurements at different solution compositions (C= 78, 89, 102 and 115 mg/ml) and at different temperatures within the MSZW. Each selected temperature has 16 samples and the orizontal lines indicate the time of the experiment. a) Results for 78 mg of INA in 1 ml of ethanol. The analysed temperatures are T_i= 21°C (orange), 20.5°C (purple), 20°C (green), 19.5°C (red) and 19°C (blue). b) Results for 89 mg of INA in 1 ml of ethanol. The screened temperatures are T_i= 26°C (purple), 25.5°C (green), 25°C (red) and 24.5°C (blue). c) Results for 102 mg of INA in 1 ml of ethanol. The temperatures for induction time measurements are T_i=30.5°C (purple), 30°C (green), 29.5°C (red) and 29°C (blue). d) Results for 115 mg of INA in 1 ml of ethanol. The presented temperatures are T_i= 35.5°C (purple), 35°C (green), 34.5°C (red) and 34°C (blue).

3.3.1.2. Probability Distribution of Induction times

The induction times are all measured at specific temperature T_i using r=5°C/min as specific cooling rate to reach the desired conditions for each composition.

The induction time probability *P(t)* is the experimental probability of measuring a certain induction time *t* or smaller and it is defined using the equation 1 explained in section 2.3.4.

Figure 3 shows the cumulative induction time probability distributions at different temperatures and concentrations. At the lower selected temperature, always indicated with dark blue symbols but with different values depending of the composition, the probability *P(t)* approaches value 1 in a shorter time, indicating a higher nucleation rate. If the temperature is regularly increased, a reduced nucleation rate is detected.

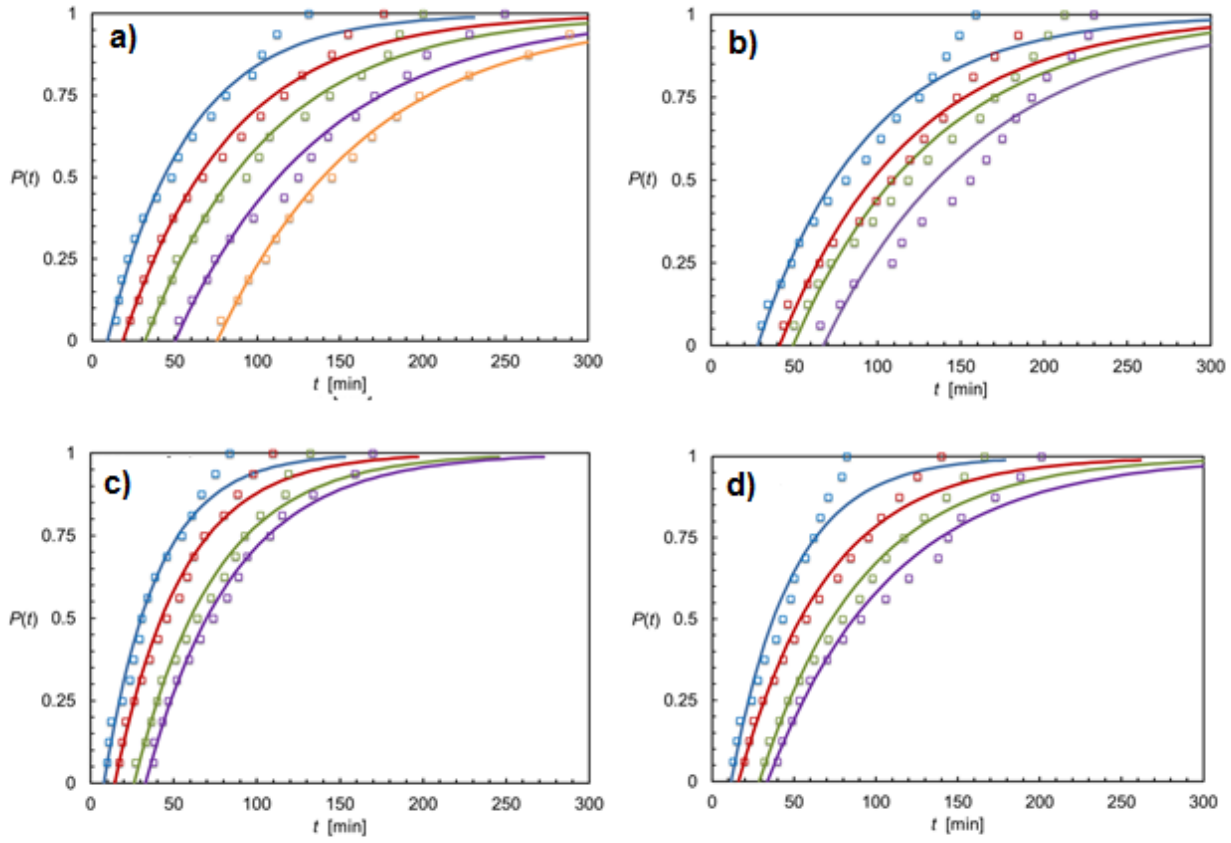

Figure 3: Obtained probability distribution of induction time using different concentrations of INA in ethanol. a) Probability distribution of 78 mg of INA in 1 ml of ethanol. Orange squares indicate a T_i=21.0°C, purple squares are

T_i=20.5°C, green squares are T_i=20.0°C, red squares are T_i=19.5°C, light blue are T_i=19.0°C. The solid lines represent the fit of each cumulative probability distribution b) Probability distribution of 89 mg of INA in 1 ml of ethanol at T_i=26.0°C (purple), T_i=25.5°C (green), T_i=25.5°C (red), T_i=24.5°C (light blue). c) Probability distribution of 102 mg of INA in 1 ml of ethanol at T_i=30.5°C (purple), T_i=30.0°C (green), T_i=29.5°C (red), T_i=29.0°C (light blue). d) Probability distribution of 115 mg of INA in 1 ml of ethanol at T_i=35.5°C (purple), T_i=35.0°C (green), T_i=34.5°C (red), T_i=34.0°C (light blue).

3.3.1.3. Nucleation rate

Once the cumulative probability distribution was measured for each composition and temperature, it is possible to estimate the nucleation rate *J* by fitting the experimental induction time probabilities to the induction time probability distribution function *P(t)* using the nucleation rate and growth time as fitting parameters in the equation 2 reported in section 2.3.4.

Figure 4 presents the obtained nucleation rates *J* as a function of the reached supersaturation *S*. The values of nucleation rates results in the same order of magnitude included in a range between 100-500 $m^{-3}s^{-1}$.

The observed fluctuation is due to the variation in terms of supersaturation ratio indicating that even minimal changes of solution environments lead to different nucleation rates.

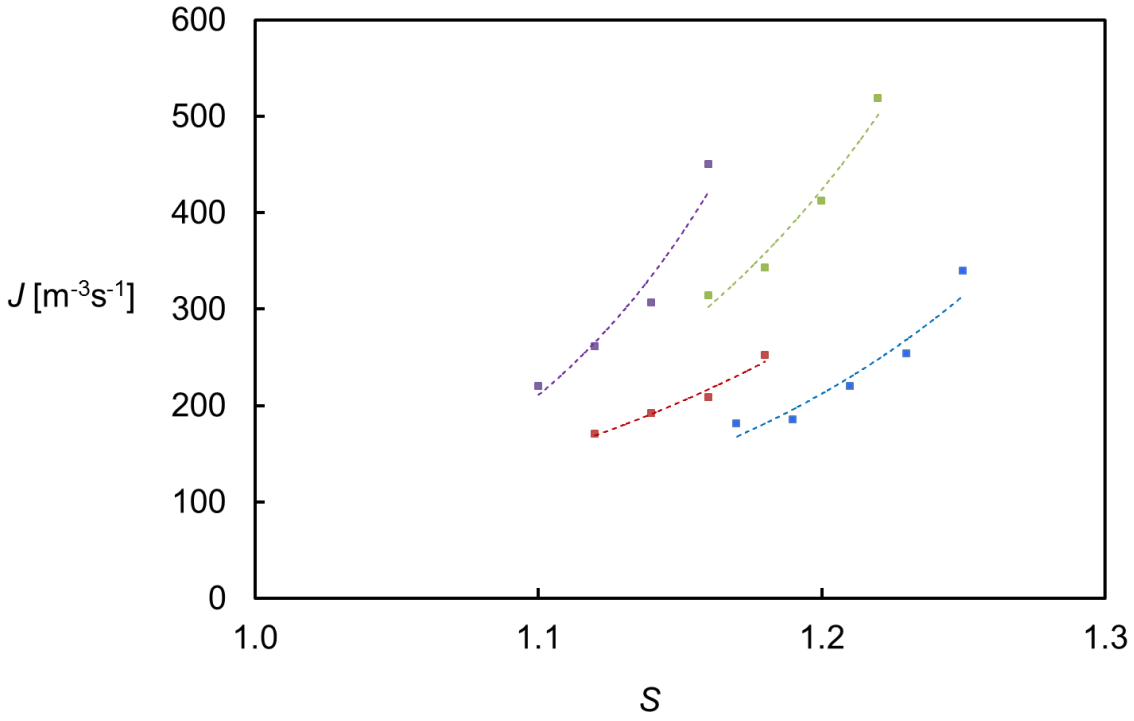

Figure 4: Relation of experimental nucleation rates at different concentrations of INA in ethanol with the reached supersaturation values. The purple symbols indicate the results at four levels of supersaturation ratios for a

concentration of 78 mg/ml. The green symbols shows the results for four levels of supersaturation ratios for a concentration of 89 mg/ml. The red marks present the result for a concentration of 102 mg/ml at four supersaturation conditions. The light blue are the symbols for the nucleation rates calculated at 5 different supersaturation rates. The presented dushed lines are just guides for each used composition.

3.3.2. 65 nl droplets

3.3.2.1. Nucleation within droplets

Nucleation within supersaturated droplets is a complicate event because the conditions to ensure nucleation need to be established. The volume that needs to host nucleation passes from V=1 ml in the stirred solution to V=65 nl and this implies a much longer induction time.

Therefore, the perfect ratio of supersaturation is a must in order to nucleate crystals in a reasonable range of time. If the supersaturation is too low, the nucleation time becames to long and it can take more than 1 week before the droplets can contain a crystal. Figure 5 presents a variety of nucleation events within nanodroplets generated through microfluidic using 125 mg and 137 mg of INA in 1 ml of ethanol and storing them at T_x= 20.0°C, 25.0°C and 30°C. The droplets were generated aiming the same size and shape; however in some samples few bubbles of oil are stored within the capillary. This defect of formulation can be reduced but not completely removed because of the viscosity of the oil compared to the alcoholic solution.

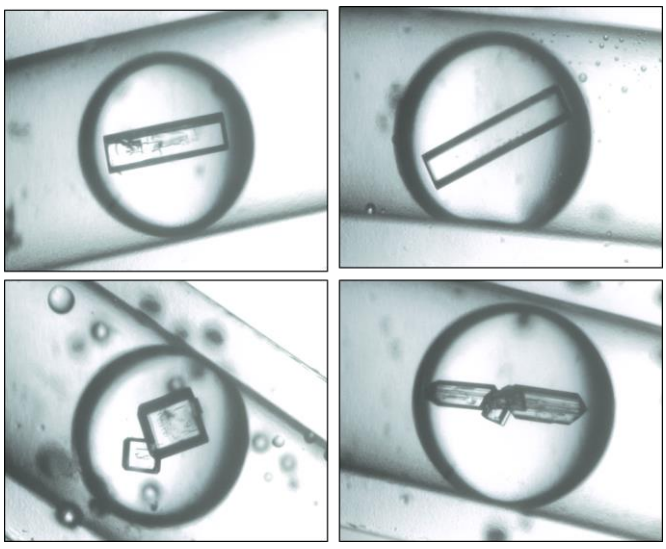

Figure 5: Some examples of crystals nucleated within the nanodroples. The used capillaries have a diameter of 0.5 mm,

therefore the estimated volume of each droplets is 65 nl. The optimal conditions to ensure nucleation within supersaturated droplets were established. Two concentrations (C=125 mg/ml and C=137 mg/ml) with saturation temperatures (T_s =45.0°C and T_s =50.0°C respectively) and crystallisation temperatures (T_x =20, 25 and 30°C) were selected to nucleate INA in ethanol.

3.3.2.2. Stability of droplets

Once the conditions to nucleate the crystals within the droplets were found, the stabilty of the formed droplets was tested. Several cycles of dissolution and crystallisation were performed for droplets generated using a concentration of 137 mg/ml of INA in ethanol. This composition has a saturation temperature T_s=50.0°C and for this reason the dissolution was conducted in the oven at T=60.0°C for 1 hour. The crystallisation within the droplets was observed at T_x= 20.0°C, at which the sample was kept for 2 hours. Figure 6 shows the percentage of crystallisation for each cycle starting from a capillar with 100 droplets. After 5 cycles of dissolution and re-crystallisation, the total number of droplets in the capillary reduces from 100 to 53 because the droplets collapse at the extremity of the capillaries. Moreover, the percentage of nucleated droplets after 2 h decreases with the number of cycle. These results indicate that the droplets are not stable under the temperature cycles and the number of droplets that are able to nucleate is reduced.

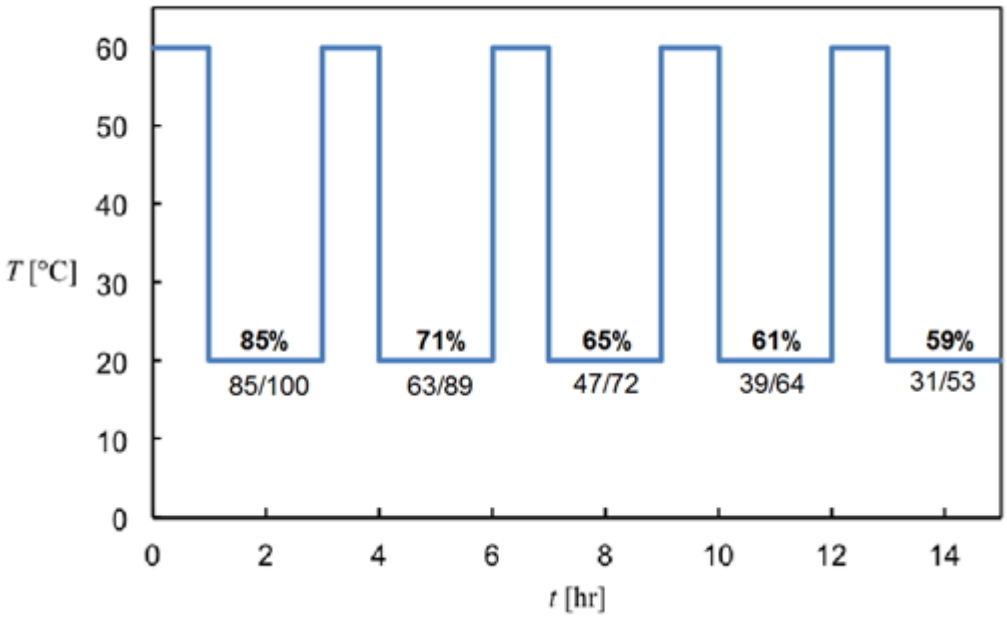

Figure 6: Test for droplets stability. Five cycles of dissolution and crystallisation were performed on droplets with a composition of C=137 mg/ml. The dissolution was conducted at T=60.0°C and the crystallisation at T_x=20.0°C. At each cycle the percentage of droplets that are able to crystallise is reduced because some droplets collapse at the extremity of the capillaries. The original capillary hosted 100 droplets (85% of which nucleated), at the end of the five cycles only 53 droplets remain intact and only 31 of them are still able to nucleate (59%).

According to the results presented in figure 6, the droplets during cycles of dissolution and crystallisation reduce their "power of nucleation" from 85 to 59%. Therefore, a new experiment cycling droplets was run in order to measure the probability distribution of induction times and the related nucleation rate. For the new purpose of the experiment, a capillary with 50 samples was used and the holding time at the desired temperature to reach the wanted supersaturation ratio was 4 hours. Figure 7 shows the obtained probability distribution of induction time for four cycles of one capillary with 50 droplets originally. The first cycle is represented by the purple symbols. All 50 samples nucleated in a range of induction times between 83 minutes and 238 minutes. In the first cycle, the number of droplets reach the maximum value of 1 and it indicates that all the analysed droplets nucleate. The other cycles are indicated by the other colours (blue, green and orange). They do not reach the probability distribution value of 1 and it means that not all sample nucleate. The reduction of nucleated sample is due to the destruction during the cycles procedure and also due to the lack of nucleation during the investigated time.

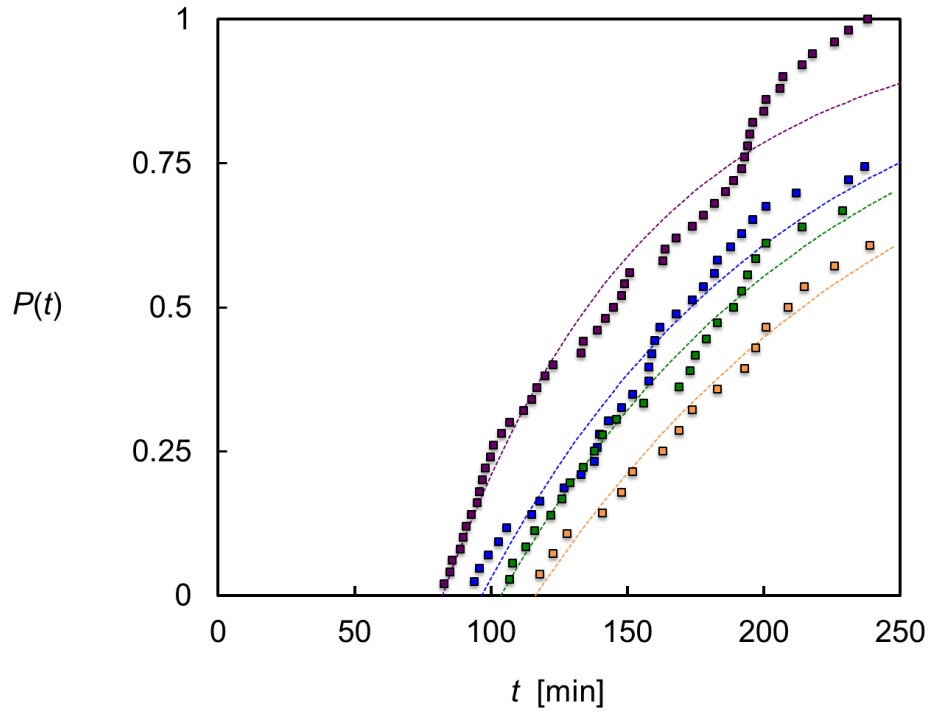

Figure 7: Experimental cumulative distribution of induction times measured during subsequent cycles of the same samples. The inital conditions presented with the purple symbols indicate 50 droplets in the capillary, which are formed with a concentration of C=137 mg/ml of INA in ethanol. The second cycle is represented by the blue symbols, the third cycle by the green colour and the fourth by the orange symbols. Only the first cycle nucleates all the sample reaching the value of $P(t)$=1in a shorter time.

3.3.2.3. Induction time measurements

In the light of these results, it seems better to analyze the droplets contained in the capillary only for one dissolution and one crystallisation cycle. Therefore, more occurate studies of induction times within the droplets, after this point, will be conducted using fresh solution in new capillaries. Three capillaries with 50 droplets each with a concentration of 125 mg/ml of INA in ethanol and a saturation temperature of T_s =45.0°C were generated through microfluidic device. Each capillary was stored at different desired temperatures (T_i= 20.0°C, 25.0°C and 30.0°C) for a reasonable time until all the droplets nucleated. Exactly the same procedure was applied for droplets with a concentration of 137 mg/ml of INA in ethanol and a saturation temperature of T_s =50.0°C. Figure 8 shows the obtained results for the induction time measurments at different concentrations and temperatures. At equal constant temperature the two compositions show different results. Figure 8a at T_i=20.0°C (purple symbols) has the first induction time t_i=92 minutes, while figure 8b at the T_i has a t_i=83 minutes. These results are due to the value of supersaturation reached: droplets with a

C=125 mg/ml at T_i=20.0°C (fig.8a) have a S=1.92, while droplets with a C=137 mg/ml at the same temperature (fig.8b) presents a S=2.11, which speeds the induction time.

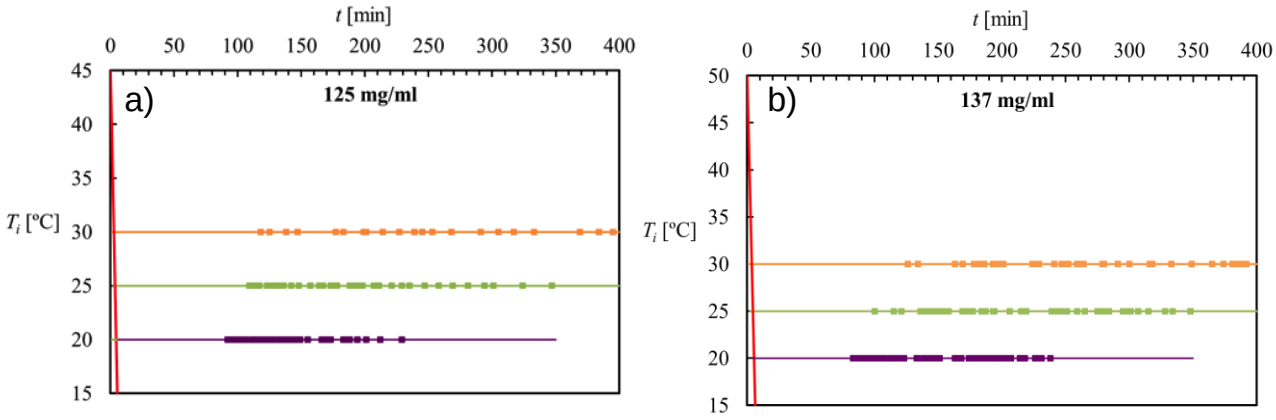

Figure 8: Induction time experiments for INA in ethanol at two different concentrations: C=125 mg/ml (a) and C=137 mg/ml (b). The desired temperatures for the induction time measurements are T_i= 20.0°C (purple), T_i= 25.0°C (green) and T_i= 30.0°C (orange). The horizontal lines indicate the time of the experiment at each costant temperature and the squares represent the individual samples.

Using the same approach applied for the obtained induction time measurements in 1 ml stirred solution of INA in ethanol, the cumulative probability distributions at the selected experimental conditions were calcualted. Figure 9 shows the results for the induction time obtained within droplets with a composition of 125 mg/ml (figure 9a) and droplets with a composition of 137 mg/ml (figure 9b). At lower concentration (figure 9a), the probability distribution never reaches the value of 1 meaning that under these conditions, not all samples nucleated in the screened time. When the droplets are formulated using 137 mg/ml of INA in ethanol, all samples nucleate. Therefore, the purple symbols indicate a value of $P(t)$=1.

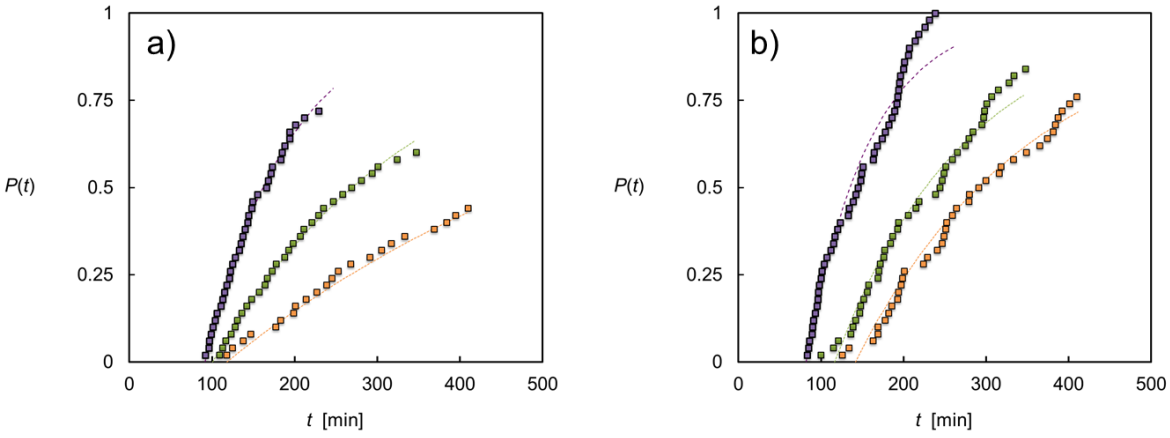

Figure 9: Probability distribution *P(t)* of isothermal induction times at different supersaturation ratios within droplets obtained through microfluidic . a) *P(t)* of 50 induction times for *C*=125 mg of isonicotinamide in 1 ml of ethanol. b) *P(t)* of 50 induction times for *C*=137 mg. For each concentrations 3 different crystallisation temperatures were tested: T_x=20.0°C (violet); T_x=25.0°C (green) and T_x=30.0°C (orange).

From the cumulative probability distribution *P(t)*, the nucleation rate was calculated using the equation $\mathrm{P}(t) = 1 - \mathrm{e}^{[-JV(t-t_g)]}$. Figure 10 shows the obtained results of nucleation rates at the analysed concentrations. The orange symbols indicate the three nucleation rates obtained at the investigated temperature of T_x= 20.0°C, 25.0°C and 30.0°C. In terms of supersaturation they correspond to *S*= 1.39, 1.60 and 1.92 respectively when the used concentration is *C*=125 mg/ml. When the *C*=137 mg/ml the supersaturation ratios are *S*= 1.53, 1.76 and 2.11 and in figure 10 these results are indicate by the blue light symbols. The y-axis indicates a order of magnitude of million (x 10^6) to quantify the nucleation rate. It means that the nucleation rate within the nanodroplet is very fast and order of magnitude higher than the nucleation rates obtained for 1 ml stirred solutions.

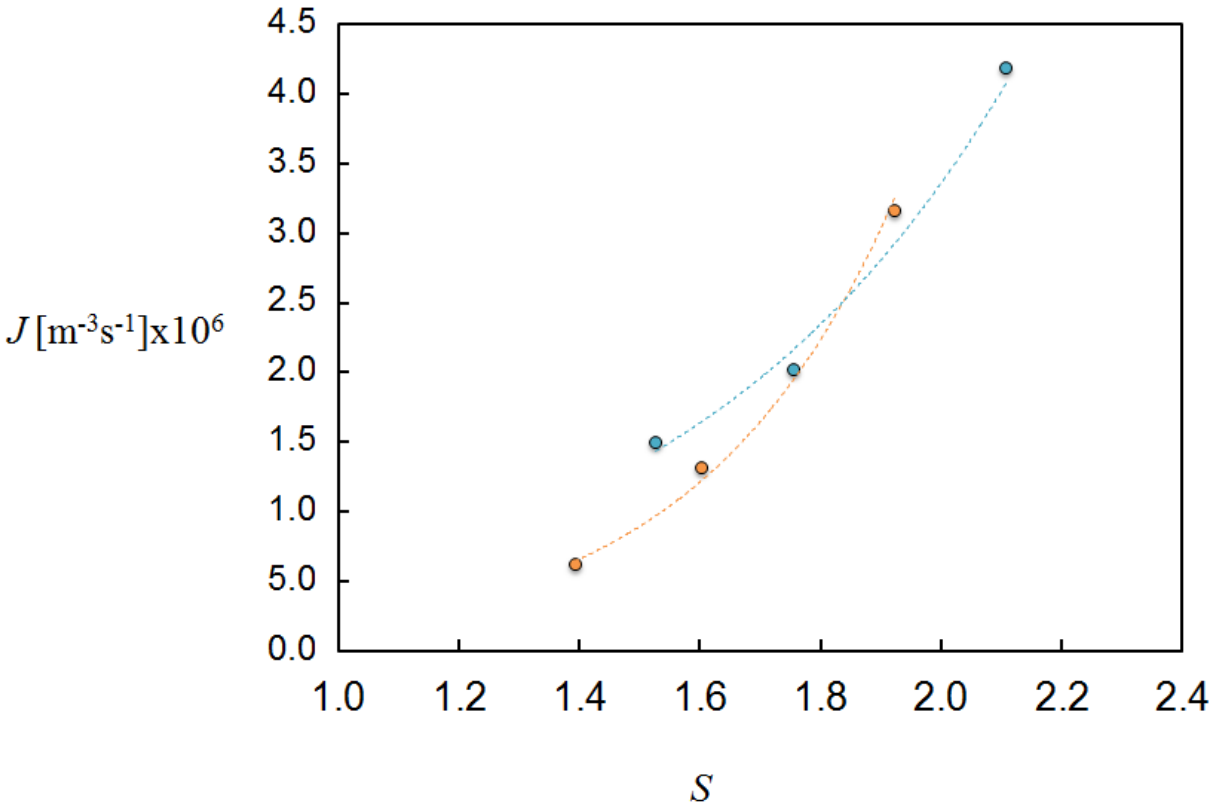

Figure 10: Relation of experimental nucleation rates at different concentrations of INA in ethanol with the reached supersaturation values. The orange symbols shows the nucleation rate obtained at three levels of supersaturation for

droplets formed with 125 mg/ml of INA in ethanol. The light blue symbols shows the results for three levels of supersaturation for a concentration of 137 mg/ml.

3.4. Discussion

In this project, the nucleation rates are obtained from two different experimental methods: one set of results comes from 1ml stirred solution and the second data set is generated through microfluidic. Table 1 summarizes the conditions of the two applied methods. All the differences are listed in the table. In 1 ml stirred vessel, the used concentration are much lower compared to the compositions in the microfluidic method. The range of the screened supersaturations for the 1 ml stirred solution is $1.11< S <1.24$, while for the microfluidic is $1.39< S <2.11$. One of the most clear difference in the two used method is the volume available for nucleation. In the stirred solution, the volume is 1 ml, while in the microfluidic the volume is only 65 nl and it estimated considering a perfect sphere with a diameter of 0.5 mm. Another important difference is the nature of the interface. In 1 ml stirred solution, there is the glass between the solution and the air. In the microfluidic the droplet is formulated using oil, which cover completely the surface of the droplet.

Table 1: Parameters used for the two methods for nucleation rate calculation. The stirred vessel method differes from the microfluidic method for concentration, supersaturation, volume, stirred envirnoment and interface.

	C [mg/ml]	S	Volume	Stirred	Interface	Surface/Volume [mm^2/ml]
Stirred Vessel	78	1.15-1.24	1 ml	Yes	Glass-Air	$1.3x10^3$
	89	1.12-1.17				
	102	1.13-1.18				
	114	1.11-1.16				
Microfluidic	125	1.39-1.92	65 nl	No	Oil	$3.1x10^6$
	137	1.53-2.11				

Considering all the listed differences between the two methods, the comparison between the two data set results as it is presented in figure 11. From the showed results and due to volume

consideration, it is clear that the microfluidic experiments need to be performed at higher supersaturations in order to detect crystals in a reasonable time period.

The differences in terms of magnitude for the calculated J is almost 1000 times and it is probably due to the different surface, which hosts the nucletion event and due to the hydrodynamics.

Interfacial and hydrodynamic effects play a fundamental rule in the nucleation mechanism. The solution in 1 ml glass vial is mixed with a magnetic stirrer bar, while there is not mixing in the microfluidic droplets, which are quiescent in oil.

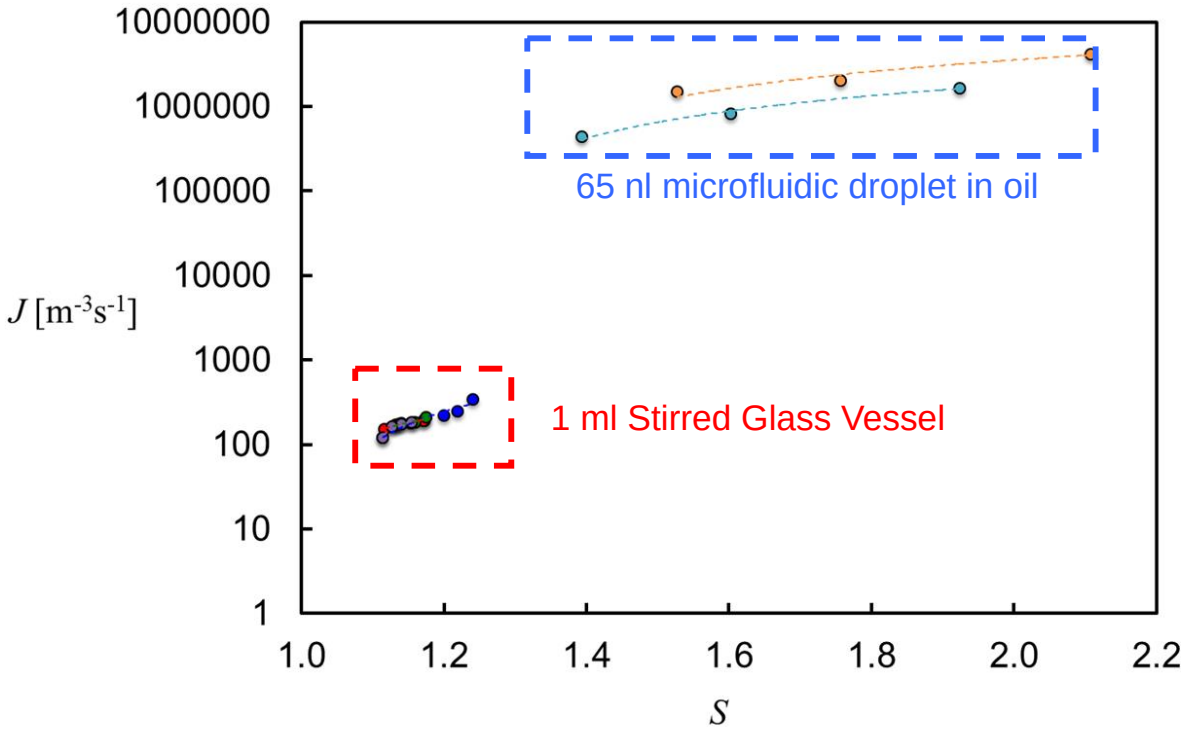

Figure 11. Comparison of the obtained nucleation rates with 1 ml stirred glass vessel (symbols in the red dashed box) and with 65 nl microfluidic droplet in oil (symbols in the blue dashed box).

3.5. Conclusions

The experiments conducted with the microfluidic method had a higher nucleation rate *J* compared to the values obtained with the Crystal 16 procedure. In order to obtain crystallisation within droplets in a reasonable time period, the supersaturation levels needed to be higher. This factor can be explained looking at the different volume available for nucleation in the two methods. In microfluidic, the crystalliser is a droplet of few nanoliters, while the vial in Crystal 16 can accommodate 1 ml of supersaturated solution; therefore, the volume in microfluidic is many orders of magnitude smaller. Furthermore, the hydrodynamic and interfaces are completely different in the two tested systems. Solution-oil interface is present for unstirred droplets while solution-glass (and air) interface is present for stirred vials. Surface to volume ratio is much higher for droplets, which indicates that interfacial effects can be most likely responsible.

3.6. References

1) Kashchiev, D. Nucleation: Basic Theory with Application; Butterworth-Heinemann: Oxford, 2000.

2) Kashchiev, D.van Rosmalen, G.M. 2003. Review: Nucleation in solutions revisited. Cryst.Res.Technol.2003,38,555-574.

3) Pound, G. M.; V. K. La Mer, V.K. 1952. Kinetics of Crystalline Nucleus Formation in Supercooled Liquid Tin. J. American Chemical Society. 74, 9, 2323.

4) Lu, J., Litster, J.D., Nagy, Z.K. 2015. Nucleation studies of Active Pharmaceutical Ingredients in an Air-Segmented Microfluidic Drop-Based Crystallizer. Cryst. Growth Des. 15, 3645–3651.

5) Jiang, S., ter Horst, J.H. 2010. Crystal Nucleation Rate from Probability Distribution of Induction Times. Crystal Growth & Design, Vol. 11, No. 1

6) Shim, J., Cristobal, G., Link, D.R., Thorsen, T., Jia, Y., Piattelli, K., Fraden, S. 2007. Control and measurement of the phase behavior of aqueous solutions using microfluidics. J. Am. Chem. Soc., 129, 28, 8825–8835.

7) Ildefonso, M.; Candoni, N.; Veesler S. 2011. Using microfluidics for fast, accurate measurement of lysozyme nucleation kinetics. Cryst. Growth Des. 11, 5, 1527-1530.

8) Akella, S.V., Mowitz, A., Heymann, M., Fraden, S. 2014. Emulsion-based technique to measure protein crystal nucleation rates of lysozyme. Crystal Growth and Design, 14, 4487-4509.

9) Laval, P., Lisai, N., Salmon, J.B., Joanicot, M. 2007 A microfluidic device based on droplet storage for screening solubility diagrams. Journal of Crystal Growth. 303,622-628.

10) Dombrowski, R.D., Lister, J.D., Wagner, N.J., He, Y. 2017. Crystallisation of alpha-lactose monohydrate in a drop-based microfluidic crystalliser. Chem.Eng. Sci. 62, 4802-4810.

11) Zhang, S.; Ferté, N.; Candoni, N.; Veesler, S. 2015. Versatile Microfluidic Approach to Crystallization. Organic Process Research & Development.19, 1837-1841.

12) Janse, A.H.; de Jong, E.J. 1978. On the width of the metastable zone. Trans. Inst. Chem. Eng. 56, 187−193.

Chapter 4

Measuring Secondary Nucleation through Single Crystal Seeding

4.1. Introduction

Crystallisation is an intricate purification process that produces a final crystalline product through crystal nucleation, crystal growth and agglomeration[1]. Nucleation is the formation of new and small crystalline entities in a supersaturated liquid phase and, therefore, for a large part responsible for the final crystal size distribution[2]. Nucleation can be classified based on the presence or the absence of the crystalline material in solution. If nucleation occurs in the absence of crystalline material of its own kind, it is referred as primary nucleation. If new crystals appear due to other large crystals in a suspension it is classified as secondary nucleation. Thus, for secondary nucleation parent crystals serve as catalyst for the formation of small new crystals [3,4].

For most industrial crystallizers which operate at high crystal slurry density and supersaturation in the metastable regime, secondary nucleation represents the dominant mechanism for generation of new nuclei [5].

With increasing use of continuous crystallisation processes in pharmaceutical industry, it is increasingly important to control and predict secondary nucleation in Continuous Stirred Tank Crystallizer (CSTR) type processes and to prevent it in Continuous Oscillatory Baffled Crystalliser (COBC) type processes[6]. In continuous processes insufficient secondary nucleation can have catastrophic effects because supersaturation may rise due to the lack of crystal growth surface. The system will then reach a metastable zone of activated nucleation that will largely affects the state of successive process, such as crystal growth and therefore the wanted crystal size distribution (CSD)[7].

During batch cooling crystallization, the nucleation step can be carried out as unseeded or seeded crystallizations relying on spontaneous or induced nucleation respectively. The unseeded procedure does not allow a full knowledge on nucleation since there is not a complete mechanism understanding and control. Normally, a well-known and often applied strategy to improve batch-wise crystallization processes and crystal quality control is seeding[8,9,10,11,12,13]. Seeded batch crystallizations are performed with the aim of generating a product with a specific particle size

distribution[14]. However, seeding procedures are generally characterized by a lack of systematic methodologies.

Currently, secondary nucleation has mainly been described so far through empirical power law models, relating observed nucleation rates to operational parameters[15]. Elaborate mechanistic models are available for attrition-induced secondary nucleation [16,17] but are difficult to apply in practice. A semi-empirical model has been suggested for predicting contact secondary nucleation [18]. More research on knowledge of the metastable zone width (MSZW) is required for more precise control and for better estimation of nucleation rates in industrial crystallizers [19].

It is important to assess secondary nucleation rate in terms of under which supersaturation ratios and seed sizes secondary nucleation is negligible and under which conditions is controllable.

The aim of this work is to develop a new approach to study and quantify the secondary nucleation process. Using Isonicotinamide (INA) in ethanol and Paracetamol (APAP) in 3-methyl-1-butanol (Isoamyl alcohol), we developed a single crystal seeding method in a small batch crystalliser to follow the appearance of crystals during the experiment, which determines the rate of secondary nucleation. This method allowed for studying effect of seed crystal size and supersaturation ratio on the secondary nucleation rate using a systematic approach.

4.2. Method

INA, APAP, isoamyl alcohol and ethanol, with a purity of ≥ 99%, 99%, 98% and 99.8% respectively, were obtained from Sigma-Aldrich.

4.2.1. MSZW determination

A known amount of API (INA or APAP) was added to 1 mL of ethanol generating different concentrations and measuring the saturation and the crystallisation temperatures. The 1.5 mL glass vials were tightly closed with a lid and sealed with para-film to avoid solvent evaporation and then

placed in the Crystal16 (Technobis Crystallization Systems B.V.). The heating and cooling rates were set to 0.3°C/min from -10.0°C to 60.0°C for INA in ethanol and to 0.5°C/min from 10.0°C to 80.0°C for APAP in isoamyl alcohol. The samples were stirred with a controlled stirring speed of 700 rpm, using a PTFE coated magnetic stirring bar. This stirrer speed was kept as 700 rpm because of previously successful studies. The determined Metastable Zone Width (MSZW) is defined as the difference of temperatures for clear points and cloud points. The clear point is detected when the suspension upon a constant heating rate turns into a solution and the transmission of the light reaches 100%. The temperature at which the clear solution turns into a suspension is considered as a cloud point and it is determined by the moment when the 100% transmission drops.

4.2.2. Induction Time experiments

The samples were prepared using the same method of the MSZW identification. However, there were few differences when the vials were placed in the reactors. First of all, the volume of the crystallisation experiments was 3 mL because Crystalline (Technobis Crystallization Systems B.V.) can accommodate larger vials (each vial can contain maximum V=8 ml) but only 8 vials per time. A recalibration of the Crystalline temperature was performed because of a small constant temperature difference between the actual and the set temperature of the walls.

40 samples were tested for each supersaturation value at S=1.06 and S=1.10 of INA in ethanol, while only 12 induction times experiments were conducted at S=1.05 and S=1.15 due to the availability of the instrument. Each sample was cooled to the temperature T_i =18.0°C using a specific cooling rate r =5º C/min. 12 samples were tested for the 4 selected supersaturation values (S=1.9, 2.0, 2.1 and 2.2) of APAP in isoamyl alcohol. Each sample was cooled to the temperature T_i =20.0°C using a specific cooling rate r =5º C/min. In both case studies, the moment the solution reached the temperature T_i, was taken as time zero for the induction time measurements. Fouling and crowning were never observed for APIs as in previous study[20].

4.2.3. Preparation of supersaturated stock solutions for seeded experiments

Table 1: Stock solutions of INA in ethanol and APAP in isoamyl alcohol were prepared under different supersaturation conditions. Using a defined concentration (C) and knowing the saturation temperature (T_s), the crystallisation temperature (T_x) was determined accordingly providing the desired supersaturated ratios.

Sample	C [mg/ml]	T_s [°C]	T_x [°C]	Supersaturation (S)
INA in ethanol	62.0	18.6	18.0	1.05
	63.6	19.2	18.0	1.06
	66.0	20.3	18.0	1.10
	70.0	21.9	18.0	1.15
APAP in isoamyl alcohol	52.7	30.0	20.0	1.90
	55.5	32.5	20.0	2.00
	58.2	35.0	20.0	2.10
	60.4	37.5	20.0	2.20

All the stock solutions were prepared using the concentration reported in table 1 and ensuring the dissolution at 20°C above the saturation temperatures (T_s) for two hours on a hot stirrer plate at 500 rpm. The suspension was completely dissolved and stabilized. The stock solution was quickly filtered and transferred into a pre-warmed bottle, ensuring the absence of heterogenous particles and avoiding any possible nucleation. The filter was placed into a ceramic funnel and the flask was connected to the vacuum pump. All the procedures were performed inside an incubator. Both filtered and warm stock solutions were then divided into 24 Crystalline vials (8 ml screw neck vial) through a pre-warmed syringe. Each sample contained 3 mL of solution. 12 vials were used to perform seeded experiments and the remaining 12 for unseeded experiments.

A magnetic stirrer bar (VWR, micro 1x0.3) was added and the vials were tightly closed with a lid before they were located in the Crystalline at a stirrer speed of 700 rpm for bottom stirrer.

4.2.4. Seeding experiments

Crystalline is a multiple reactor setup and all reactors are independents and each of them contains an in-situ camera with a resolution of 2.8μm/pixel and a depth of field of 2.5 mm. The presence of the camera ensures particles count from images providing a tool for nucleation rate studies. A series of 8 vials per time were placed inside the reactors and the solutions were heated up at 40.0°C and 45.0°C for the solution at S=1.06 and S=1.10 respectively for INA in ethanol. These temperatures were kept constant for 20 minutes in order to ensure a complete dissolution of any particles of solute that could form during sample preparation. At the highest temperature, the transmissivity reaches 100% indicating a clear solution. The solution at this stage was under-saturated, therefore a cooling profile of r=1°C/min was applied generating the desired supersaturation ratio. The requested temperature to ensure the chosen experimental conditions was T=18.0°C. Once the solutions reach the desired temperature, the experiments start (t'). Two crystalline vials were taken out from the two reactors. One vial was seeded with a single crystal previously characterized. The single crystal was precipitated from a 1.5 ml vial into the Crystalline vial, which contains the supersaturated solution. The second vial did not receive any crystal but it received the same treatment of the seeded sample. The moment when the vials are replaced inside Crystalline represents time zero (t_0). Isonicotinamide in Ethanol does not agglomerate in Ethanol; however, the count above 200 particles is not reliable because the detected particles are too many and it is not possible to identify the single particles. Different seed sizes were analysed for both supersaturation ratios.

Exactly the same procedure was applied for APAP in isoamyl alcohol. However, only 4 vials were placed inside the crystalline reactors and the solutions were heated up at 50.0°C, 52.5°C, 55.0°C and 57.5°C for the solution at S= 1.90, S=2.00, S=2.10 and S=2.20 respectively. The requested temperature to ensure the desired supersaturation conditions was T=20.0°C.

4.2.5. Definition of times for crystallisation

After the dissolution of the crystalline material, the clear solution sample was brought to a temperature of 18.0°C as presented in figure 1. Time t', represents the starting point of the experiment; after t' the solution is at a constant supersaturation and it is possible to seed. The moment when the single crystal is added is defined as t_0 from which moment we start the observation of secondary nucleation. t_0- t' for the performed experiments in this study was never longer than 10 minutes. t_n is the time from which primary nucleation can be expected to occur. t_n-t_0 depends on the induction times of the unseeded samples. Figure 1 shows that there is sufficient time after time t' to seed the supersatured clear solution in order to distinguish effects caused by primary and secondary nucleation.

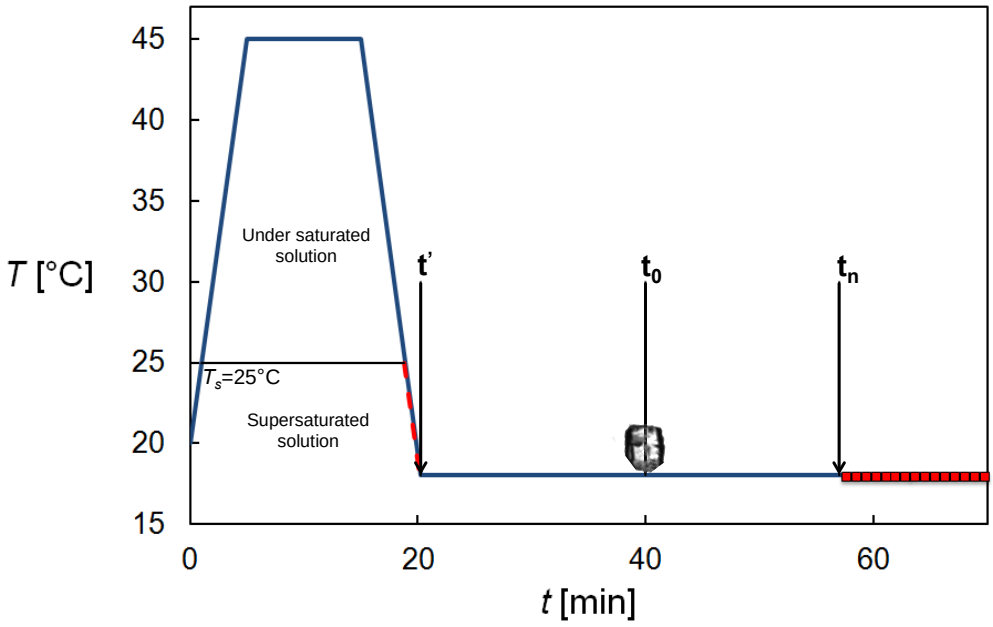

Figure 1: Definition of times during the seeding procedure for a single crystal of INA at T=18.0°C in a supersaturated solution of ethanol at S=1.10. First, undersaturated conditions were created in order to dissolve the crystalline material at higher temperature than saturation (T_s=25.0°C). Then, the supersaturation ratio S=1.10 was generated and isothermal conditions were reached by cooling to T=18.0°C. Time t' represents the time that isothermal conditions start; time t_0 is the moment that the single crystal is added; time t_n is the time for spontaneous primary nucleation (indicated by the red squares).

4.2.6. Seeds characterization

A large amount of single crystals of INA in ethanol and APAP in isoamyl alcohol were formed by cooling crystallisation and by subsequent solvent evaporation. Well-defined single crystals with a

plate-like shape were obtained for both APIs. Each single crystal was isolated and quickly washed with a solution of pure cold ethanol for INA and pure cold isoamyl alcohol for APAP to remove any residues of materials and to avoid possible initial breading mechanism during the seeding procedure. Microscope images were used for seed size characterisation. All the crystals were sized circumscribing a circumference and calculating the projected area in mm^2.

4.2.7. Calibration of the analysed volume in the Crystalline window

In order to estimate the analysed unit per volume observed within the Crystalline window, a calibration of the particles in focus was conducted using different concentrations of polystyrene spheres. The used spheres had a density of d=1.05 g/cm^3 which results in a volume for single spheres of V= $1.25x10^{-7}$ mL.

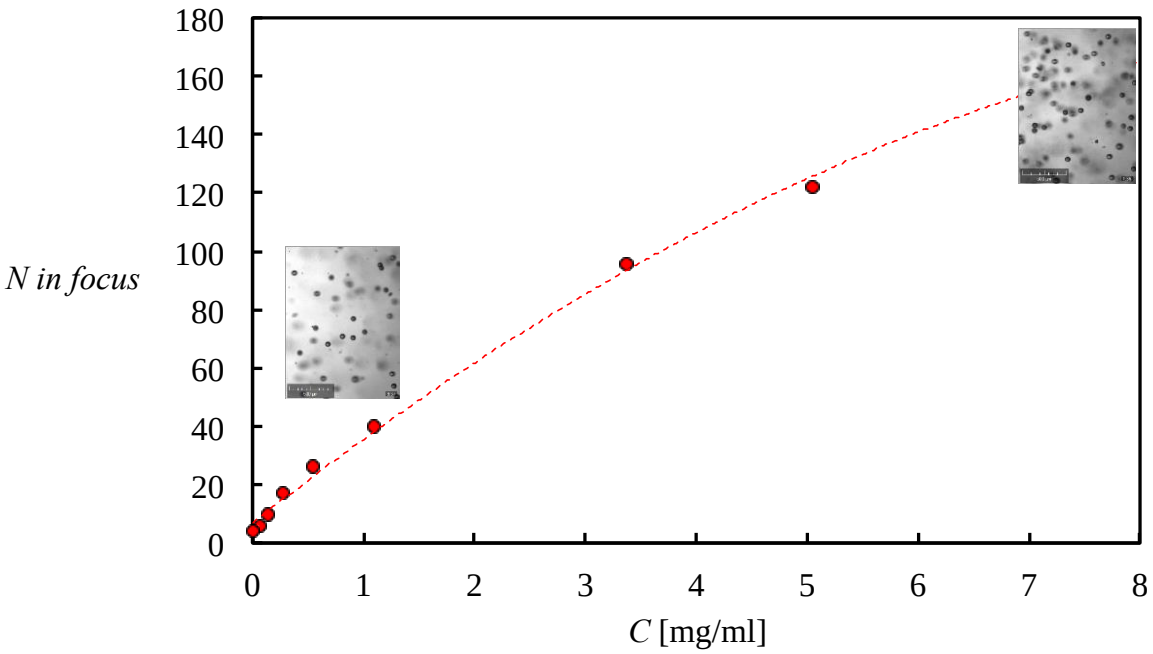

Figure 2: Calibration of the Crystalline window using polystyrene microspheres. Different concentrations of spheres were used to calculate how many particles are detected in focus through the Crystalline camera.

This determined particle count increase rate gives the increase in particles in a certain arbitrary volume of unknown size. If assumed that only the single crystal is responsible for the secondary crystals observed we can determine a value for the secondary nucleation rate due to the presence of

this crystal counting the number of particles in focus. If we consider only the initial linear part of the graph presented in figure 2, it is possible to work out how many nanospheres are present in the analysed sample. Then, considering for each selected concentration the number of particles in focus, the analysed volume in the Crystalline window can be calculated. In principle, this procedure allows to calculate the nucleation rate *B* (number of particles/time) in a know volume resulting in a real nucleation rate and not just a relative secondary nucleation rate.

4.3. Results

First, secondary nucleation measurement conditions are established by measuring the metastable zone of the model compounds in the selected solvents and the induction time probability distribution for spontaneous nucleation. Then, the secondary nucleation after seeding a single crystal of each API in supersaturated solutions is studied using different seed sizes and diverse solution environments.

4.3.1. Metastable Zone Width

Nucleation occurs within the metastable zone, which is the working window where supersaturation drives and balances the formation of new nuclei and the growth of existing crystalline entities [21]. During nucleation studies supersaturation needs to be monitored because excessive supersaturation will result in extreme nucleation. A too low supersaturation will slow the growth and nucleation rates, thus creating the need for longer residence times, adding to the capital costs of the equipment[15]. Therefore, a good knowledge of the supersaturation range is essential for an optimum performance of a crystallizer. We want to measure secondary nucleation behaviour under well-defined conditions at which primary nucleation is, in comparison, negligible. In order to establish these conditions, the metastable zone (MSZ) is measured. The MSZ is here defined as the zone between the solubility line and the MSZ limit in which spontaneous nucleation is negligible while

growth and secondary nucleation can occur if seed crystals are present. The MSZ usually is measured through obtaining clear and cloud point temperatures. The cloud points are influenced by cooling rate and measurement volume [20] . When a faster cooling rate is used to determine the cloud points, the system has less time to respond to the variation of supersaturation ratios and it results as a smaller metastable zone. In a larger volume, the presence of heterogeneous particles plays a fundamental role for the width of the metastable zone. It is very frequent that heterogeneous particles induce faster nucleation reducing the MSZW.

Figure 3 shows the measured average clear and cloud points and the resulting MSZ for INA in ethanol and for APAP in isoamyl alcohol. Three clear and cloud point temperature measurements were performed for each sample, showing a variation of less than 1.0°C per sample. Therefore, the error bars are smaller than the measurements.

The obtained solubility results show a good agreement with literature data at the investigated conditions [20].

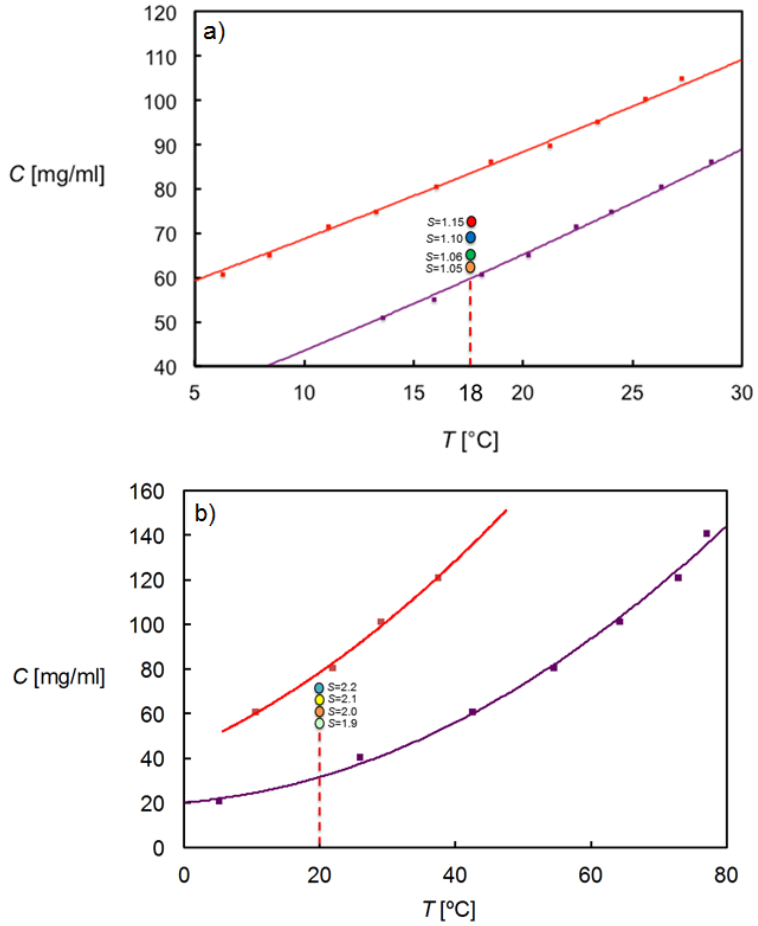

Figure 3: The Metastable Zone Width of INA in ethanol (a) and APAP in isoamyl alcohol (b) at different concentrations *C*. The purple curve is the solubility line constructed from clear point temperatures (purple squares), while the red curve shows the metastable zone limit constructed from cloud point temperatures (red squares). The applied cooling rate was 0.3°C/min. a) Within the metastable zone, the area between solubility line and the MSZ limit line, four experimental concentrations at a temperature of T=18.0°C were been selected to perform secondary nucleation studies. The orange, green, blue and red dots indicate the seeding conditions at a supersaturation value of respectively S=1.05, S=1.06, S=1.10 and S=1.15. b) Four experimental concentrations at a temperature of T=20.0°C were been selected. The light green, the orange, the light yellow and the light blue show the conditions at supersaturation values of S=1.9, S=2.0, S=2.1 and S=2.2 respectively.

The width of the metastable zone has been measured using the difference of temperatures between clear and cloud points. For instance, in INA in ethanol experiments (figure 3a), for a concentration of 60.8 mg/ml a clear point of T=18.1°C and a cloud point of T=6.3°C were measured, resulting in a MSZW of 11.8°C. In the presented temperature range, the obtained average values of MSZW are measured to be around 10.0±1.1°C. The same procedure was followed to define the MSZW for APAP in isoamyl alcohol (figure 3b).

The solubility and metastable zone width allow the choice of conditions for the study of secondary nucleation by single crystal seeding of a supersaturated solution. First, a working temperature of

T=18.0°C and *T*=20.0°C conveniently close to room temperature were chosen for INA in ethanol and for APAP in isoamyl alcohol respectively. The solubility of INA at *T*=18.0°C is 60.5 mg/mL of ethanol, while the solubility of APAP at *T*=20.0°C is 33.9 mg/mL of isoamyl alcohol. At these temperatures the supersaturation conditions should be mild to minimize the possibility for spontaneous primary nucleation. Therefore, at *T*=18.0°C the supersaturation ratios *S*=1.06 and *S*=1.10, for INA in ethanol (figure 3a), were chosen. At *T*=20.0°C the supersaturation ratios *S*=1.90, S=2.00, S=2.10 and *S*=2.20, for APAP in isoamyl alcohol (figure 3b), were selected.

4.3.2. Induction Time Measurements

Still, under these supersaturated conditions eventually primary nucleation will occur. It is therefore important to know the level of primary nucleation at these conditions. This was measured by determining the experimental induction time probability distribution in unseeded clear solutions at the chosen conditions[22]. Figure 4 shows the obtained induction time probability distribution. In all 40 experiments no crystals were detected until 59 and 37 minutes for the supersaturations of *S*=1.06 and *S*=1.10, respectively. After this time is increasingly more samples crystals appeared. After a time of 97 and 79 minutes, crystals were detected in all experiments crystals for both supersaturation ratios *S*=1.06 and *S*=1.10, respectively.

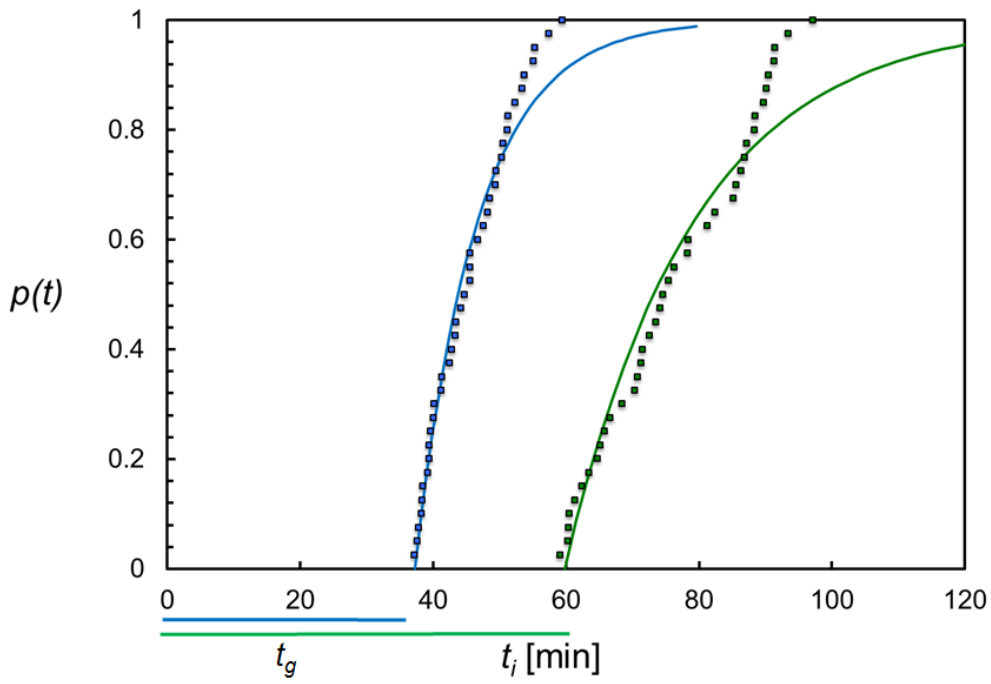

Figure 4: Experimental induction time probability distributions for 40 unseeded experiments of INA in ethanol at a supersaturation of *S*=1.06 (green squares) and *S*=1.10 (blue squares) at a temperature of *T*=18.0°C. The lines represent the fits of the probability function[20] with the experimental data series. The horizontal lines below the time axis represent the time period during which in all samples no nucleation was detected. The induction times for S=1.05 and S=1.15 are not presented in this figure because the probability distribution is based only on 12 samples.

The same analysis was conducted with induction time experiments for APAP in isoamyl alcohol at different supersaturated conditions. Figure 5 shows the obtained results. At the lowest supersaturation investigated *S*=1.9, the first sample nucleates only 286 minutes after reaching the desired experimental conditions. The induction times for APAP in isoamyl alcohol indicate a long time of waiting before nucleation can be detected.

These results show that at the chosen conditions an extended interval of time exists during which unwanted primary nucleation is avoided. The points in figure 3a and 3b were therefore determined to be optimal conditions for studying the secondary nucleation rate.

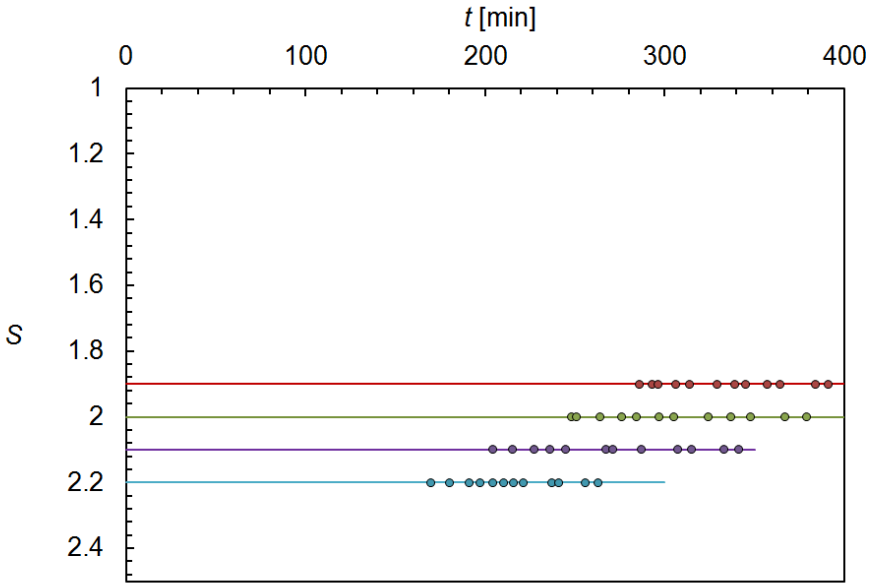

Figure 5: Induction time measurements of APAP in isoamyl alcohol at four different supersaturations: S=1.9 (red), 2.0 (green), 2.1 (purple) and 2.2 (light blue). At each supersaturation 12 experiments were conducted.

4.3.3. Secondary nucleation rate Measurements

Figure 6 presents the particle count in a small part of the volume during two parallel experiments, a seeded (green symbols) and an unseeded one (red symbols), as a function of time t-t_0. Time t-t_0=0 is the point in time at which one of the experiments is seeded with a single crystal. The unit of count is the results of the calibration experiments run using the polystyrene microspheres presented in the method section.

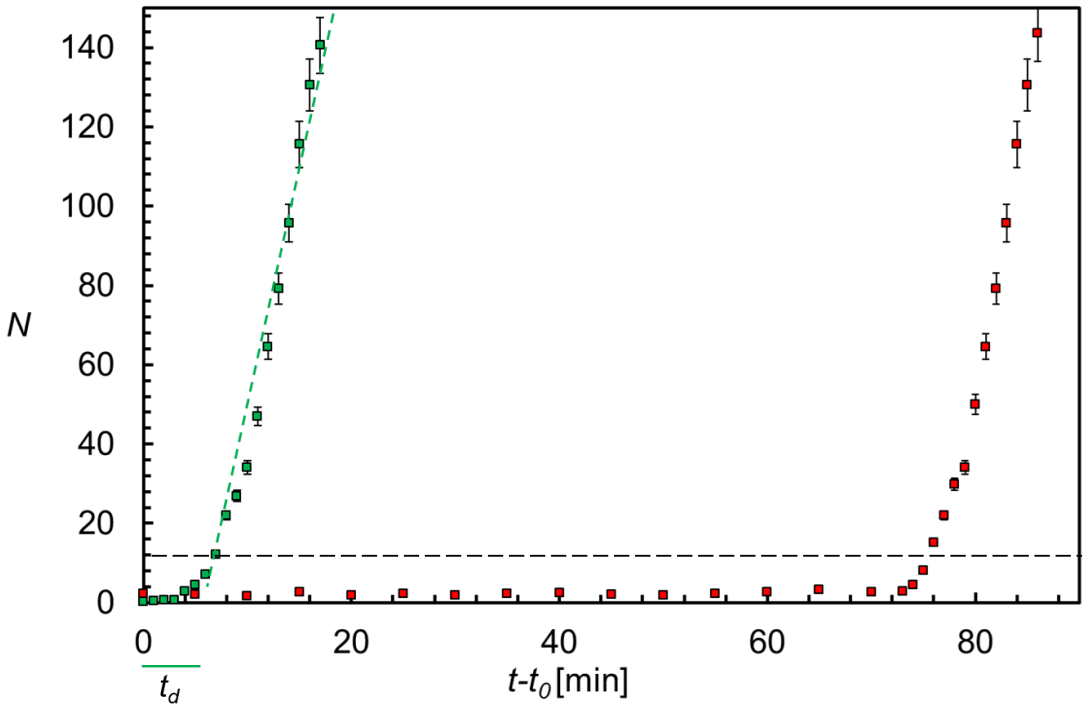

Figure 6: Particle count *N* during a seeded experiment (green squares) and an unseeded experiment (red squares) run in parallel for INA in ethanol at *S*=1.10 and *T*=18.0°C. For the seeded experiment, the solid line shows the delay time t_d, the green dashed line indicates the slope *m* before secondary nucleation occurs and the dashed black line shows the cut-off value for secondary nuclei count.

The seeded experiment shows an increased particle count 6 minutes after the experiment starts. In the unseeded experiment the particle count raises only after 75 minutes, which means that spontaneous nucleation occurs much later compared to secondary nucleation induced by the seeding procedure. Before this rise the measured particle count fluctuates around a value of 4 ± 2 particles/investigated volume. This is due to impurity particles such as dust particles present in the samples. In order to properly and consistently identify a particle count rise, it was assumed that a particle count larger than 10 paricles/investigated volume indicated the presence of crystals. The last count before this value of 10 particles presents the delay time in the experiment. The delay time is interpreted as the time needed for the parent crystal to undergo secondary nucleation. The delay time in the seeded experiment in figure 6 was determined to be 6 min. The seeded experiment shows a particle count rise up to around 140 particles/investigated volume after 18 minutes of experiment.

The number of particles is monitored using the Crystalline camera, which allows, as presented in figure 7, the count of crystals in focus during the time of the experiment. For counts of over 140 particles/investigated volume the suspension is too dense and the particles overlapped in the suspension images. It was therefore decided not to include particle counts of over 140 particles/investigated volume.

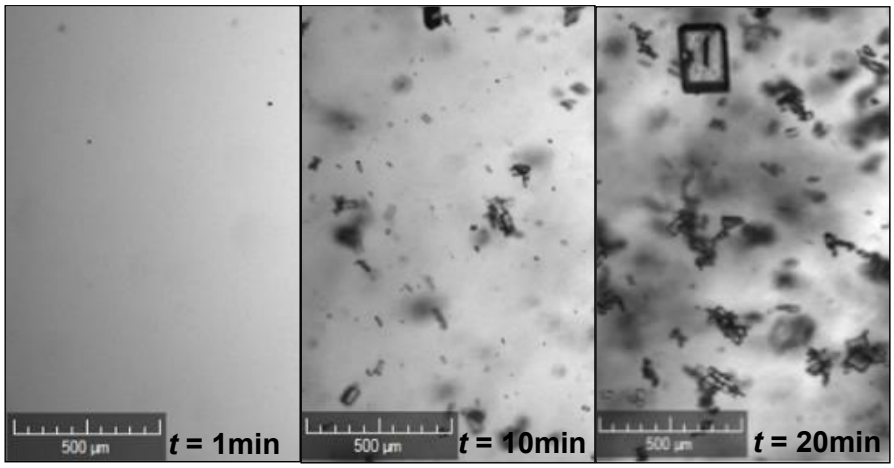

Figure 7: Sequence of images detected during a seeded experiment. A limitation of this method of detection is that individual crystals are not accurately recognized anymore at high suspension densities. Indeed, generally, the maximum count is 250 particles per image.

Between the established upper and lower limits of the particle count it was observed that the rise was roughly linear enabling the determination of a rate *m* of particle count increase. For the seeded experiment in figure 4 this rate was determined as 12.8 particles per minute particles/investigated volume.

Exactly the same procedure was conducted for single crystal seeding of APAP in isoamyl alcohol. Figure 8 shows the results for particle count during the run of the experiments for four different investigated supersaturations. The lower supersaturation S=1.9 indicated by the yellow symbols presents a slower increasing in particle count N resulting in a lower nucleation rate. When supersaturation increases, the number of particles raises up faster and secondary nucleation rate is higher.

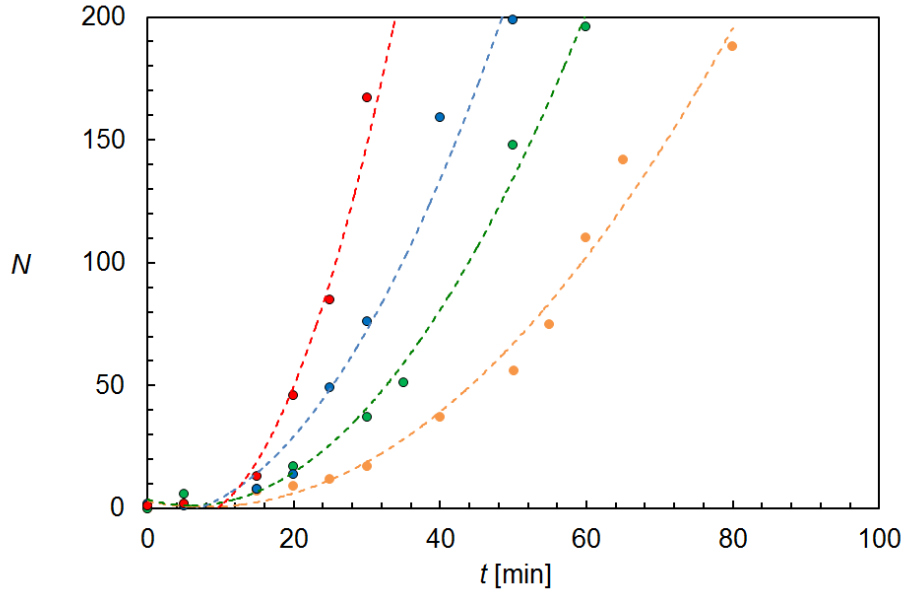

Figure 8: Single Crystal Seeding of APAP in isoamyl alcohol. Number of particles *N* is plot against the time *t* monitoring the increased number of particles due to secondary nuclei formation. Four supersaturation ratios were investigated: *S*=1.9 (yellow), *S*=2.0 (green), *S*=2.1 (blue) and *S*=2.2 (red).

The developed single seed crystal method allows us to establish a secondary nucleation rate under specific conditions of temperature and supersaturation and as a function of seed crystal properties such as seed size. Different seed sizes with a projected area between 9.0-1.3 mm^2 were used to determine secondary nucleation rates.

Figure 9 shows how the particle count for differently sized seeded crystals generated. We chose to use the projected area, which was between 9.0-1.3 mm^2, as a measure for the size of the seed crystals. Clearly, the seed crystal size influences the secondary nucleation rate. A larger seed crystal (e.g., blue squares in figure 7) produces a faster rise in the particle count leading to a higher secondary nucleation rate.

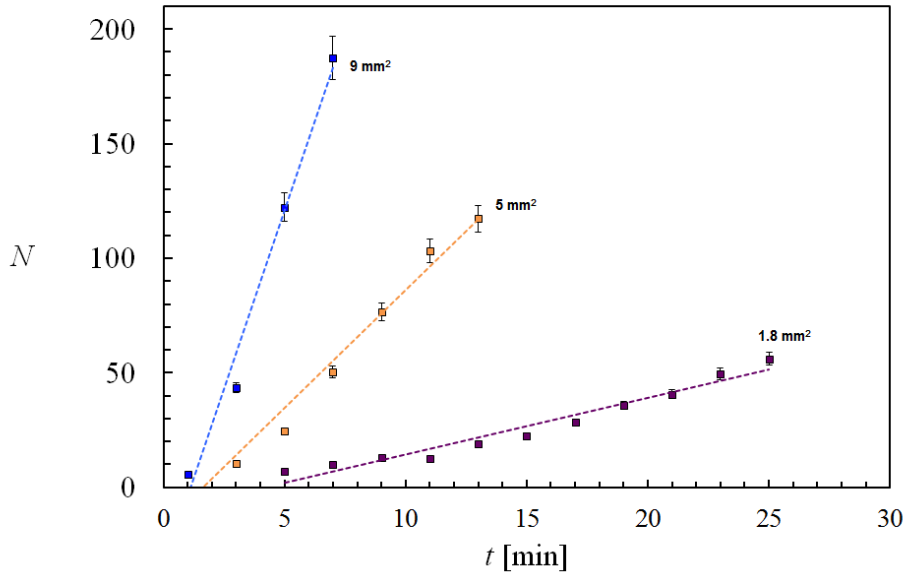

Figure 9: Particle count N against time t of single seed crystal experiments for INA in ethanol at a supersaturation S=1.10. Different colours of the symbols represent different single seed size, given in projected area: purple (1.8 mm^2), ornate (5 mm^2), blue (9 mm^2). There is a clear relation showing a larger slope for larger seed sizes.

The measured delay time depends on the parent crystal size. This delay time decreases if the seeded crystal is larger, as shown in figure 9. Once the single crystal is in contact with the supersaturated solution, it needs to grow to a certain size before secondary nuclei can form. Secondary nucleation rates for INA in ethanol using different seed sizes were determined at S=1.05, 1.06, 1.10 and 1.15 and all the obtained results are presented in figure 10. The obtained secondary nucleation rates for S=1.05 and S=1.06 almost overlap because the considered conditions are too close. A large range of seed sizes were used for all four supersaturation ratios and the experiments show that the secondary nucleation rate is increased by both seed size and supersaturation.

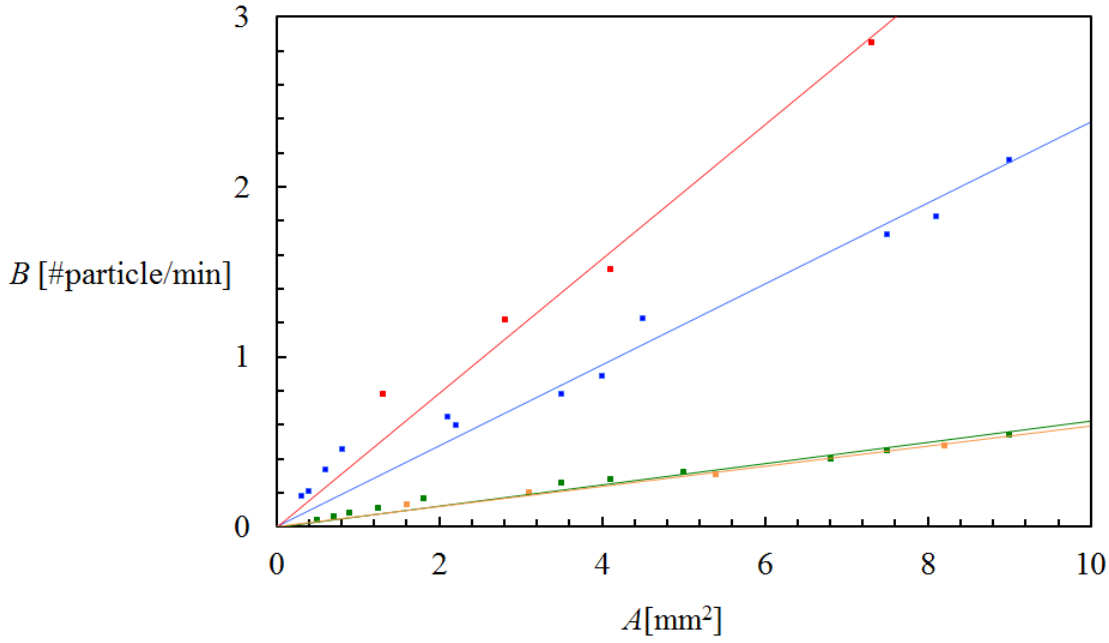

Figure 10: Secondary nucleation rate *B* [#particles/min] against seed size (*A*) for supersaturations *S*=1.05 (orange squares) *S*=1.06 (green squares), *S*=1.10 (blue squares) and *S*=1.15 (red squares) at temperature *T*=18°C. For each supersaturation 12 different seeds sizes were used.

According to the results presented in figure 10 for INA in ethanol, if the seeded crystals have similar size, the number of crystals produced after seeding reduces with decreasing of supersaturation. Considering a seeded crystal size between 3-6 mm^2, secondary nucleation rate *B* are compared for three repetitions under similar conditions. Figure 11 reports the obtained results. At *S*=1.05 (orange points), the number at the end of the experiment raises only 30 particles and this indicates that supersaturation is consumed and there is not any other driving force to generate new crystals. The depletion of supersaturation was confirmed looking at the mass balance, which is presented in table 2. The seed was weighted at the beginning of the experiment and the amount of material that can be crystallised was calculated knowing the initial concentration C_s and the level of supersaturation *S*. At the end of the experiment all the solid material was recovered through filtration and weighing the residual material remained in the vial.

Table 2: Mass balance for seeding experiments of INA in ethanol at a S= 1.05 using different seeds mass (m_s). The table reports: the mass of crystals that can be formed at the used level of supersaturation (m_c), the theoretical total mass that is the results of m_s+ m_c and the real total mass weight at the end of the experiment (m_t). Only three example of experiments are reported just to give the idea of how the measurements were conducted.

m_s [mg]	m_c [mg]	m_s + m_c [mg]	m_t [mg]
0.7	9.3	10.0	10.4
0.9	9.3	10.2	10.6
1.2	9.3	10.5	10.9

The m_t results in all experiments, also in those are not presented in the table, higher than the theoretical mass (ms+mt) and this is due to the filtration procedure, where probabily the cake remains wet and increases the final weight.

Therefore, the mass balance confirmes that the supersaturation is depleted and it is not possible to form other secondary nuclei through attrition or fluid shear.

In figure 11, projecting the line through the analysed supersaturated conditions, *S*=1.03 represents the secondary nucleation threshold where the seeded crystal will just grow slightly without undergoing secondary nucleation.

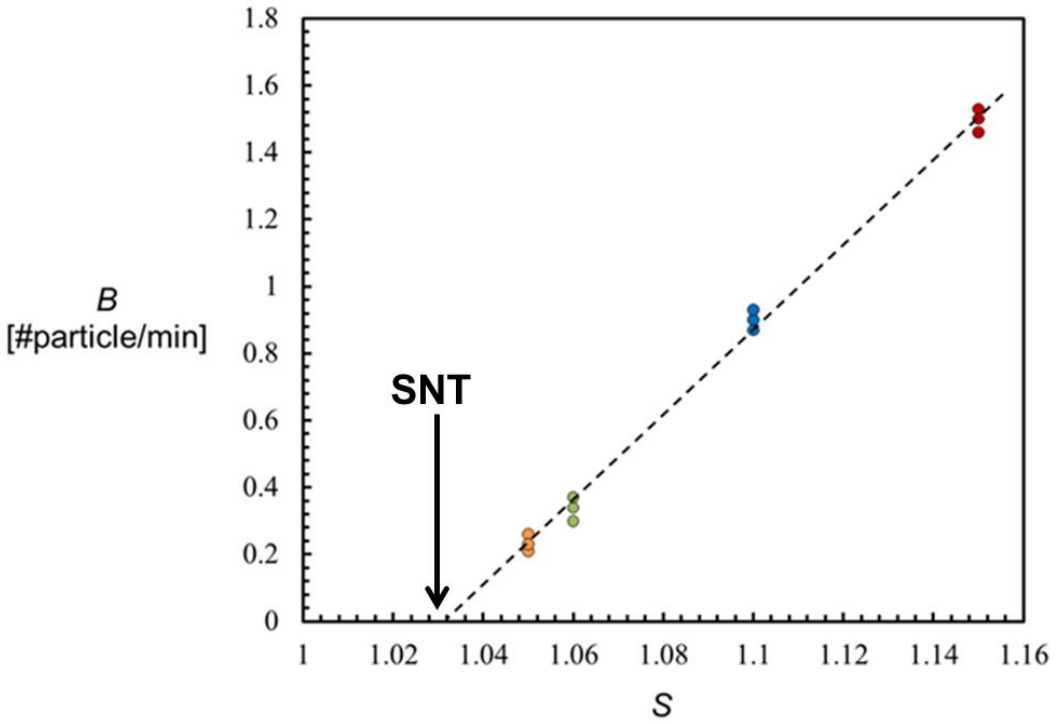

Figure 11: Secondary Nucleation Threshold (SNT) of INA in ethanol seeding single crystals in a range of size between 3-6 mm^2. Secondary nucleation rate *B* was measured at four supersaturated conditions: *S*=1.05 (orange dots), *S*=1.06 (green dots), *S*=1.10 (blue dots) and *S*=1.15 (red dots). Three repetitions were conducted at each supersaturation. The arrow indicate the obtained value of SNT, which in this case is *S*=1.03.

The same procedure was applied to calculate the secondary nucleation threshold for APAP in isoamyl alcohol and the results are presented in figure 12. In this case the size of the used seeded crystal was between 4-5.5 mm^2. Only one repetition for each supersaturation was conducted. Each coloured square indicates the obtained nucleation rate B at a specific value of supersaturation: *S*=1.9 (light green), *S*=2.0 (orange), S=2.1 (yellow) and S=2.2 (light blue). The determined SNT results as S=1.68.

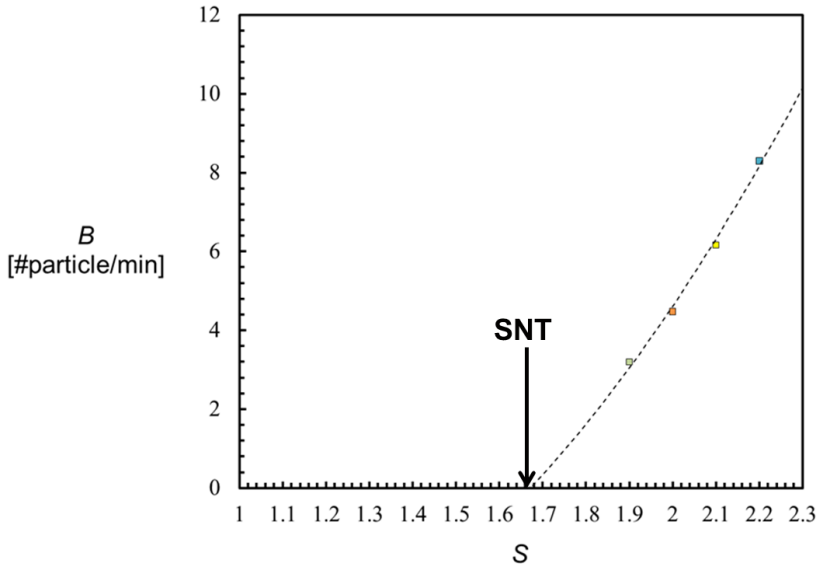

Figure 12: Secondary Nucleation Threshold (SNT) of APAP in isoamyl alcohol seeding single crystals in a range of size between 4-5.5 mm^2. Secondary nucleation rate B was measured at four supersaturated conditions: S=1.9 (light green dot), S=2.0 (orange square), S=2.1 (yellow square) and S=2.2 (light blue square). Three repetitions were conducted at each supersaturation. The arrow indicate the obtained value of SNT, which in this case is S=1.03.

4.4. Discussion

The reproducibility of the presented results, especially when different solution conditions are applied, indicates the reliability of this novel method applicable for different compounds in different experimental environment. However, as for all nucleation detection techniques, there are limitations for detection of new crystals born[23,24] also in this methodology. In Crystalline device,

the early born crystals are easily recognized since the lower detection limit is 3μm. When secondary nucleation occurs, the number of particles faster increases. When it reaches a value larger than 200 particles, the secondary nucleation rate detection needs to be stopped because the Crystalline camera is not able to discriminate between crystals on focus and background. Furthermore, agglomeration of crystals can cause problems for the counting procedure affecting the secondary nucleation rate determination.

This method represents a suitable technique for simultaneous studies of primary and secondary nucleation events. Apparently, the two subsequent events can be considered different, but it is interesting to note the similarity in the particle count increase in figure 6. The similarity of seeded and unseeded experiments might be an indication that the underlying mechanisms in these crystallizing solutions are the same. This seems to show then that in the unseeded experiment the single nucleus mechanism[19] is active. Once the primary nucleated single crystal is sufficiently large, it induces secondary nucleation, generating a similar raise in particle count as in the case of the secondary nucleation in the single seed experiment.

The developed method enables a systematic study of secondary nucleation kinetics and the validation of new secondary nucleation theories. A systematic study for secondary nucleation improves the control on this crucial step of crystallization. This novel seeding procedure can be incorporated in workflow procedures allowing rapid development of industrial crystallisation processes.

The series of steps that need be followed are presented in figure 13. The described workflow presents a logic way of thinking and gives guidance for a rational discrimination between primary and secondary nucleation events. The workflow consists of 6 steps and it starts from the basic knowledge of solubility and MSZW in order to define the crystallisation window for INA in ethanol. Once the MSZW is determined, the first decision needs to be made: the desired supersaturation ratios within the MSZW will be chosen and the induction time measurements will be calculated. The levels of supersaturation need to be quite close to the solubility curve in order to

facilitate the procedure for seeding and avoid unwanted primary nucleation. Spontaneous nucleation will be monitored through induction time measurements. In the meantime, the seeds are characterized and then added into the supersaturated solution providing a method for secondary nucleation rate determination. The procedure is repeatable at different supersaturation ratios, which allows the secondary nucleation threshold determination.

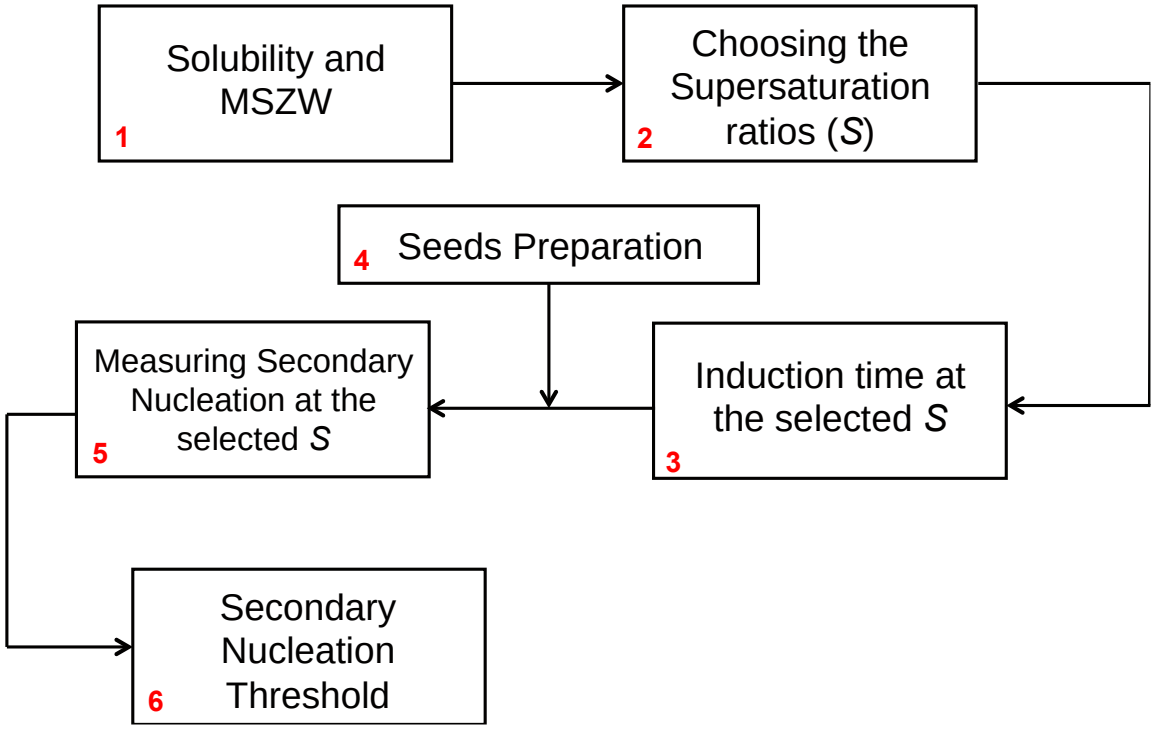

Figure 13: Workflow for secondary nucleation. The scheme describes the steps need to be followed in order to get systematic information on secondary nucleation rate aiming the determination of the secondary nucleation threshold. Step 1: The solubility and the MSZW are the starting points to indentify the conditions to crystallize the material at the selected concentration and temperature. Step 2: The supersaturation ratios for secondary nucleation studies are selected within the previous defined MSZW. Step 3: Induction time experiments at the selecred supersaturation ratios are required in order to understand the time frame for seeding experiments avoiding unwanted primary nucleation. Step 4: The crystals that will be used as seeds need to be well-characterized. Step 5: The conditions for the secondary nucleation experiments are established and now the seeded crystals can be added and secondary nucleation can be monitored at the selected conditions of supersaturation. Step 6: Analyzing the value of secondary nucleation rates obtained at different supersaturated conditions, the secondary nucleation threshold can be calculated finally understanding at which supersaturation ratio secondary nucleation is negligible.

4.5. Conclusions

A meticulous and reproducible seeding procedure for cooling crystallisation process has been developed. The used method permits a parallel discrimination of primary and secondary nucleation through well-controlled conditions within the MSZW. Once the single parent crystal is seeded in a supersaturated solution, the number of secondary nuclei starts increasing and it allows secondary nucleation identification and nucleation rate measurements.

The size of the seeded parent crystals plays a fundament role in secondary nucleation. A minimum crystal size is needed before secondary nuclei can be generated. For a small single crystal, it was observed that the time, elapsed between the seeding and the moment the number of secondary nuclei start increasing, is longer.

Furthermore, the seed crystal size affects the rate of increase of number of crystals. A bigger parent crystal produces more secondary nuclei during shorter time.

The developed method provides a framework for designing a crystallisation process for secondary nucleation rates determination through seeding well-characterized seed crystals.

4.6. References

1) Nyvlt, J., 1984. Nucleation and Growth Rate in Mass Crystallization. Prog. Crystal Growth and Charact. 9, 335-370.

2) Mullin, J. W. Crystallization, 4th ed.; Butterworth-Heinemann: London, 2001.

3) Myerson, A. S. Handbook of Industrial Crystallization, 2nd ed.; Butterworth-Heinemann: Woburn, MA, 2002

4) Frawley, P.J., Mitchell, N.A., O´Ciardha, C.T., Hutton, K.W., 2012. The effects of supersaturation, temperature, agitation and seed surface area on the secondary nucleation of paracetamol in ethanol solutions. Chemical Engineering Science. 75, 183–197.

5) Kobari, M., Kubota, N., Hirasawa, I., 2012. Secondary nucleation mediated effects of stirrer speed and growth rate on induction time for unseeded solution. Cryst.Eng.Comm. 14, 5255-5261.

6) Verdurand, E., Bebon, C., Colson, C, Klein, J.P, Blandin, A.F, Bossountrot, J.M., 2005. Secondary nucleation and growth of organic crystals in industrial crystallization Journal of Crystal Growth. 275, e1363–e1367.

7) Meadhra, R.O, Kramer, H.J.M, Van Rosmalen, G.M., 1996. Model for Secondary nucleation in a suspension crystalliser, AIChE, 42, 972-982.

8) Adi, H., Larson, I., Stewart, P., 2007. Use of milling and wet sieving to produce narrow particle size distributions of lactose monohyrate in the sub-sieve range. Powder Technol. 179, 95-99.

9) Jagadesh, D., Kubota, N., Yokota, M., Doki, N., 1999. Seeded effect on Batch Crystallisation of Potassium Sulfate under Natural Cooling mode and a simple Design Method of Crystallizer. J. Chem. Eng. Jpn. 32, 514-520.

10) Kalbasenka, A.N., Spierings, L.C.P., Huesman, A.E.M., Kramer, H.J.M., 2007. Application

of seeding as a process actuator in a model predictive control framework for fed-batch crystallisation of ammonium sulphate. Part. Part. Syst. Charact. 24, 40-48.

11) Kubota, N., Doki, N., Yokota, M., Sato, A., 2001. Seeding policy in batch cooling crystallisation. Powder Technol. 121, 31-38.

12) Ludwick, J.C., Henderso, P.L., 1968. Particle shape and inference of size from sieving. Sedimentology 11, 197-235.

13) Lung-Somarriba, B.L.M., Moscosa-Santillan, M., Porte, C., Delacroix, A., 2004. Effect of seeded surface area on crystal size distribution in glycine batch cooling crystallisation: a seeding methodology. J Cryst. Growth 270, 624-632.

14) Beckmann, W., Nickisch, K., Budde U., 1988. Development of a Seeding Technique for the Crystallization of the Metastable A Modification of Abecarnil. Organic Process Research & Development 2, 298−304.

15) Agrawal, S.G., Paterson, A.H.J., 2015. Secondary Nucleation: Mechanisms and Models, Chemical Engineering Communications 202, 698-706.

16) Chianese, A., Sangl, R.G., Mersmann, A.B., 1996. On the size distribution of fragments generated by crystal collisions. Chemical Engineering Communication 1, 146.

17) Gahn, C., Mersmann, A., 1999. Brittle fracture in crystallization processes. Part A. Attrition and abrasion of brittle solids. Chemical Engineering Science 54, 1273-1282.

18) Garside, J., Rusli, I.T., Larson, M.A., 1979. Origin and size distribution of secondary nuclei, AIChE 25, 57.

19) Kadam, S.S., Kramer, H.J.M., ter Horst, J.H. 2011. Combination of a Single Primary Nucleation Event and Secondary Nucleation in Crystallization Processes. Cryst. Growth Des. 11, 1271–1277.

20) Kulkarni,S.A; Kadam,S.S; Meekes, H.; Stankiewicz, A.I.; ter Horst, J.H. 2013. Crystal Nucleation Kinetics from Induction Times and Metastable Zone Widths. Cryst. Growth Des. 13, 2435−244

21) Ulrich, J., and Strege, C. (2002). Some aspects of the importance of metastable zone width and nucleation in industrial crystallizers, J. Cryst. Growth, 237–239, 2130–2135.

22) Jiang, S., ter Horst, J.H. 2011. Crystal nucleation rates from probability distributions of induction times. Cryst. Growth Des. 2011, 11 (1), 256−261.

23) Kashchiev, D., van Rosmalen, G. M. 2003. Review: Nucleation in solutions revisited. Cryst. Res. Technol. 38, 555–574.

24) Groen, H., Roberts, K.J. 2004. An Examination of the Crystallization of Urea from Supersaturated Aqueous and Aqueous-Methanol Solutions as Monitored In-Process Using ATR FTIR Spectroscopy. Cryst. Growth Des. 4, 930–936.

Chapter 5

A general method for secondary nucleation rates under industrial conditions

5.1. Introduction

Nucleation is typically avoided or minimized in industrial crystallisation processes since it is difficult to control resulting in undesired varibility of the product size [1]. Solutions exibit a metastable zone that defines the supersaturation conditions at which a specific compound can grow without significant crystal nucleation[2]. Industrial crystallizers, which use continuous mixed-suspension, mixed-product removal (MSMPR) crystallisation need to operate at a supersaturation that maintains a balance between growth rate and nucleation rate. When the crystallisation is conducted in batch crystallizers, crystal nucleation is avoided and seeding is the preferred choice[3]. Supersaturation plays a fundamental role for crystallisation decisions: excessive supersaturation will result in extreme nucleation leading to the formation of fines. A low supersaturation will create conditions to circumvent crystal nucleation by seeding strategies but also will decrease crystal growth, thus creating the need for longer residence times, adding to the capital costs of the equipment, for instance[4]. The limit in terms of supersaturation that defines the good balance between nucleation and growth is defined as secondary nucleation threshold (SNT)[5]. At a supersaturation less than the secondary nucleation threshold, seeds will grow in absence of secondary nucleation. At greater supersaturations, seed crystals will induce secondary nucleation. The secondary nucleation threshold, sometimes also referred to as the seeded metastable limit[6]. Therefore, an accurate determination of the secondary nucleation threshold is essential for obtaining control over the product size from seeded batch crystallization as well as continuous MSMPR crystallization processes [7].

The aim of this work is to systematically study the SNT and the effect of crystallizer volume and seed loading. In the previous chapters of this thesis, a method to meticulously study primary and secondary nucleation events within the Metastable Zone Width (MSZW) has been developed leading to the determination of a detailed secondary nucleation workflow in crystallization process design. This secondary nucleation workflow (figure 1) consists of 6 steps starting from the basic

knowledge of solubility and MSZW.

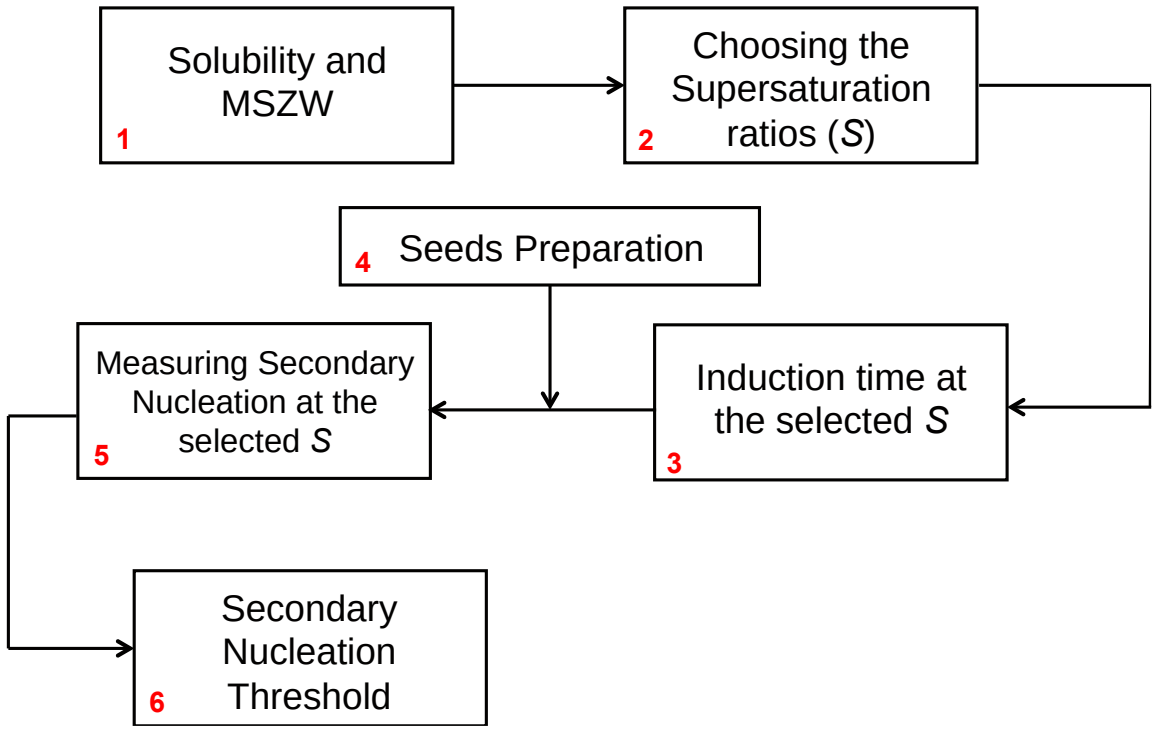

Figure 1: Workflow for secondary nucleation. The scheme describes the sequence of steps to measure secondary nucleation rate and determine secondary nucleation threshold.

Once the MSZW is known the supersaturation ratios for the secondary nucleation rate measurements within the MSZW are chosen. The levels of supersaturation need to be quite close to the solubility curve in order to prevent unwanted primary nucleation during the secondary nucleation rate measurements. Spontaneous nucleation will be monitored through induction time measurements. In the meantime, the seed material is selected and characterized. Subsequently, secondary nucleation rate measurements are done by adding the seed material into the supersaturated solution. The procedure is repeatable at different supersaturation ratios, which allows the secondary nucleation threshold determination.

5.2. Method

5.2.1. Solubility and Metastable Zone Width Determination

5.2.1.1. *V*= 3 ml (Crystalline)

Section 4.2.1. of Chapter 4 deeply describe the method for MSZW determination using Crystalline. The determined Metastable Zone Width (MSZW) is defined as the difference of temperatures for clear points and cloud points. This concept was largerly described in previous chapters. The clear point is detected when the suspension upon a constant heating rate turns into a solution and the transmission of the light reaches 100%. The temperature at which the clear solution turns into a suspension is considered as a cloud point and it is determined by the moment when the 100% transmission drops.

5.2.1.2. *V*=100 ml (EasyMax)

A known amount of INA was added to V=100 mL of ethanol generating different concentrations and measuring the saturation and the crystallisation temperatures. The 100 mL glass vessel of EasyMax (Mettler Toledo) was closed with the lid. EasyMax is a double reactor setup where two different experiments can be run in parallel. For the solubility and metastable zone width experiments, four concentrations were examined. The heating and cooling rates were set to 0.5°C/min from -10.0°C to 50.0°C. The samples were stirred with a controlled stirring speed of 200 rpm, using the impeller with the metallic helix incorporated in the EasyMax. The turbidity probe was added in one of the available holes of the lid and the rest of the holes were sealed with para-film to avoid solvent evaporation. The turbidy probe detectes the MSZW at each investigated concentration, determing the clear and cloud points, which represents the solubility and the crystallisation moment respectively. The clear point was obtained at the temperature when the suspension turns into a solution and the turbidity reaches 0%. The temperature at which the clear

solution turns into a suspension is considered as a cloud point and it is determined by the moment when the turbidity probe indicates 100%.

5.2.1.3. *V*= 700 ml (Optimax)

Exactly the same procedure was used to determine the solubility and the MSZW in a larger volume of V=700 ml. At this scale, the used crystalliser was the Optimax (Mettler Toledo), which presents the same properties of EasyMax in terms of temperature control and possibility of using probes that fit in the lid. Optimax differs from EasyMax because of the volume of the vessel (1L) and for the number of the vessel (only one). At this crystalliser scale, the samples were stirred again using a stirring speed of 200 rpm and using the incorporated impeller with the metallic helix at the end, as it was done for the EasyMax experiments. However the stirrer layout in the Optimax is bigger and it remains suspended in the vessel at an higher height compared to the EasyMax. The same principles were applied to determine the clear and cloud points using the turbidity probe.

5.2.2. Induction Time Measurements

The samples for the induction time experiments were prepared using the same method of the MSZW identification. The moment the solution reached the desired temperature T_i, was taken as time zero for the induction time measurements. At some point in time, the transmission decreased due to the presence of crystals. The difference between the time at which the transmission started to decrease and time zero was taken as the induction time. Fouling and crowning were never observed for INA in ethanol.

At 100 ml scale, four samples were tested for each supersaturation value of S=1.10, 1.15, 1.20 and 1.25. The induction time detection was determined using turbidity and FBRM probes. The FBRM is a probe that can be inseted directly into the process stream allowing the flow of particles across the probe window where the measurement takes place. A laser beam is launched down the probe tube

through a set of optics and focused to a tight beam spot at the sapphire window. The optics rotate at a fixed speed (typically 2m/s) resulting in the beam spot rapidly scanning across particles as they flow past the window. As the focused beam scans across the particle system, individual particles will backscatter the laser light to the detector. These distinct pulses of backscattered light are detected, counted, and the duration of each pulse is multiplied by the scan speed to calculate the distance across each particle. This distance is defined as the chord length, a fundamental measurement of the particle related to the particle size. When the crystals start appearing, the turbidity increases the displayed value from 0% to 100% and almost simultaneously the FBRM starts raising the total particle count indicating the occurred crystallisation. At 700 ml volume scale, the supersaturation values were slightly different: S=1.05, 1.10, 1.15 and 1.20.

5.2.3. Seeding Experiments

All the stock solutions were prepared ensuring the dissolution at 20°C above the saturation temperatures (T_s) for two hours on a hot stirrer plate at 500 rpm. The suspension was completely dissolved and stabilized. The stock solution was quickly filtered and transferred into a pre-warmed bottle, ensuring the absence of heterogenous particles and avoiding any possible nucleation. The filter was placed into a ceramic funnel and the flask was connected to the vacuum pump.

At larger volume (V= 100 ml and V=700 ml) only one stock solution at the lowest used supersaturation was prepared in order to avoid the excessive use of material. For the experiment at higher supersaturation, the constant temperatures were adjusted in order to ensure the desired conditions.

For each experiment, the scheme presented in figure 1 and largely described in section 4.2.4 and 4.2.5 was applied. One important difference in terms of crystal detection must be counted. The secondary nuclei in Crystalline (V= 3 ml) are counted through the camera and using the transmissivity method. In larger scales with EasyMax and Optimax (V=100 ml and 700 ml) the

particles are detected using the FBRM probe. It records the chord lenght distribution and it allows the total particle count in the vessel.

The solutions were heated up again 20°C above the saturation temperatures for each selected concentration. These temperatures were kept constant for 20 minutes in order to ensure a complete dissolution of any particles of solute that could form during sample preparation. At the highest temperature, the chord lengh distribution of the FBRM reached a value very closed to 0 indicating a clear solution. The solution at this stage was under-saturated, therefore a cooling profile of r=5°C/min was applied generating the desired supersaturation ratio. Once the solutions reach the desired temperature, the experiments start ($t^{'}$) and the amount of selected seeds can be added. At V=100 ml, the EasyMax layout allows the two parallel runs of one seeded and one unseeded experiment. In Optimax V=700 ml, the unseeded experiments were conducted separately. Initally, single crystal seeding experiments were conducted at V=100 ml and V=700 ml in order to compleate the applicability test of the developed workflow in larger cyrstalliser volumes. The used single crystal were in a range of size between 1 mm^2<x<3 mm^2.

5.3. Results

5.3.1. Solubility and Metastable Zone Width

We want to measure secondary nucleation behaviour under well-defined conditions at which primary nucleation is negligible. In order to establish these conditions the metastable zone (MSZ) is measured. The MSZ is here defined as the zone between the solubility line and the MSZ limit in which spontaneous nucleation is negligible while growth and secondary nucleation can occur if seed crystals are present. The solubility line is represented by the obtained clear points detected when the turbity is 0% and the suspension turns into a solution. The metastable limit is the combination of the cloud points obtained when the turbidity probe shows 100% and the solution

becomes a suspension. Figure 1 compare the obtained MSZW at the analysed volumes: *V*= 3ml, *V*=100 and 700 ml.

Each point indicates the measured average of clear and cloud points for different concentrations of INA in ethanol.

The measured MSZW depends on the volume used as is salso known from previous studies.[8] For instance, in a volume of *V*=100 ml a concentration of 60.8 mg/ml leads to a clear point temperature of *Ts*=18.3°C and a cloud point of *Tc*=1.1°C, resulting in a MSZW of 17.8°C. In a volume of *V*=700 ml at the same concentration of material, the MSZW is 13.4°C. In a volume of *V*= 3 ml, the MSZW is 11.8°C. Therefore, the MSZW calculated in 100 ml results larger than 3 ml and 700 ml.

The difference of volume and crystalliser types affect the nucleation of the same material at equal concentrations and cooling rates. The induced secondary nucleation using different crystalliser layouts is responsible for this variation and it depends on mechanism of attrition and fluid shear.

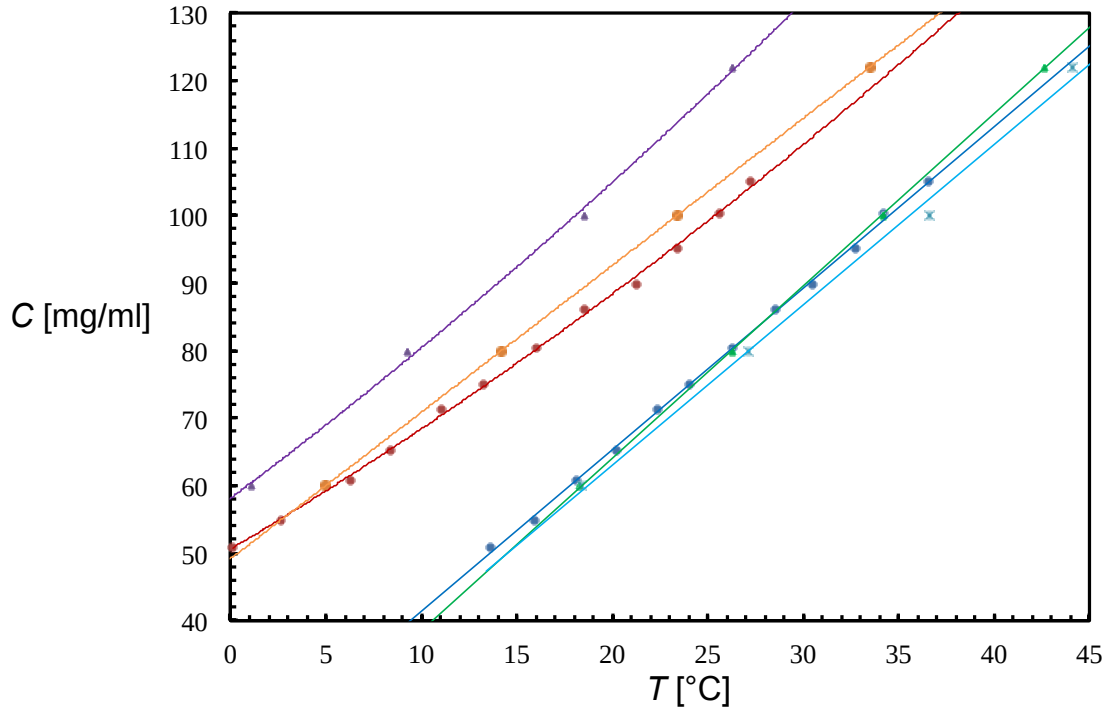

Figure 1: The Metastable Zone Widths of INA in ethanol at different concentrations *C* in different volumes. The blue and the red lines show the solubility and the metastable limit using a *V*= 3 ml. The green and the orange lines indicate the solubility and the metastable results using a *V*=700 ml. The light blue and the purple lines represent the results of solubity and metastable limit for a *V*=100 ml. The clear and cloud points in a *V*=3 ml are obtained using the transmissivity detection, while in a *V*=100 and 700 ml are obtained from the turbidity probe. The applied cooling rate was 0.5°C/min for all different volumes.

5.3.2. Choosing the Supersaturation ratios

Once the crystallisation windows are defined, it is possible to select the supersaturations to study both primary and secondary nucleation within the MSZW. Table 1 summarizes the selected supersaturation ratios for the different volumes.

Table 1: Selected supersaturation ratios for each volume of crystalliser.

Volume [ml]	**3**	**100**	**700**
Supersaturation *S*	1.06	1.10	1.05
	1.10	1.15	1.10
	1.15	1.20	1.15
	1.20	1.25	1.20

The selected supersaturation ratios are positioned within the metastable zone in figure 3, figure 4 and figure 5 for V= 3ml, V=100 ml and V=700 ml respectively.

One important difference that needs to be noticed is that for V=3 ml the concentration of INA in ethanol changed to reach the desired supersaturation. For V=100 ml and V=700 ml, Only one concentration was kept constant and then the temperature was adjusted to reach the desired supersaturation ratio. A constant concentration of C=80 mg/ml of INA in ethanol was used for the experiments in order to avoid any waste of material.

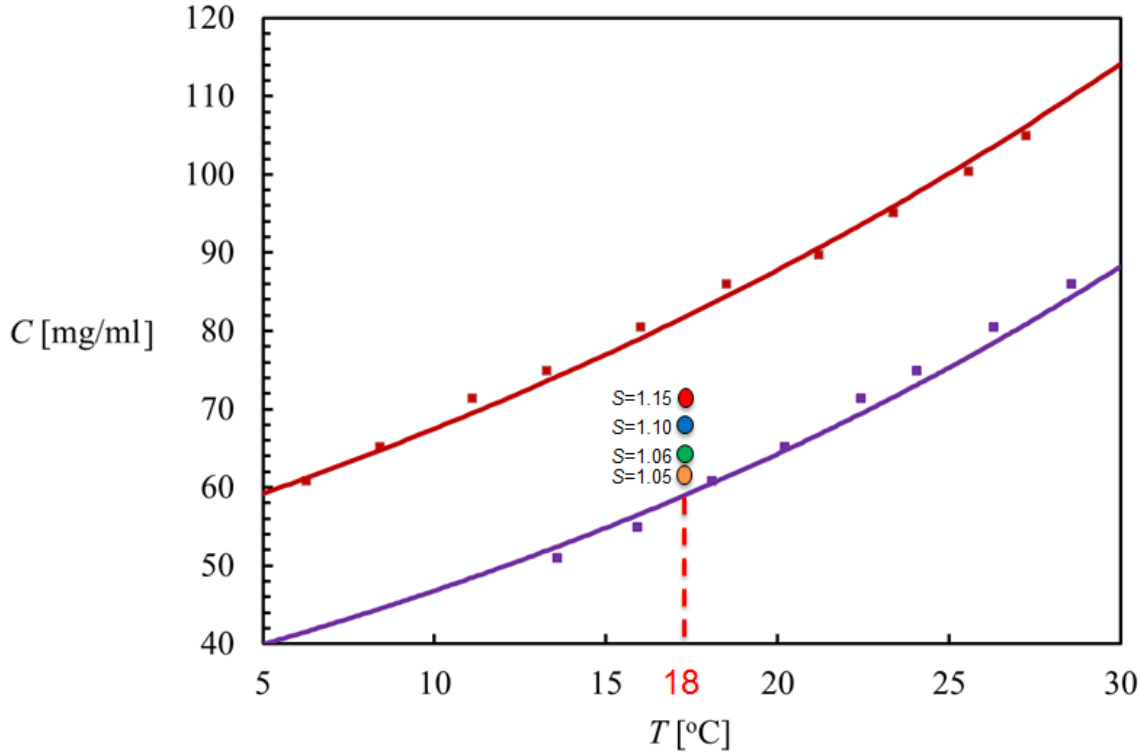

Figure 3: Within the metastable zone detected in a V= 3ml, the area between solubility line and the MSZ limit line, two experimental concentrations at a temperature of T=18.0°C were been selected to perform secondary nucleation studies. The orange, green, blue and red dots indicate the seeding conditions at a supersaturation value of respectively S=1.05, S=1.06, S=1.10 and S=1.15.

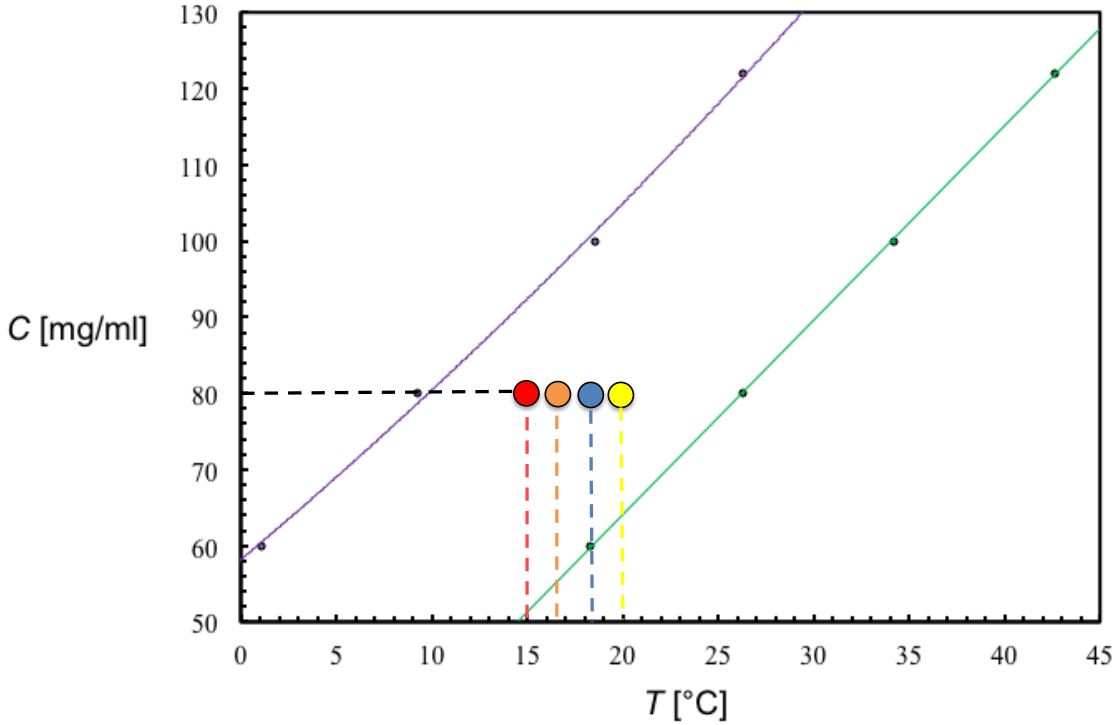

Figure 4: Selected Supersaturations within the MSZW in V=100 ml volume for a concentration of C=80 mg/ml. The red point indicates a S=1.25 when the crystallisation occurs at a temperature T_x=15°C; the orange point shows a S=1.20 with a temperature T_x=16.5°C; the blue point is at a S=1.15 with a T_x=18°C and the yellow point is at a S=1.10 with a T_x=20°C.

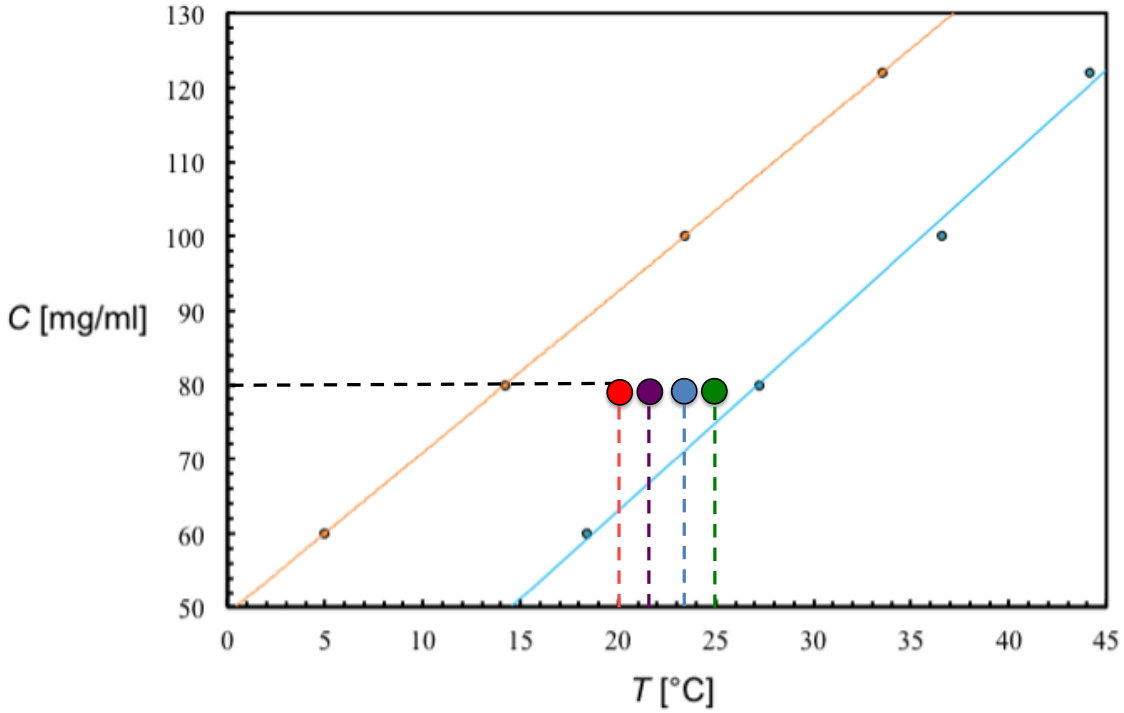

Figure 5: Selected Supersaturated conditions within the MSZW in V= 700 ml volume. Using a constant concentration of C=80 mg/ml, 4 supersatured ratios were selected. The red point indicates a S=1.20 when the crystallisation occurs at a temperature T_x=20°C; the purple point shows a S=1.15 with a temperature T_x=21.5°C; the blue point is at a S=1.10 with a T_x=22.5°C and the green point is at a S=1.05 with a T_x=25°C.

5.3.3. Induction Times at the selected Supersaturations

The level of primary nucleation at the selected supersaturated conditions showed in figure 6 and 7 was tested determining the experimental induction time in unseeded clear solutions. Figure 6 presents the induction time measurements for a V=100 ml and figure 7 shows the obtained results for a V=700 ml. The induction time experiments for a V=3 ml were discussed in section 4.3.2.

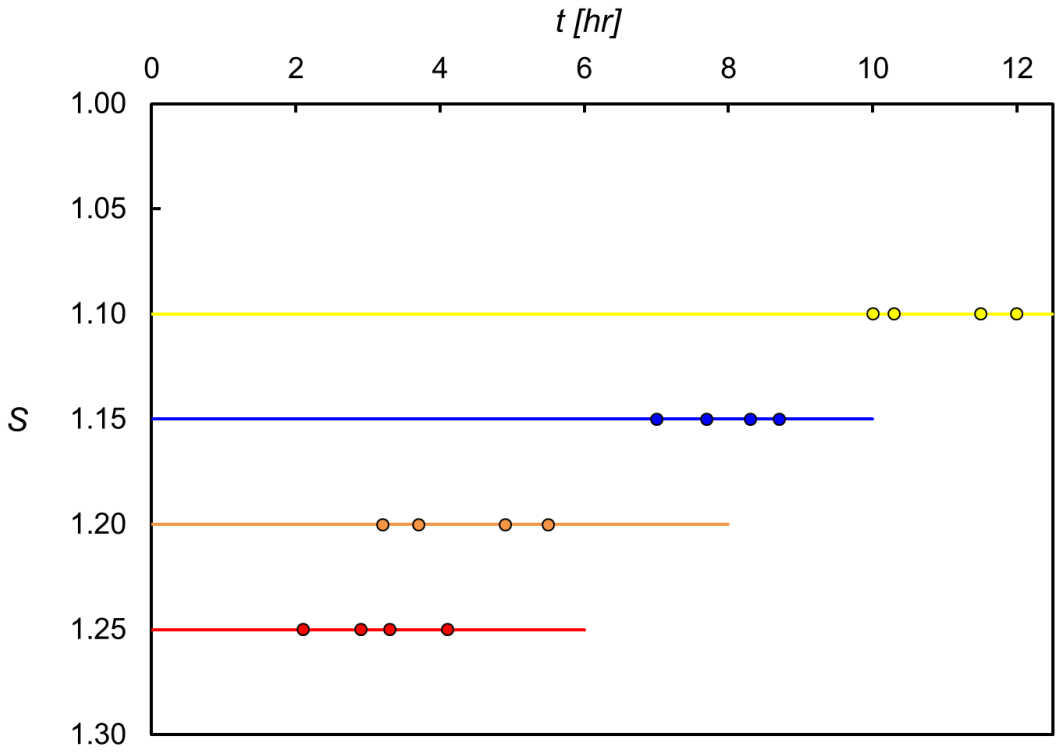

Figure 6: Induction time measurements at different supersaturation ratios for INA in ethanol using a volume of *V*=100 ml. Four measurements for each supersaturation were conducted and always the same solution was used. The yellow symbols show the resulta at *S*=1.10, the blue at *S*= 1.15, the orange at *S*=1.20 and the red at *S*=1.25. The horizontal lines indicate the time of the experiments.

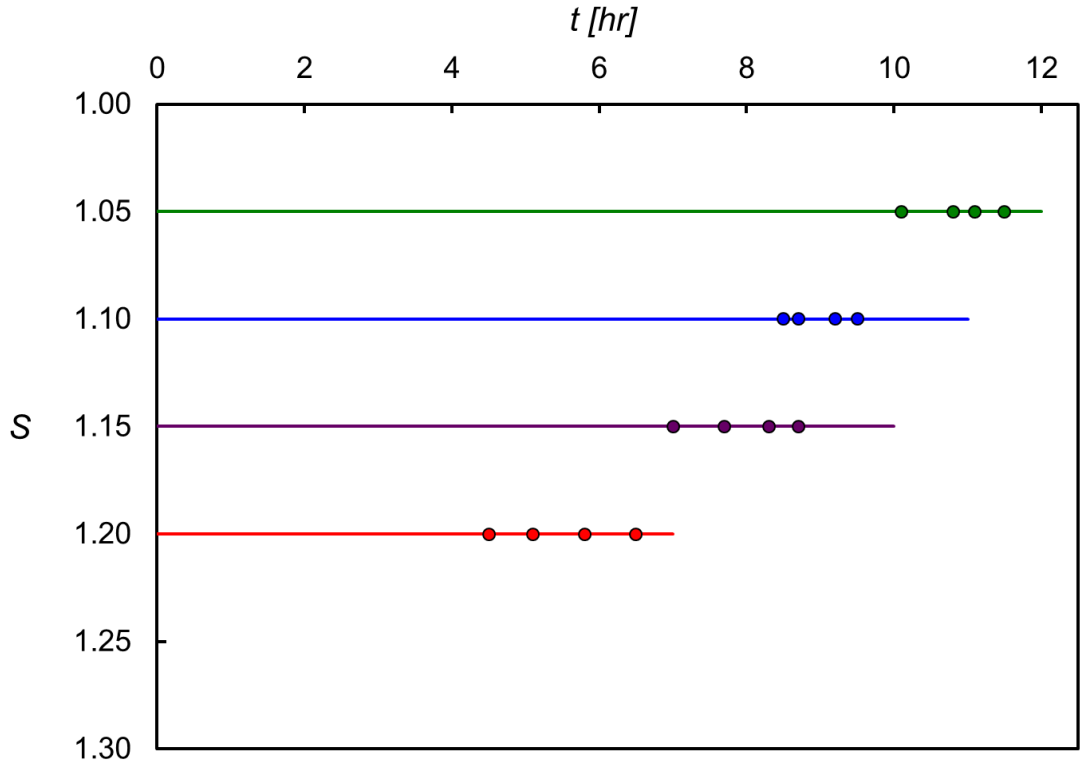

Figure 7: Induction time measurements at different supersaturation ratios for INA in ethanol using a volume of *V*=700 ml. Four measurements for each supersaturation were conducted and always the same solution was used. The green symbols show the resulta at *S*=1.05, the blue at *S*= 1.10, the purple at *S*=1.15 and the red at *S*=1.20. The horizontal lines indicate the time of the experiments.

In *V*=100 ml, at the highest supersaturation *S*=1.25, in all 4 experiments no crystals were detected until 2.1 hours. After this time in increasingly more samples crystals appeared. After 4.1 hours, crystals were detected in all experiments. Reducing the supersaturation, the induction time measurements become longer. In *V*=700 ml, the highest investigated supersaturation ratio was *S*=1.20. Under these conditions, crystals were detected only after 4.5 hours and all four experiments terminate after 6.5 hours. Comparing the obtained results in both volumes at *S*=1.20, the induction time measurements at *V*=700 ml are longer than those at *V*=100 ml. The selected supersaturation ratios can be used for the secondary nucleation rate experiments since there is sufficient time to control unwanted primary nucleation.

5.3.4. Seeds Characterisation

A large amount of crystals of INA in ethanol were formed by cooling crystallisation and by subsequent solvent evaporation as it was described in section 4.2.6. However this time, the wanted range of size for the seeded crystals needs to be smaller in order to increase the number of the seeded crystals . Therefore, seaves were used to fractionate the crystals using sieves with a size range of 125 μm <x< 250 μm and 250 μm <x< 500 μm. The decided crystal amount loading was calculated by weight and it was 0.5% and 1% of the w/w of the entire solution. After this procedure, they were quickly washed with a cold solution of ethanol in order to remove any residues of materials and to avoid possible initial breading mechanisms during the seeding procedure.

5.3.5. Secondary Nucleation Experiments

For the 3ml experiments the same procedure was used as in chapter 4 (Section 4.3.3). In larger volumes, the particles were analysed using the FBRM probe, which provides a total count of particles.

Figure 8 shows one example of particle count as a function of time in *V*=100 ml for a supersaturated solution *S*= 1.2, after seeding 1% w/w of a seed size range of 250 μm<x<500 μm. The represented

chord lenght indicates that the total count increases 25 minutes after the seeding moment, which is represented by t=0.

Before the rise the measured number of particles fluctuates and these values represent the seeded crystals, which are growing before secondary nucleation is triggered. In order to properly identify and consistently quantify the secondary nucleation rate, it was assumed that a total count larger than 1000 indicate the formation of new crystals. The cut-off value is indicated in figure 8 by the horizontal dashed line. The measurement of the total count stops when the chord length of FBRM probe reaches a plateau value, which in figure 8 is not presented to avoid any counting confusion. In this case, the total count reaches this plateau value above 25000 particles. Between the upper and lower limits of the total count, the chord lenght shows a linear behaviour enabling the determination of the secondary nucleation rate B. This method was applied for all the combinations of supersaturations, seed sizes and seeds loading. The obtained results are reported in table 2.

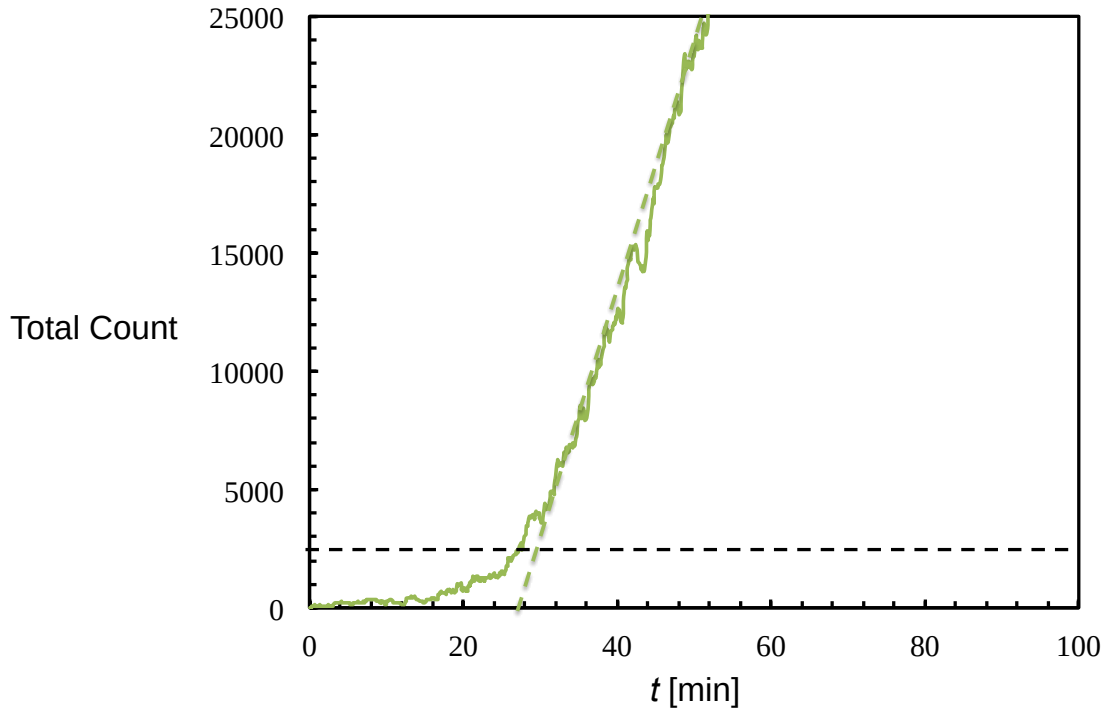

Figure 8: Total count during a seeded experiment for INA in ethanol at S=1.25 in V=100 ml. The seeds loading was 1% w/w and the range seeds size was 250 µm<x<500 µm. The green dashed line indicates the slope that represents the secondary nucleation rate B and the dashed black horizontal line represents the cut-off value for secondary nuclei count.

The measured secondary nucleation rates *B* increase with the crystal size and the amount of seeds added. For instance, at a *S*= 1.20 in *V*=100 ml, for the seed size range 125 µm<x<250 µm, the secondary nucleation rate *B* for 0.5% w/w seeds loading results as *B*=28 particles/minute. At the same conditions, but with a 1% seeds loading, *B*=42 particles/minute. Increasing the crystal size, *B* for 0.5% w/w is 51 particles/minute and for 1% w/w results as 72 particles/minutes.

Comparing the obtained results for *S*=1.2 in a larger volume *V*=700 ml, the secondary nucleation rate is even higher. The comparison is not possible for a smaller volume (*V*=3 ml) because in Crystalline the particle count is based on transmissivity and not on the chord lenght distribution.

Table 2 shows the obtained secondary nucleation rate B for the different seeds size, seeds loading and volumes.

***V* [ml]**	**Supersaturation *S***	**Secondary Nucleation Rate *B* [# particles/min]**			
		125µm<x<250µm		250µm<x<500µm	
		0.5 % w/w	1% w/w	0.5% w/w	1% w/w
3	1.06	11	19	24	39
	1.10	22	38	48	74
	1.15	43	54	80	136
	1.20	65	94	142	189
100	1.10	4	9	14	22
	1.15	16	26	37	58
	1.20	28	42	51	72
	1.25	34	56	66	91
700	1.05	8	14	21	30
	1.10	21	32	42	59
	1.15	36	50	61	81
	1.20	44	62	74	100

5.3.6. Secondary Nucleation Thresholds

According to the presented results in table 2, a large quantity of secondary nucleation rates were obtained under different conditions of supersaturation ratios, seeds size range and seeds loading at different volume of crystallisers. Using all obtained data, it is possible to determine the secondary nucleation thresholds (SNT) for each volume of analysed crystalliser. Figure 9, 10 and 11 present the obtained results for the all combination of multiple crystals seeded in a volume of 3 ml, 100 and 700 ml respectively.

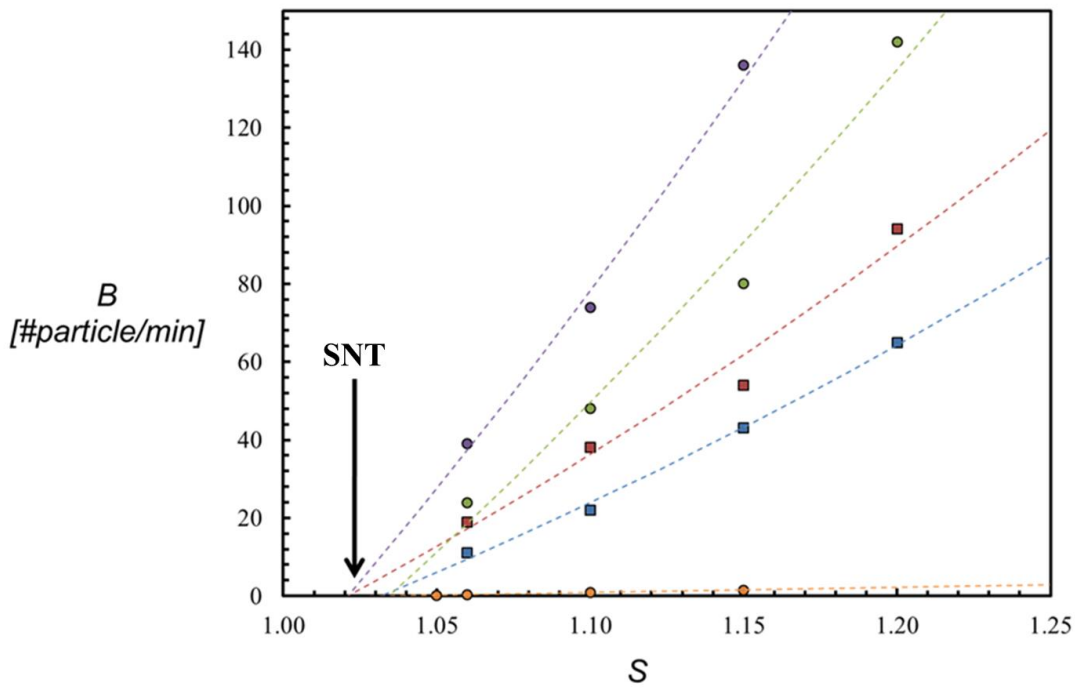

Figure 9: SNT for different seeds loading and seed sizes of INA in ethanol at different supersaturated solutions (*S*= 1.05, 1.06, 1.10 and 1.15) in *V*=3 ml. The multiple seeding experiments are compared with the single crystal experiments (orange symbols) conducted at the same supersaturated conditions. The circles represent the seeding experiments with a seed size range of 250 µm <x< 500 µm for 1% w/w seeds loading (purple) and 0.5% w/w (green). The square symbols indicate the seeding experiments with a seed size range of 125 µm <x< 250 µm for 1 % w/w seeds loading in the red squares and 0.5% w/w for the blue squares. The lines are guides for eyes and they terminate on the x-axis of supersaturation where the arrow indicates the calculated SNT.

Under the conditions the highest value of supersaturation at which secondary nucleation is negligible changes with the kind and amount of seeds used. For a *V*=3 ml the SNT is around *S*= 1.02, for *V*=100 ml it is around *S*=1.06 and for V=700 ml it is around *S*=1.03. The results suggested a relevant implication of volumes, stirred types and crystalliser layouts in the SNTs determination.

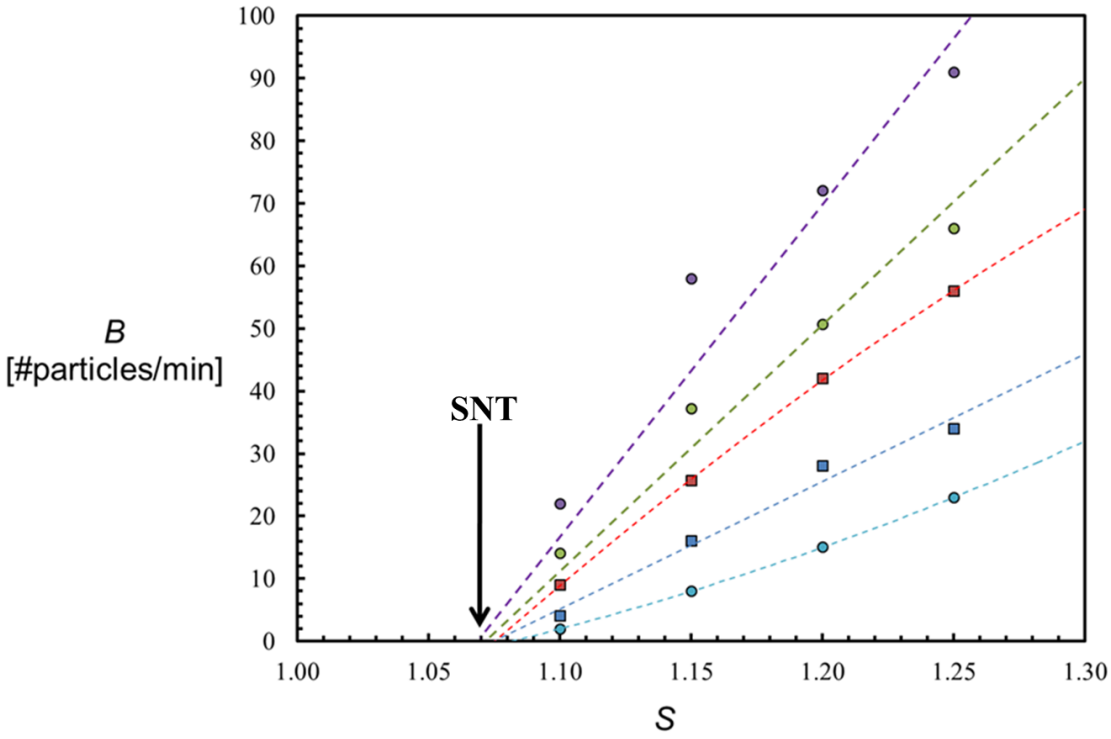

Figure 10: SNT for different seeds loading and seed sizes of INA in ethanol at different supersaturated solutions (*S*= 1.10, 1.15, 1.20 and 1.25) in *V*=100 ml. The multiple seeding experiments are compared with the single crystal experiments (light blue symbols) conducted at the same supersaturated conditions. The dot symbols represent the seeding experiments with a seed size range of 250 µm <x< 500 µm for 1% w/w seeds loading in the purple dots and 0.5% w/w for the green dots. The square symbols indicate the seeding experiments with a seed size range of 125 µm <x< 250 µm for 1 % w/w seeds loading in the red squares and 0.5% w/w for the blue squares.

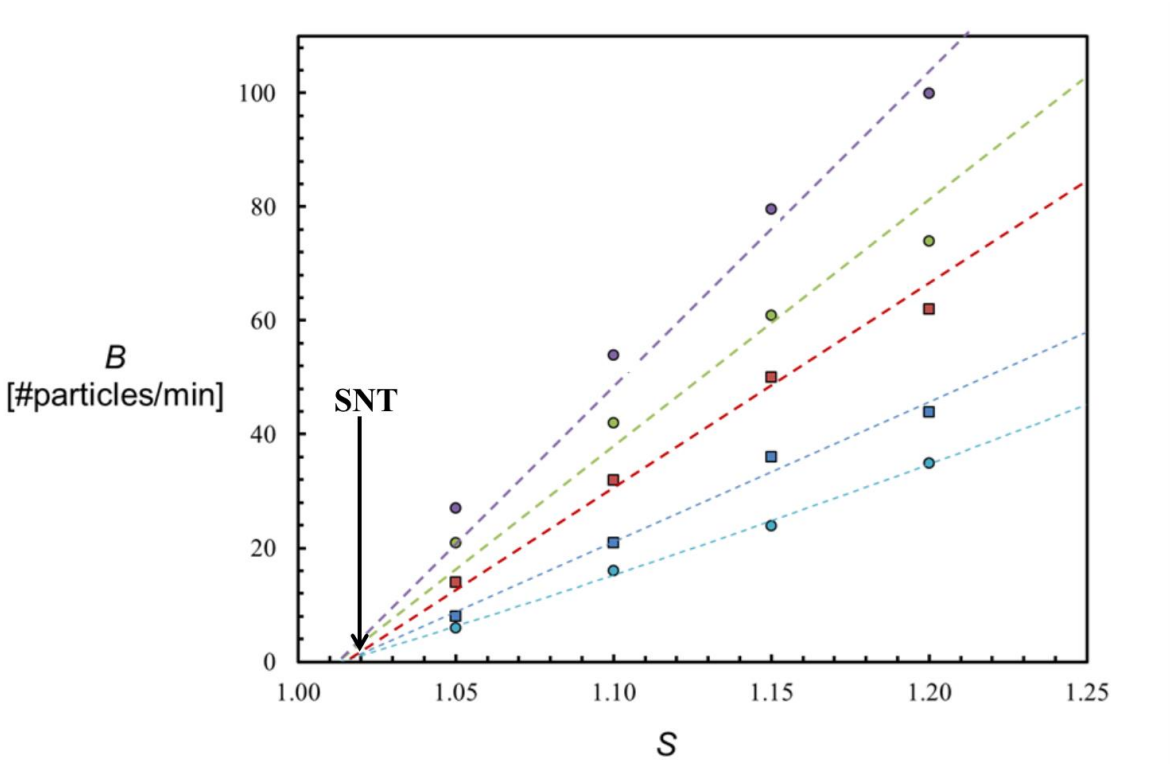

Figure 11: SNT for different seeds loading and seed sizes of INA in ethanol at different supersaturated solutions (*S*= 1.10, 1.15, 1.20 and 1.25) in V=700 ml. The multiple seeding experiments are compared with the single crystal experiments (light blue symbols) conducted at the same supersaturated conditions. The dot symbols represent the seeding experiments with a seed size range of 250 µm <x< 500 µm for 1% w/w seeds loading in the purple dots and 0.5% w/w for the green dots. The square symbols indicate the seeding experiments with a seed size range of 125 µm <x< 250 µm for 1 % w/w seeds loading in the red squares and 0.5% w/w for the blue squares.

5.4. Discussion

Secondary Nucleation Thresholds were identified applying the developed workflow for secondary nucleation assessment. Especially for industrial scale, it is important to rationalize and standardize procedures using workflows. The procedure reduces the variation of results determined by different used methods from various researchers. It is possible to screen a larger quantity of compound with this developed workflow comparing the results under similar conditions.

The systematic method addresses the determination of an important step of crystallisation at different scales. It was first developed for small laboratory lab scales and then tested to measure secondary nucleation rates and secondary nucleation threshold in larger scales. The applied workflow for different scales meet several drawbacks, which sometimes are difficult to rationalise.

For example, in general the MSZW is larger in a small volume due to the higher probability of heterogeneous nucleation[9]. However, in this work, the MSZW at V=700 ml vessel is smaller than the obtained results at V=100 ml. The detected difference is due to the crystallizer type of the 100 ml and 700 ml stirred vessels. First of all the different volumes affect the heat transfer during the cooling profile to reach a desired supersaturated condition within the MSZW. In 100 ml vessel the temperature shows less variations. The other difference between the two crystallisers is due to the probe positioning inside the vessel. In 700 ml there is more space to accommodate the probes and they perturb the agitated solution differently compared to the smaller volume. This causes faster attrition after the primary nucleation event occurs encouraging secondary nucleation and resulting in a smaller metastable zone width.

The systematic determination of secondary nucleation thresholds addresses an important challenge for industrial crystallisation. Using the developed approach, the control of nucleation through the seeding approach is guaranted. Knowing the SNT, there will not be riskes of dissolving seeds because the operating conditions are below the secondary nucleation threshold.

5.5. Conclusions

The systematic workflow for secondary nucleation assessment has been applied at different crystallizer volumes using various seed loadings to obtain relative secondary nucleation rates *B* and secondary nucleation thresholds. Each step was meticulously respected for all different scales indicating that next to volume and seed loading,crystalliser & stirrer type and probe position also affect secondary nucleation. With this research, it has been proven that the novel seeding procedure described in Chapter 4 can be incorporated in design procedures enabling rapid, accurate and reliable design for industrial crystallisation processes.

5.6. References

1) Srisa-nga, S., Flood, A.E., White, E.T., 2006.The secondary nucleation threshold and crystal growth of α-glucose monohydrate in acqueous solution. Crystal Growth and Design. 6, 795-801.
2) Mullin, J. W. Crystallization, 4th ed.; Butterworth-Heinemann: London, 2001.
3) Ulrich, J., and Strege, C. 2002. Some aspects of the importance of metastable zone width and nucleation in industrial crystallizers. J. Cryst. Growth, 237–239, 2130–2135.
4) Agrawal, S.G., Paterson, A.H.J., 2015. Secondary Nucleation: Mechanisms and Models, Chemical Engineering Communications 202, 698-706.
5) Coles, S.J., Threlfall, T.L. 2014. A perspective on a century of inert seeds in crystallisation. CrystEngComm.16, 4355-4364
6) Threlfall, T.L., Coles, S.J. 2016. A perspective on the growth-only zone, the secondary nucleation threshold and crystal size distribution in solution crystallisation. CrystEngComm. 18, 369-378.
7) Verdurand, E., Bebon, C., Colson, C, Klein, J.P, Blandin, A.F, Bossountrot, J.M., 2005. Secondary nucleation and growth of organic crystals in industrial crystallization, Journal of Crystal Growth. 275, e1363–e1367.
8) Kadam, S.S., Kramer, H.J.M., ter Horst, J.H. 2011. Combination of a Single Primary Nucleation Event and Secondary Nucleation in Crystallization Processes. Cryst. Growth Des. 11, 1271–1277.
9) Myerson, A.S. Handbook of Industrial Crystallization. Second ed., Butterworth-Heinemann: Woburn, 2002.

Chapter 6

Primary and Secondary Nucleation Kinetics of Chiral Crystals

6.1. Introduction

In a crystallization process, nucleation generates the crystal population which grows out during the process time[1]. Nucleation, therefore, impacts on the product quality aspects of crystal structure, crystal size distribution, purity and morphology of the resulting crystalline particulate product[2]. A fundamental understanding of the crystal nucleation stage is needed for meticulous control and accurate prediction of the produced product quality.

Especially for chiral compounds, in which typically either the left or right-handed form is needed, controlled nucleation plays a strategic role to form exclusively one chiral form.

In this work, sodium chlorate ($NaClO_3$) and sodium bromate ($NaBrO_3$) are used as model compounds to investigate primary and secondary nucleation processes of chiral compounds. Although achiral in solution, sodium bromate resembles a conglomerate-forming chiral molecule as it crystallizes in a non-centrosymmetric space group, making it chiral in the solid state[3]. The opposite handedness crystal configurations, here denoted by *A* and *B*, are related to each other by mirror symmetry[4,5]. The conglomerate-forming crystals of pure $NaBrO_3$ and $NaClO_3$ are isostructural and it is shown that they show solid-solution behavior [6,7]. While $NaBrO_3$ readily builds into $NaClO_3$ crystals leading to high concentrations of BrO3-ions in NaClO3 crystals, even at low solution concentrations, ClO_3 ions are hardly incorporated in $NaBrO_3$ crystals[8]. Interestingly, for the same configuration the sign of the optical rotation of $NaClO_3$ is opposite to that of $NaBrO_3$ [4, 9].

Crystallization of such a salts from a stagnant solution results in multiple primary nucleation events. This leads to a mixture of both chiral configurations (*A* + *B*) [10]. Interestingly, crystallization under stirred conditions leads to crystals, which are all of same chiral configuration (*A* or *B*) [11]. This can be explained by the formation of a single parent crystal by primary nucleation that subsequently induces secondary nucleation to give smaller daughter crystals that have the same configuration[12]. These crystals deplete the supersaturated solution, which suppresses the nucleation of the opposite chiral form[13]. Mechanisms and models of secondary nucleation have been proposed[14.] With relation

to studies involving chiral compounds, both attrition[15] as well as shear forces[16] can provide the autocatalytic effect of secondary nucleation. The *A*-configuration of each compound can be crystallized from solution by using seed crystals with the *A*-configuration of either the same compound (self-seeding) or from its isomorphous counterpart (foreign-seeding)[17-19]. These results also apply to the *B*-configuration. The seed crystal must be above a minimal size to be able to induce secondary nucleation with retention of chirality[15]. Seeded experiments at high supersaturations and conditions in which primary nucleation is not possible could still lead to nucleation of the opposite chiral form through Embryos Coagulation Secondary Nucleation (ECSN)[20-22]. In ECSN, the solution phase contains chiral clusters of both forms which are attracted to the seed crystal by van der Waals forces after which they crystallize near the seed crystal. Indirect experimental proof of the existence of chiral clusters has been reported[23].

In this research, we applied the developed workflow for secondary nucleation assessment (Chapter 4) to understand the following points:

1. Does the mechanism of secondary nucleation differ between self-seeding and foreign-seeding?
2. Is there a difference between the two types of foreign-seeding (i.e. seeding of $NaBrO_3$ in $NaClO_3$ solution and seeding of $NaClO_3$ in $NaBrO_3$ solution?)

The secondary nucleation workflow described in Chapter 4, provides a systematic tool to obtain secondary nucleation kinetics information. Secondary nucleation rate measurement conditions are established by first measuring the metastable zone of the model compound in the selected solvents and then, within the MSZ, the induction time probability distribution for spontaneous nucleation at specific supersaturation ratios.

6.2.Method

Sodium chlorate ($NaClO_3$) and sodium bromate ($NaBrO_3$) were both purchased from Alfa Aesar and used as received. A Milli-Q water purification system was used to purify water before it was used as a solvent in the experiments.

All the reported steps in the secondary nucleation workflow were followed to determine the conditions and the kinetic data for secondary nucleation assessment.

6.2.1. MSZW and Induction Time Measurements

The Metastable Zone Width (MSZW) was determined using the same method explained in Section 4.2.1. The heating and cooling rates were set to 0.5°C/min from -25.0°C to 50.0°C for $NaBrO_3$ in water and from 10.0°C to 70.0°C for $NaClO_3$ in water. The samples were stirred with a controlled stirring speed of 700 rpm, using a PTFE coated magnetic stirring bar. The induction time experiments at different supersaturation ratios are needed in order to understand at which conditions spontaneous nucleation occurs. 8 samples were used to estimate the induction times at T_x=20.0°C and T_x=25.0°C, which result of a value of S= 1.1 and S= 1.2 for $NaBrO_3$ and T_x=25.0°C and T_x=30.0°C with a S= 1.2 and S=1.3 for $NaClO_3$.

6.2.2. Seeding experiments

The seed crystals were prepared through evaporative crystallization of a saturated solid-free solution, which was filtered beforehand. The $NaBrO_3$ crystal has a triangular shape, while $NaClO_3$ has a more cubic shape.

After about three days, the crystals were large enough to be distinguished by polarization microscopy. The polarizer was set at 0° and the analyzer was set at 90°. When the crystal turns dark after clockwise rotation of the analyzer, the crystals are dextrorotatory (D). When the crystal turns dark after counter-clockwise rotation of the analyzer, the crystals are levorotatory (L). From this information, the configuration of the solid-state could be established as is explained in Table 1.

The formed crystals were washed with cold water in order to remove any possible residual particles, which could otherwise result in initial breading. After the characterization through the polarized microscope, the single crystals were weighted and classified for their size.

Table 1: Relationship between the optical activity and solid-state configuration of $NaClO_3$ and $NaBrO_3$

Compound	Optical activity	Configuration
$NaClO_3$	D	*A*
	L	*B*
$NaBrO_3$	D	*B*
	L	*A*

From each experiment, three drops of slurry were taken and transferred to a small petri dish, which was covered with filtration paper. The samples were allowed to evaporate slowly until the solvent was completely removed. To test whether primary nucleation occurs during evaporation, a sample of the slurry, in which the solid phase was only of one chiral form, was evaporated through the aforementioned method. After complete evaporation of the solvent, all the crystals were of one chiral form proofing that no primary nucleation occurs under these circumstances. After complete evaporation, the crystals were large enough to be distinguished by polarized microscopy (Table 1). More than 100 crystals of each sample were characterized and counted and the %EE was determined by:

$$E = \frac{(n_a - n_b)}{(n_a + n_b)} \times 100$$

in which n_a is the number of crystals having the A-configuration and n_b is the number of crystals having the B-configuration. The reported *E* are averaged over the three samples taken per experiment.

Two stock solutions at different supersaturation ratios for $NaBrO_3$ and two for $NaClO_3$ were prepared. Table 2 shows the selected concentrations and the supersaturation ratios for the four stock solutions.

Table 2: Concentration and supersaturated conditions for the four supersaturated stock solutions. Two solutions were prepared for $NaBrO_3$ in water and the other two for $NaClO_3$ in water. For each solution is reported the saturation temperature (T_s), the crystallization temperature (T_c) and the supersaturation ratio (S).

Stock Solution	***C* [g/100ml of solvent]**	T_s	T_c	***S***
$NaBrO_3$ in water	39.4	24.0	20.0	1.1
	42.9	29.9	25.0	1.2
$NaClO_3$ in water	105	31.0	25.0	1.2
	110	35.9	30.0	1.3

The solutions were left stirring for two hours at 20°C above the saturation temperatures in order to be sure that the suspensions turned into solutions. The stock solutions were quickly filtered and transferred into a pre-warmed bottle, ensuring the absence of heterogeneous particles and avoiding any possible nucleation. The four stock solutions are used to conduct the various combinations for the seeding experiments of $NaBrO_3$ and $NaClO_3$. Figure 1 shows a schematic representation of the performed experiments. First of all, the seeding experiments are classified as self-seeding and foreign seeding. The self-seeding indicates the addition of a single crystal of the same form of the supersaturated solution (e.g. a single crystal of $NaBrO_3$ is seeded into a supersaturated solution of $NaBrO_3$). These types of experiments are represented in the left part of figure 1. The foreign seeding is obtained when a crystal with a different nature compared to the supersaturated solution is added (e.g. a single crystal of $NaBrO_3$ is seeded into a supersaturated solution of $NaClO_3$).

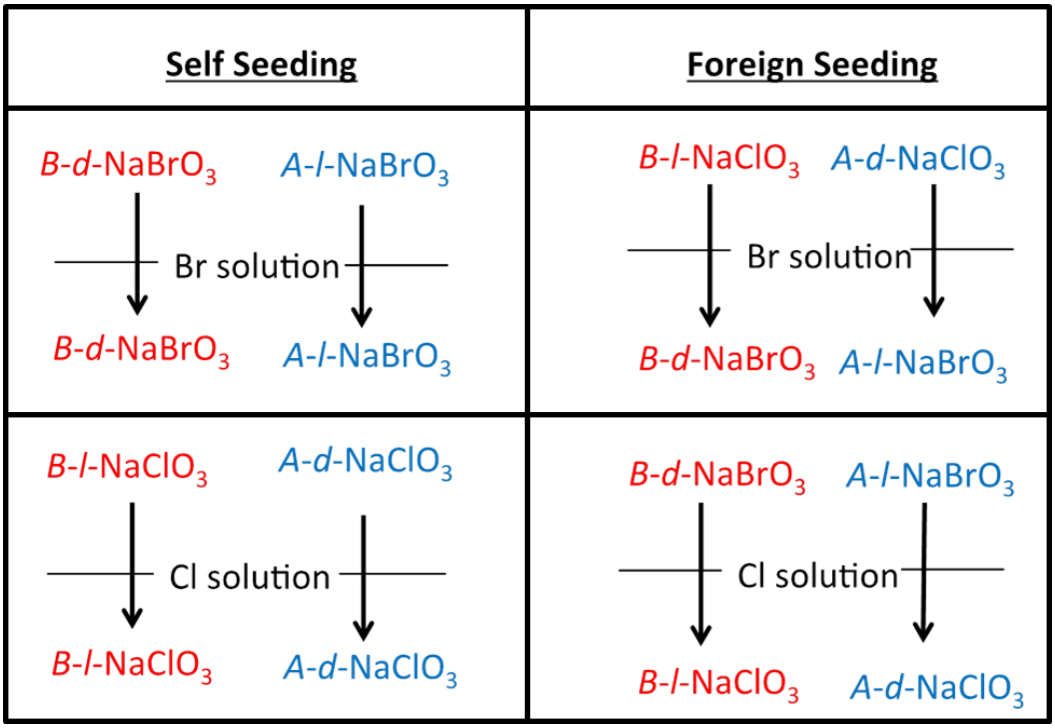

Figure 1: Seeding experiments of $NaBrO_3$ and $NaClO_3$ under different conditions. Depending on the nature of the seeding (self or foreign) all the possible combinations are represented. On the left part of the table the self-seeding is shown: on the top left a single crystal of $NaBrO_3$ is seeded into a $NaBrO_3$ supersaturated solution; on the bottom left a single crystal of $NaClO_3$ is seeded into a $NaClO_3$ supersaturated solution. On the right part of the table the foreign seeding is represented. On the top right a single crystal of $NaClO_3$ is seeded into a supersaturated solution of $NaBrO_3$, on the bottom right a single crystal of $NaBrO_3$ is added to a supersaturated solution of $NaClO_3$. The optical rotations of the crystals are identified by *d* and *l* symbols. The same optical rotation is obtained when there is a self-seeding procedure, while the optical rotation is reversed with foreign seeding.

Figure 1 shows the chiral outcome (*A* or *B*) and optical rotation (*d* or *l*) of the self and foreign seeding experiments. In the self-seeding experiments the formed crystals have the same chirality of the seeded crystal; in the foreign seeding the particularity is that when a supersaturated solution is seeded with a single crystal of D-$NaBrO_3$, the resulting crystals are L-$NaClO_3$. Therefore the optical rotation is reversed.

6.2.3. IR Experiments

The FTIR was conducted analyzing the dry powder in a range of wavelength of λ=1100-400 cm^{-1}. The samples were prepared evaporating the solvent from the terminated seeded experiments. The unseeded experiments of $NaBrO_3$ and $NaClO_3$, one seeded experiment of $NaBrO_3$ in $NaClO_3$ solution and one experiment of $NaClO_3$ in $NaBrO_3$ solution were filtered and grinded obtaining the solid material for direct analysis with the FTIR.

6.3. Results

6.3.1. Steps of the secondary nucleation workflow

Solubility and MSZW

Figure 2 shows the MSZW of $NaBrO_3$ and $NaClO_3$ in water. The width of the metastable zone has been measured using the difference of temperatures between clear and cloud points through the transmissivity detection in Crystal 16. According to the obtained results, $NaBrO_3$ has a lower solubility compared to $NaClO_3$. For instance, using a C=0.42 g/ml of $NaBrO_3$ dissolve in water at a T_s=30°C. At the same temperature, a C=1.05 g/ml of $NaClO_3$ is able to dissolve. The solubility and metastable zone width allow the choice of conditions for the study of secondary nucleation by single crystal seeding of a supersaturated solution.

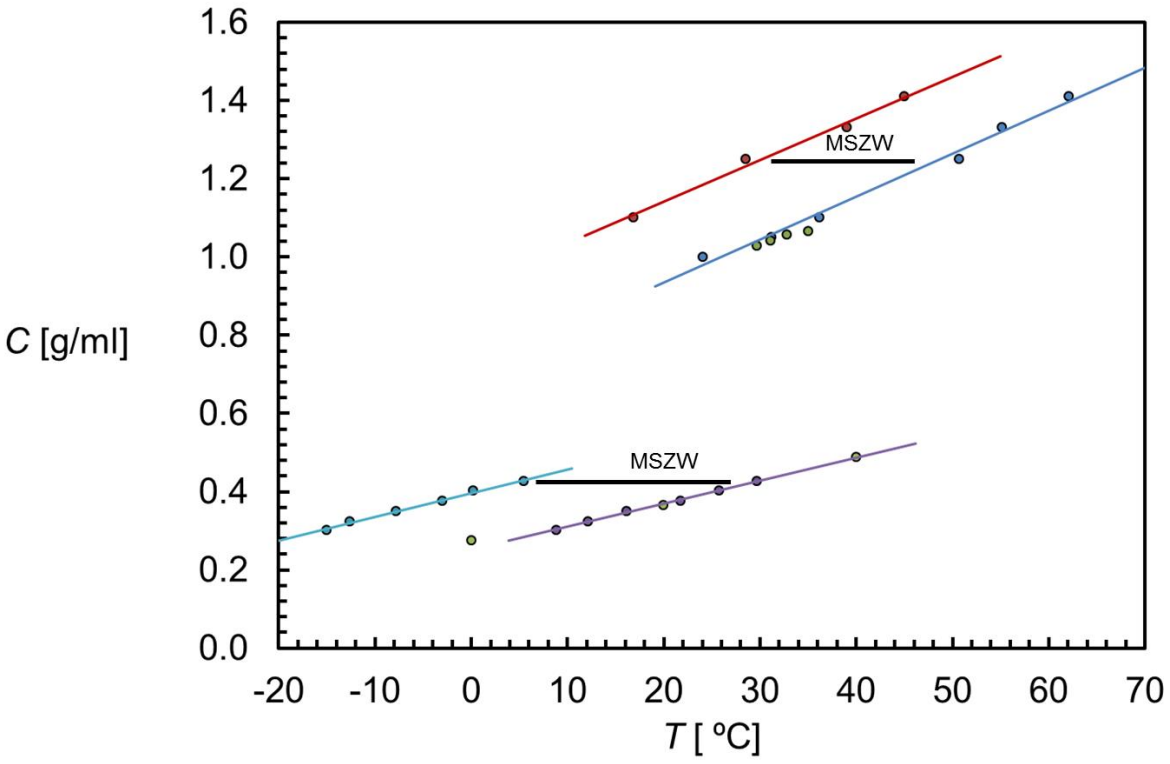

Figure 2: The solubility, Metastable Zone limit and Metastable Zone Width of $NaBrO_3$ and $NaClO_3$ in water at different concentrations *C*. The light blue and the purple lines indicate respectively the solubility and metastable limit and the solubility for $NaBrO_3$ in water. The red and the blue lines represent the metastable limit and the solubility respectively

for $NaClO_3$ in water. The applied cooling rate was 0.5°C/min. The green dots indicate the literature data for the two measured systems.

Induction time Measurements

Induction time measurements at a temperature of T_c=20.0°C and T_c=25.0°C were conducted for $NaBrO_3$ solutions in water at a supersaturation ratio of S=1.1 and S=1.2 respectively. For $NaClO_3$ solutions in water, the induction time measurements were measured at a T_c= 25.0°C and T_c=30.0°C in order to reach supersaturation ratios of S=1.2 and S=1.3. Figure 3 reports the obtained induction times.

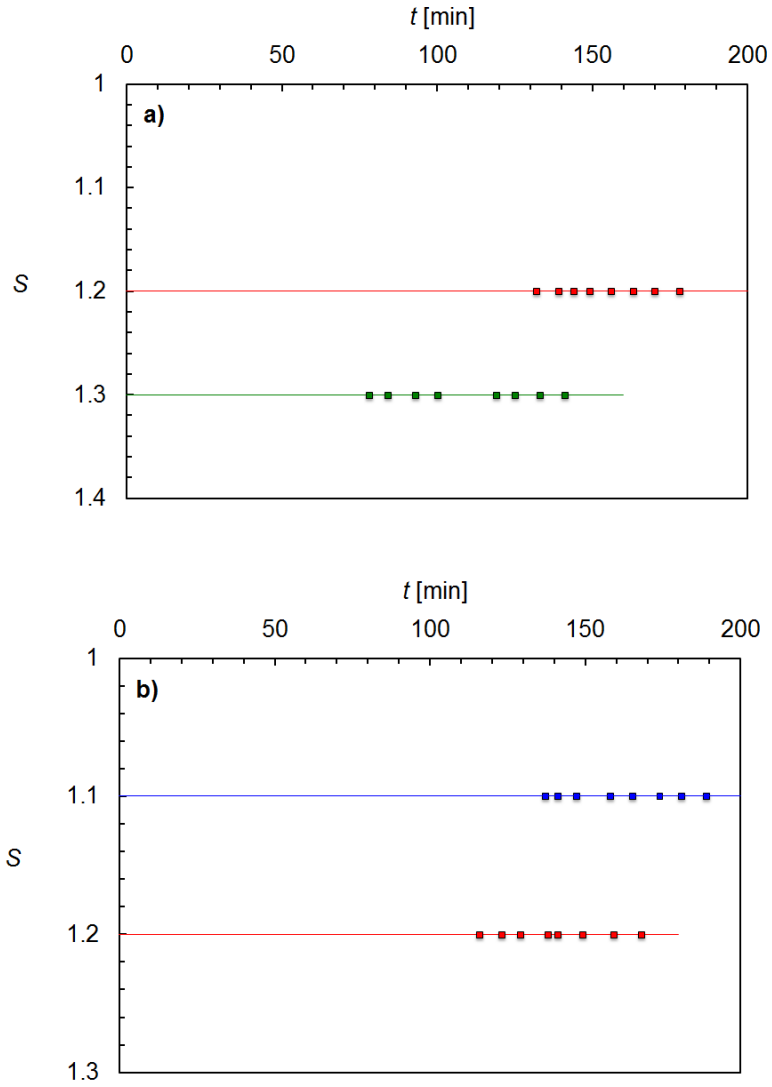

Figure 3: Induction time measurements for $NaBrO_3$ (a) and $NaClO_3$ (b) supersaturated solutions. 8 experiments were performed at each selected supersaturation ratio. a) Two unseeded stock solutions of $NaBrO_3$ at S=1.2 (red) and S=1.3 (green) were used to measure induction times. b) Two unseeded stock solutions of $NaClO_3$ at S=1.1 and S=1.2 were tested.

In all 8 experiments no crystals were detected until 78 and 132 minutes for the supersaturations of S=1.2 and S=1.3, respectively for solutions of $NaBrO_3$. For solutions of $NaClO_3$ the crystals are detected at 116 minutes for S=1.1 and 137 minutes for S=1.2. After this time in increasing more samples crystals were detected. For both systems the results indicate that the average of induction times at supersaturation S=1.2 is Δt_i= 140 min ± 18 min for $NaBrO_3$ and Δt_i =154 min ± 16 min for $NaClO_3$. Therefore, the self- and foreign seeding experiments are conducted at S=1.2.

Secondary Nucleation Rates in self- and foreign single seed crystal experiments

Under the conditions for which primary nucleation is not detected, secondary nucleation now can be studied. We chose to do secondary nucleation rate measurements seeding a single crystal in the supersaturated solutions. This single crystal is the only responsible for the generation of secondary nuclei and by following the change in the number of crystals in time in the suspension it is possible to determine the secondary nucleation rate under well-defined conditions.

Figure 4 shows the typical outcome of 4 different secondary nucleation rate experiments. The number of particles was monitored with the Crystalline camera after seeding was initialized at t=0. The number of particles is detected until 140 particles because, how it was explained in Chapter 4, it is the cut-off value for the crystalline window to discriminate particles in focus. The number of particles against time was counted using the method described in Chapter 4.

In figure 4, two seeded experiments are shown: one $NaBrO_3$ seed crystal in $NaBrO_3$ supersaturated solution (blue squares) and one $NaBrO_3$ in $NaClO_3$ solution (red squares), which indicate a self-seeding experiment and a foreign seeding experiment. They are compared with two unseeded experiments: one $NaBrO_3$ solution (green squares) and one $NaClO_3$ solution (orange squares).

All the solutions for this set of experiments had the same supersaturation ratio of S=1.2. The two seeded experiments show secondary nucleation before 50 minutes, while in the unseeded experiments nucleation is detected only after 100 minutes the experiment starts.

Figure 4 shows that the method to assess secondary nucleation is valid as it decouples the events of primary and secondary nucleation.

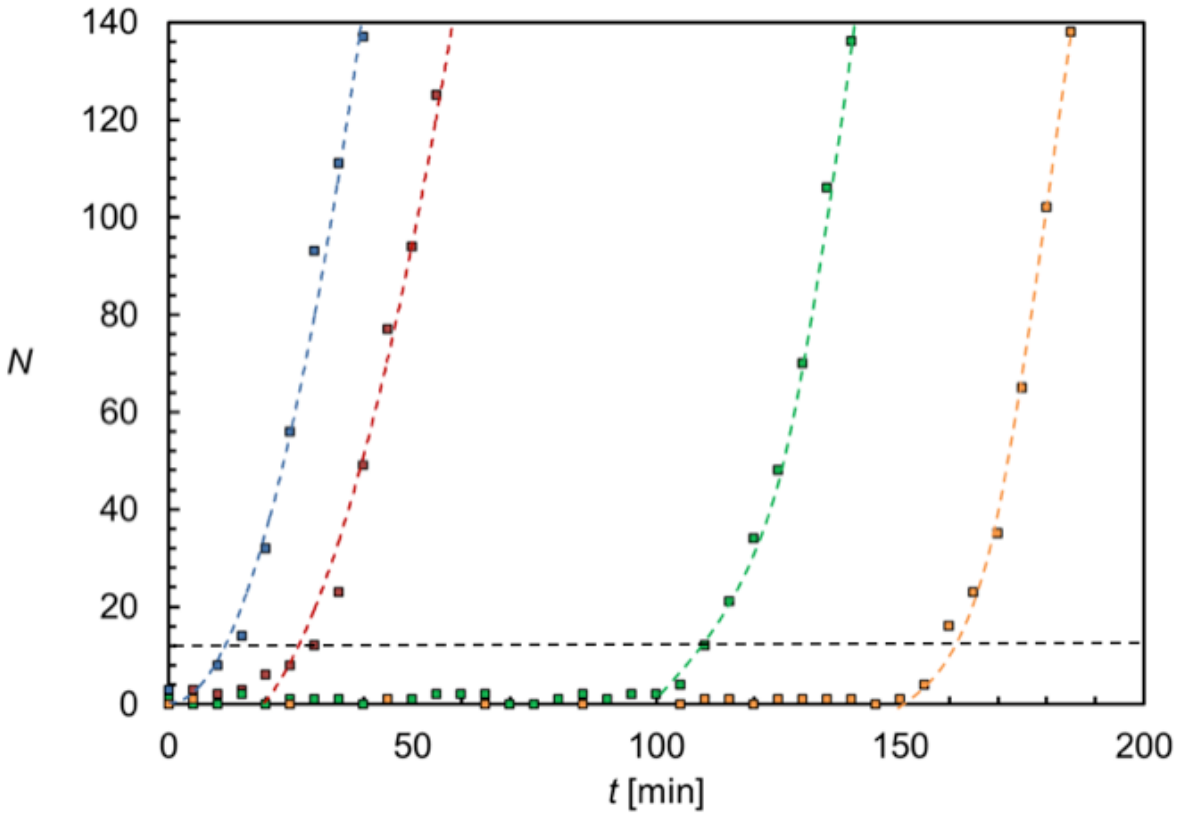

Figure 4: The changing number of crystals (in arbitrary units) in a supersaturated solution of S= 1.2 in various secondary nucleation rate experiments. Single crystal seeded (blue and red symbols) and unseeded experiments (green and orange symbols). The blue symbols indicate the self-seeding of a $NaBrO_3$ single crystal in $NaBrO_3$ solution; the red symbols represent the foreign-seeding of a $NaBrO_3$ single crystal in $NaClO_3$ solution. The parallel unseeded experiments are $NaBrO_3$ (green symbols) and $NaClO_3$ (orange symbols) solutions respectively. The supersaturation was S=1.2 at a temperature of 25.0°C. The horizontal dashed line indicates the cut-off value of 10 particles, which represents the initial stage for counting the formed secondary nuclei.

All 4 combinations for foreign and self-seeding were tested and figure 5 shows an example experiment for each type of experiment. The red dots represent an experiment of foreign seeding for $NaClO_3$ single crystal in $NaBrO_3$ solution. In the foreign seeding experiment of a $NaClO_3$ single crystal in $NaBrO_3$ solution the number of particles increases after 5 minutes. The number of particles detected at t =20 minutes subtracted from the first number of particles higher than 10 counted after the seeding moment and divided by the time of the experiments results as the relative secondary nucleation rate B. For the foreign seeding experiment involving a single crystal of

$NaClO_3$ in a $NaBrO_3$ solution, the determined secondary nucleation rate was always faster than the self-seeded experiments.

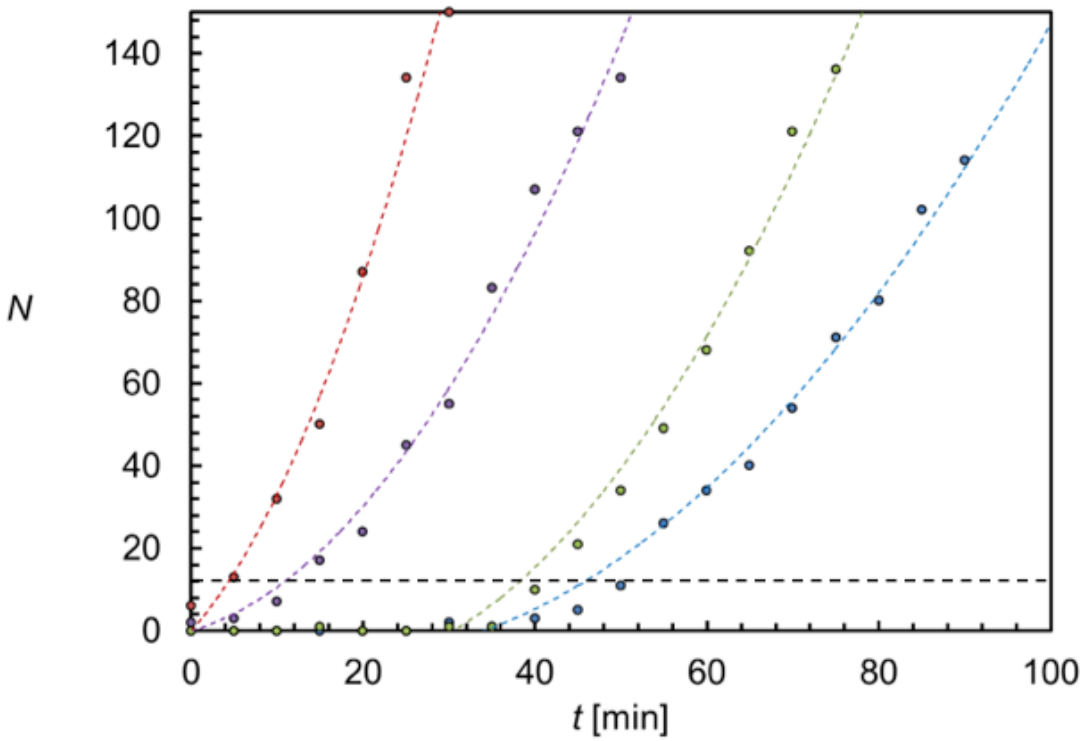

Figure 5: Different single crystal seeding experiments: A single crystal of $NaBrO_3$ in $NaBrO_3$ (blue), $NaClO_3$ in $NaClO_3$ (green), $NaBrO_3$ in $NaClO_3$ (purple) and $NaClO_3$ in $NaBrO_3$ (red). Similar single crystal seed size and weight (5.1- 5.9 mg) were used at a supersaturation ratio S=1.2 and temperature of T_c=25.0 °C. The dashed horizontal line indicates the used cut-off value for the secondary nuclei count.

6.3.2. Chirality of crystals from single crystal self- and foreign seeding experiments

In order to check whether the chirality of the seed crystal is retained in the formed suspension the enantiomeric excess in the product crystals should be determined. This hypothesis was tested by conducting a series of 8 experiments for each possible seeding combination, knowing weight and chirality of each single crystal. The seed crystals were classified depending on the ability of rotating the polarized light clockwise (D) or counter-clockwise (L) which is related to the absolute crystal configurations A and B. Table 3 reports all information on the seed crystals used and the chirality of the product.

In table 3 the experiments are characterized by the name of the experiment, which depends on the chiral nature of the seeded crystal (D or L) and by a number, which refers to the unique experiment. The experiments are ordered depending on the measured secondary nucleation rates *B*, which, as discussed in Chapter 4, is related to the weight of the single seed crystal used. The table shows the chiral purity of the final product. A positive (+) chiral purity *E* means that the crystals rotate the polarized light of the microscope in clockwise (D); if the *E* is negative (-), the obtained crystals are counter-clockwise (L). In principle, if the single nucleus mechanism takes place, seeding with a D single crystal must result in a suspension in which only D crystals are present. Similarly, single L crystal seeds would generate only L crystals in the suspension.

Table 3: Results for self- and foreign seeding experiments using different combinations of $NaBrO_3$ or $NaClO_3$ single crystals in supersaturated solutions of $NaBrO_3$ and $NaClO_3$ at supersaturation S=1.2. The results are expressed by the name of the experiment (Exp.) followed by the sign of the chirality of the seed crystal (+ or -) in the first column. Then, the mass of the seed crystal is reported in mg, followed by the calculated secondary nucleation rate *B* (#particles/min) and the calculated percentage of chiral purity (E) in the last column.

Self- Seeding				**Foreign Seeding**			
$NaBrO_3$ single crystal in $NaBrO_3$ solution				*$NaClO_3$ single crystal in $NaBrO_3$ solution*			
Exp.	Seed mass [mg]	*B* [#particles/min]	*E*	Exp.	Seed mass [mg]	*B* [#particles/min]	*E*
L1 (-)	2.4	2.70	-99	D9 (+)	0.4	1.42	-93
D1 (+)	5.5	3.10	+99	D10 (+)	0.9	1.98	-87
D2 (+)	6.5	3.65	+100	D11 (+)	1.1	3.34	-95
L2 (-)	9.5	3.90	-97	L9 (-)	2.2	4.40	+97
L3 (-)	9.8	4.10	-100	D12 (+)	4.8	4.70	-100
D3 (+)	10.6	4.30	+100	L10 (-)	5.9	5.75	+92
L4 (-)	13.7	6.04	-100	L11 (-)	6.4	7.00	+100
D4 (+)	14.4	6.46	+97	L12 (-)	11.7	10.30	+100
$NaClO_3$ single crystal in $NaClO_3$ solution				*$NaBrO_3$ single crystal in $NaClO_3$ solution*			
D5 (+)	2.1	1.76	+98	D13 (+)	1.9	2.71	-99
D6 (+)	3.4	2.13	+100	D14 (+)	3.2	3.51	-100
L5 (-)	3.7	2.40	-100	L13 (-)	3.5	3.88	+89
D7 (+)	4.6	3.34	+98	D15 (+)	5.1	4.36	-83
L6 (-)	5.1	3.72	-100	L14 (-)	5.6	4.79	+93
L7 (-)	8.4	4.97	-100	D16 (+)	6.3	5.26	-89
D8 (+)	11.5	5.36	+99	L15 (-)	8.4	6.14	+100
L8 (-)	12.1	5.50	-100	L16 (-)	10.4	8.72	+100

The self-seeding experiments ($NaBrO_3$ single crystal in $NaBrO_3$ solution and $NaClO_3$ single crystal in $NaClO_3$ solution) result in product crystals having a chiral purity higher than 97%. The determined secondary nucleation rate *B* increases with single crystal seed weight up to *B* = 6.46 particles/min for a seed weight of 14.4 mg.

The foreign seeding experiments ($NaClO_3$ single crystal in $NaBrO_3$ supersaturated solution and $NaBrO_3$ in $NaClO_3$ supersaturated solution) indicate a chiral purity higher than E= 83%, which is lower than that for the self-seeding experiments. The highest obtained nucleation rate *B* in the foreign seeding experiment is 10.3 particles/minute at a $NaClO_3$ single crystal seed weight of 11.7 mg and 8.7 particles/minutes at a NaBrO3 single crystal seed weight of 10.4 mg. It seems that the secondary nucleation rate in foreign seeding experiments is higher than that in the self-seeding experiments.

It was possible to recover the single seed crystal at the end of all experiments except for the foreign seeding of a single crystal of $NaClO_3$ in $NaBrO_3$ solutions. Figure 6 shows polarized light images for seed crystals before and after each type of experiment. For both self- and foreign seeding, the seeded crystal appears to have increased in size over the course of the experiment. This shows that a part of supersaturation in the solution was used to grow the parent crystal before secondary nucleation could start.

It is interesting to note that the single seed crystal after the foreign seeding experiment (Experiment for $NaBrO_3$ single crystal seeded in $NaClO_3$ supersaturated solution) is completely covered by new crystals.

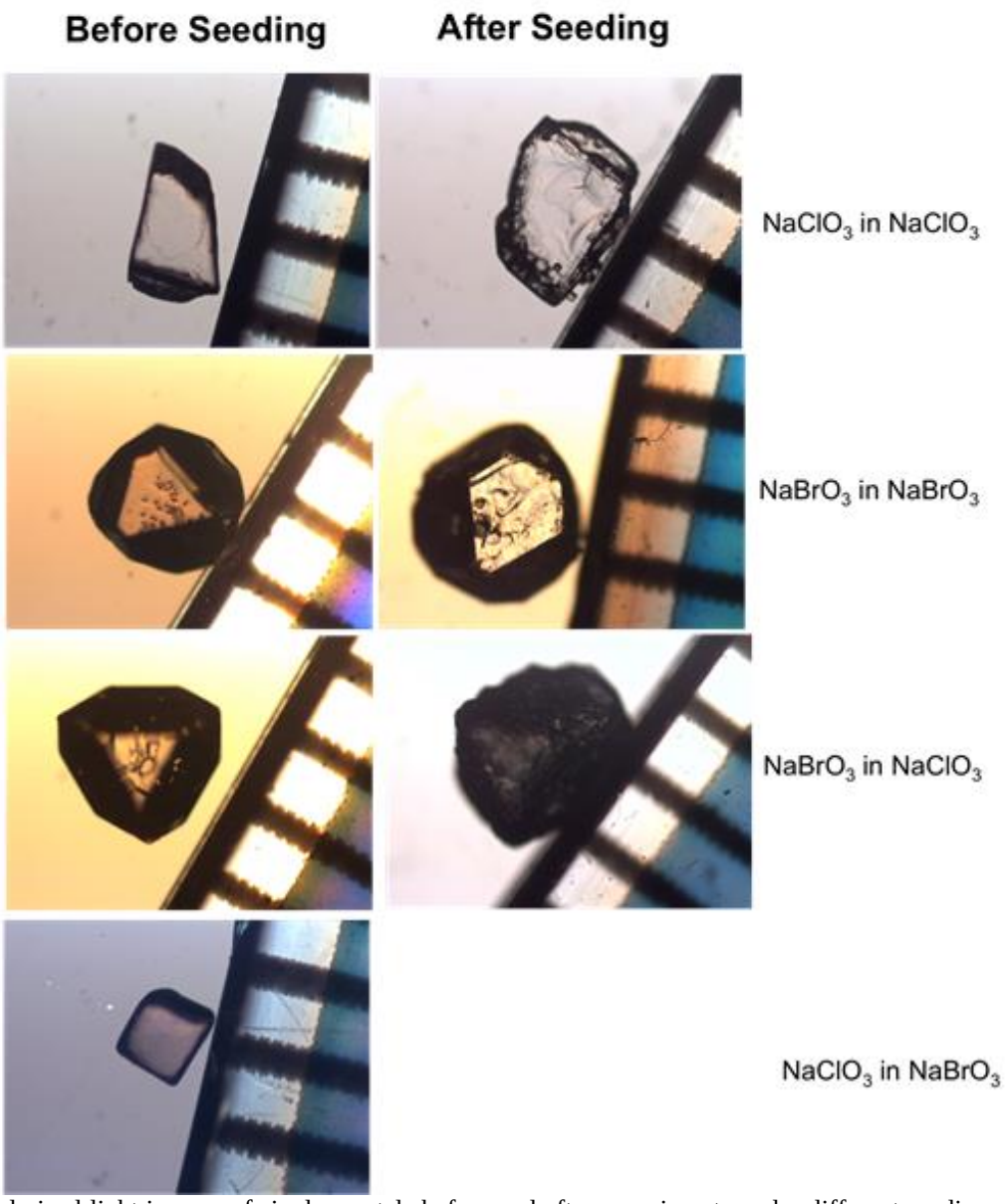

Figure 6: Polarized light images of single crystals before and after experiments under different seeding conditions For the foreign seeding of a single crystal of $NaClO_3$ in a supersaturated solution of $NaBrO_3$, the seed crystal after the experiment was never recovered and only the image before the experiment is available. A ruler (black and white image next to the crystal) was used to size the crystals. Before the experiments the single crystal used for the seeding presented a smoth surface. At the end of the experiments, when the seeded crystals were recovered, they were full covered by new secondary nuclei born on the surface.

Also the self-seeding experiments ($NaClO_3$ seed in $NaClO_3$ solution and $NaBrO_3$ seed in $NaBrO_3$ solution) behave in the same way of the foreign seeding of NaBrO3 seed in $NaClO_3$ solution. Indeed, figure 7 shows the epitaxial growth on $NaBrO_3$ single crystal surface after the seeding experiment in the $NaBrO_3$ supersaturated solution.

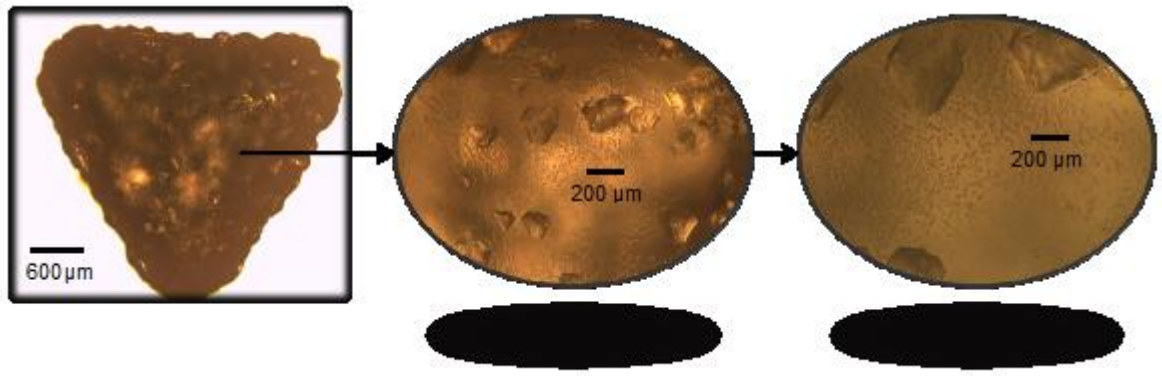

Figure 7: The presented crystal indicates a single crystal of $NaBrO_3$ after been seeded into a $NaBrO_3$ supersaturated solution (S=1.2). The surface is complitely covered by secondary nuclei formed through epitaxial growth. The zoom on the surface shows much more clearly how the tetragonal crystals are ordered at the surface.

In the foreign seeding experiment with $NaClO_3$ in $NaBrO_3$ the seeded crystal could not be recovered. However, although the seeded crystal dissolved, the final crystal product was chiral pure and it had the same configuration as the seeded crystal, see table 2.

Interestingly, in the case of $NaClO_3$ single crystal seeding in $NaBrO_3$ solutions, the secondary nucleation rate was faster than in all other seeding experiments. We investigated this seeding process by using light microscopy to follow the submerging of a seed crystal of $NaClO_3$ in a saturated solution S=1.0 of $NaBrO_3$. Just after the solution comes into contact with the crystal, small crystallites are formed and dispersed from the seed crystal. The dispersion even proceeds in the opposite direction of the flow of solution. After about a minute, many crystallites have formed around the seed crystal while the seed crystal slowly dissolves and reduces in size. Based on its typical tetragonal morphology the crystallites can be identified as $NaBrO_3$. We performed similar experiments for the other three seeding combinations but this formation of crystallites was not observed in these experiments.

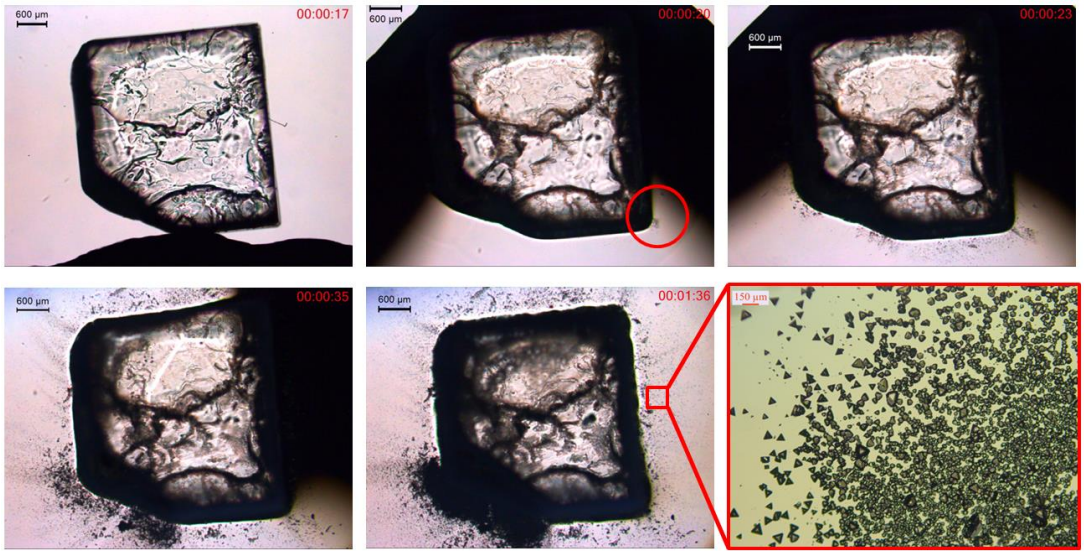

Figure 8: Microscope images taken over time during the flow of a saturated solution S=1.0 of $NaBrO_3$ over a single crystal of $NaClO_3$. The dark shadow is the edge of the incoming solution. The bottom right picture is a magnified image of the crystalline dust formed during the experiment.

Also in the secondary nucleation foreign seeding experiments involving supersaturations (S=1.2), the $NaClO_3$ seed crystal seemingly dissolved as it could not be recovered. To verify this we used FTIR spectroscopy to determine whether the $NaClO_3$ eventually is present in the solution or in the solid phase. Figure 9 shows the obtained IR spectra of solid raw material for $NaClO_3$ and $NaBrO_3$, solution phase. Traces of $NaClO_3$ were detected in the $NaBrO_3$ solution phase indicative of $NaClO_3$ single crystal seed dissolution. The dissolution of the $NaClO_3$ seed crystals in the $NaBrO_3$ solution during the foreign seeding experiment explains why the seed crystals could never be recovered in these experiments. In the other foreign seeding experiments, traces of $NaBrO_3$ were found in the $NaClO_3$ solid phase and not in the $NaClO_3$ solution phase. In this case, indeed the seed crystal survived and could be recovered.

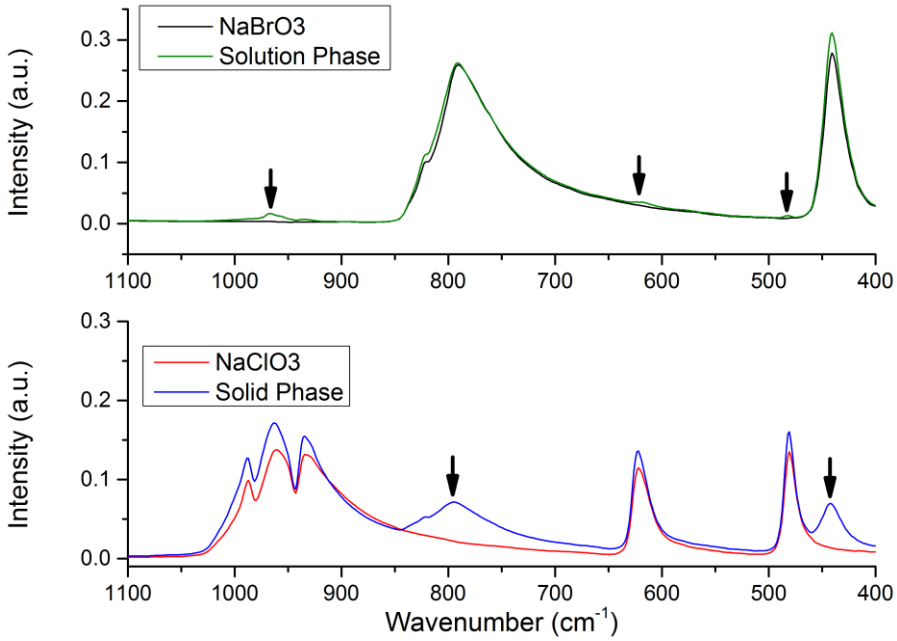

Figure 9: IR-spectra of foreign-seeding experiments: The $NaClO_3$ seeds in $NaBrO_3$ solution experiments disappear in solution (top) whereas the $NaBrO_3$ seeds do not dissolve in $NaClO_3$ solutions and remain in the solid phase (bottom). The arrows indicate the peaks representing the signals of the foreign seed crystal.

6.4. Discussion

The self-seeding experiments induced the formation of a close to chirally pure product retaining the chirality of the seed crystal. While the foreign seeding experiments showed high but slightly lower chiral purity, higher secondary nucleation rates compared to the self-seeding experiments were measured. In the light of these results, does the mechanism of secondary nucleation differ between self-seeding and foreign-seeding? In the conducted experiments, the single nucleus mechanism is reproduced: primary and secondary nucleation experiments are decoupled and the formed crystals are secondary nuclei induced by the single seed crystal. The small daughter crystals have the same chiral configuration as the seed crystal in all seeding experiments. In the foreign seeding experiments for a single crystal of $NaClO_3$ in a supersaturated solution of $NaBrO_3$ the parent crystal was never recovered after the experiments evidenced by the FTIR analysis proving that it dissolves in the solution phase. The phase diagram of $NaBrO_3$ and $NaClO_3$ in water solution can be used to understand what happens in the foreign seeding experiments. According to the phase diagram[8] of

$NaBrO_3$ and $NaClO_3$ in water the system behaves as a solid solution. However, the tie lines show that while small amounts of $NaBrO_3$ readily builds in into the $NaClO_3$ lattice, $NaClO_3$ is mainly rejected from the $NaBrO_3$ lattice. The phase diagram shows that sodium chlorate and sodium bromate behave as a solid solution at the right side of the phase diagram in which the solubility is constant with respect to the total amount of $NaClO_3$ and $NaBrO_3$. This part represents a concentrated $NaClO_3$ solution with a small amount of $NaBrO_3$. After addition the $NaBrO_3$ seed crystal starts to dissolve. The supersaturation slightly increases. Under these conditions, crystallization would lead to the formation of a mixture of $NaClO_3$ and $NaBrO_3$ as depicted by the tie lines. By moving from the linear solubility line to the left towards $NaBrO_3$, the solubility decreases to the left side of the phase diagram where a pure $NaBrO_3$ solution is depicted. The addition of a $NaClO_3$ crystal to a saturated or slightly supersaturated pure $NaBrO_3$ solution will lower the solubility which increases the supersaturation leading to crystallization of close to pure $NaBrO_3$, as is depicted by the tie lines. This explains why the $NaClO_3$ seed crystal was never recovered in $NaBrO_3$ solutions. Pure $NaBrO_3$ would crystallize over the majority of compositions except in highly concentrated $NaClO_3$ solutions.

The discontinuous phase-diagram indicates that different conditions are in place for the two types of seeding experiments but how this affects nucleation remains unclear.

On the light of the obtained results, using a chiral seed crystal it is possible to select two different seeding approaches: one foreign seeding a one self-seeding (figure 10).

Following the route of for foreign seeding ($NaClO_3$ seed crystal in a supersaturated solution of $NaBrO_3$), the seed, due to the different solubility, starts dissolving and it increases locally the supersaturation in the solution. This mechanism induces a chirally selective primary nucleation event, which allows the crystal to grow and to generate a chiral pure suspension of D or L crystals. Surprisingly, despite the seed crystal dissolved, still a high chiral control was observed in the suspension. Under these conditions, we expected a racemic suspension the be formed or chiral-pure crystals in which the chiral nature is not related to the seed crystal.

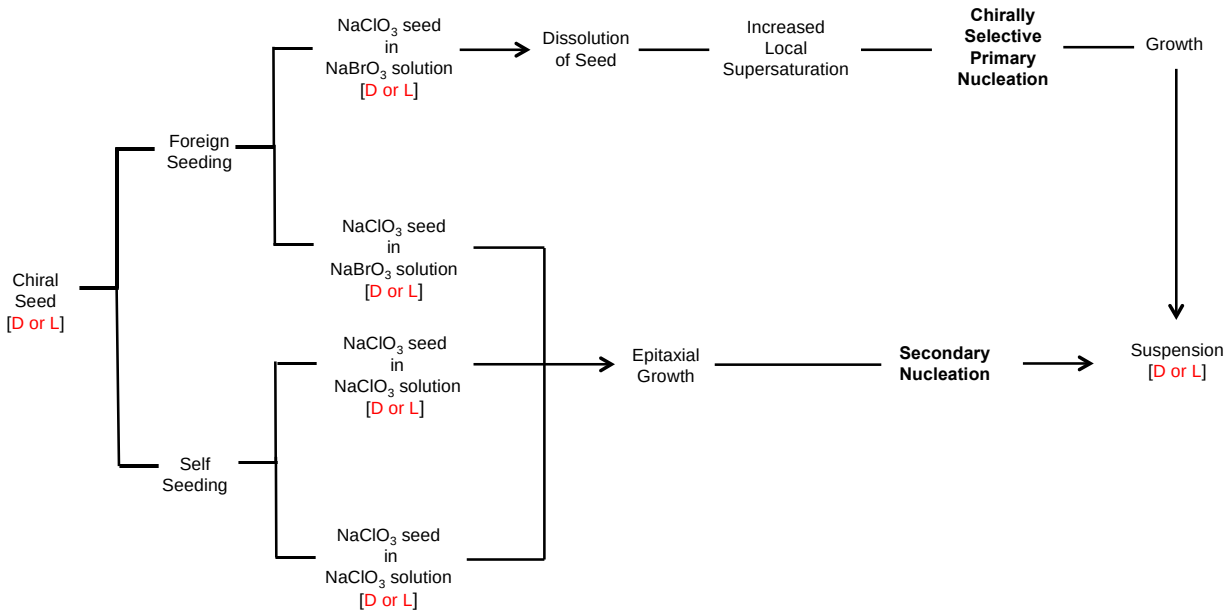

Figure 10: Schematic representation of the possible viable routes for chiral seeding procedures. Two possible approaches are applicable: foreign seeding ($NaClO_3$ seed in $NaBrO_3$ solution and $NaBrO_3$ seed in $NaClO_3$ solution) and self-seeding ($NaBrO_3$ seed in $NaBrO_3$ solution and $NaClO_3$ seed in $NaClO_3$ solution).

The alternative foreign seeding procedure ($NaClO_3$ seed in $NaBrO_3$ supersaturated solution) follows the same steps identified for the self-seeding. Once the single crystal of one specific chiral form is added into the supersaturated solution, it triggers epitaxial growth and then secondary nucleation terminating in a chiral pure final suspension with D or L crystals.

6.5. Conclusion

The developed workflow in Chapter 4 is successfully applied in the study of chiral outcomes for self and foreign seeding in experiments of the chiral crystalline phases of $NaBrO_3$ and $NaClO_3$. This systematic procedure was used to determine simultaneously the secondary nucleation rate and the chiral purity after a well- controlled seeding of a single chiral crystal. This single crystal induces secondary nuclei with the same configuration as the parent crystal, while foreign single crystal seeding induced faster secondary nucleation rates than self-seeding. The self- seeding experiments ($NaBrO_3$ single crystal in $NaBrO_3$ supersaturated solution and $NaClO_3$ single crystal in $NaClO_3$ supersaturated solution) show a higher chiral purity compared to the foreign seeding experiments

($NaBrO_3$ single crystal in $NaClO_3$ supersaturated solution and $NaClO_3$ single crystal in $NaBrO_3$ supersaturated solution), while the foreign seeding induced faster nucleation kinetic with respect to the self-seeding.

Furthermore, it seems that the foreign seeding experiments for the $NaClO_3$ and $NaBrO_3$ solutions do not behave in the same way. When a single crystal of $NaBrO_3$ is seeded into a supersaturated solution of $NaClO_3$, the parent crystal is always recoverable after the experiment and it shows epitaxial growth on the crystal surface. When a single crystal of $NaClO_3$ is seeded into a supersaturated solution of $NaBrO_3$, the parent crystal dissolves. The addition of a $NaClO_3$ crystal to a saturated or slightly supersaturated pure $NaBrO_3$ solution will lower the solubility which increases the supersaturation leading to crystallization of close to pure $NaBrO_3$, as is depicted by the tie lines. However, although the single seed crystal cannot be recovered, the chiral control remains viable.

6.6. References

1) Lee, A. Y.; Erdemir, D.; Myerson, A. S. 2011. Crystal polymorphism in chemical process development. Annu. Rev. Chem. Biomol. Eng. 2, 259−280.

2) Ter Horst, J.H., Schmidt, C.; Ulrich, J. Handbook of Crystal Growth. Nishinaga, T. & Rudolph, P. (eds.). 2015 ed. Amsterdam, Vol. II, p. 1317-1349 33 p.

3) Dickinson, R.G., Goodhue, E.A. 1921. The crystal structure of sodium bromate and sodium chlorate. J. Am. Chem. Soc. 43, 2045-2055.

4) Abrahams, S.C, Glass, A.M., Nassau, K. 1977. Crystal chirality and optical rotation sense in isomorphus sodium chlorine oxigen and sodium bromine oxigen. Solid State Communications, 24, 515-516.

5) Gopalan, P., Peterson, M.L., Crundwell, G., Kahr, B. 1993. Reevaluating structures for mixed crystals of simple isomorphous salts: sodium chlorate bromate. J. Am. Chem. Soc. 115, 3366- 3367.

6) Crundwell, G., Gopalan, P., Bakulin, A., Peterson, M.L., Kahr, B. 1997. Acta Crystallographica Section B. 53, 189-202.

7) Sivaramkrishnan, V., Arunkumar, K.A. 1976. Optical rotation of solid solutions of sodium chlorate and sodium bromate. Journal of Physics and Chemistry of Solids. 37, 799-802.

8) T. Swenson, T., Ricci, J.E. 1939. The Ternary Systems KBr03-KC103-Hz0 at 25" and NaBrO3-NaC1O3-H20 at 25°C and 50°C. J. Am. Chem. Soc. 61, 1974-1977.

9) Niederma, T, Schlenk, W. 1972. Chemische Berichte-Recueil. 105, 3470.

10) Kipping, F.S., Pope, W.J. 1898. Enantiomorphisms. Journal of the Chemical Society, Transactions. 73, 606-617.

11) Kondepudi, D.K., Kaufman, R.J., Singh. N. 1990. Sodium chlorate ($NaClO_3$) crystals are optically active although the molecules of the compound are not chiral. Science. 250, 975-976.

12) Kadam, S.S., Kramer, H.J.M., ter Horst, J.H. 2011. Combination of a Single Primary Nucleation Event and Secondary Nucleation in Crystallization Processes. Cryst. Growth Des. 11, 1271–1277.

13) Kondepudi, D.K., Bullock, K.L., Digits, J.A., Hall, J.K., Miller, J.M. 1993. Kinetic of Chiral Symmetry Breaking in Crystallisation. J. Am. Chem. Soc., 115, 10211-10216.

14) Agrawal, S.G., Paterson, A.H.J., 2015. Secondary Nucleation: Mechanisms and Models, Chemical Engineering Communications 202, 698-706.

15) McBride, J.M., Carter, R.L. 1991. Spontaneous Resolution by Stirred Crystallization Angewandte Chemie International Edition in English. 30, 293-295.

16) Buhse, T., Durand, D., Kondepudi, D., Laudadio, J., Spilker, S. 2000. Chiral Symmetry Breaking in Crystallization: The Role of Convection. Phys. Rev. Lett., 2000, 84, 4405-4408.

17) Vogl, O., Qin, M., Bartus, J., Jaycox, G.D. 1995. Chiral nucleation. Monatsh D,L-leucine with longitudinally polarized electrons. Nature. 126, 67-73.

18) Laudise, R.A., Mullin, J.B., Mutaftschiev, B., Denk, E.G.,Botsaris, G.D.1972. Crystal Growth. Journal of Crystal Growth. 13, 493-499.

19) Qian, R.Y., Botsaris, G.D. 1997. A new mechanism for nuclei formation in suspension crystallizer: the role of inter- particle forces. Chemical Engineering Science. 52, 3429-3440.

20) Qian, R.Y., Botsaris, G.D. 1998. Nuclei breeding from a chiral crystal seed of $NaClO_3$. Chemical Engineering Science. 53, 1745-1756.

21) Qian, R.Y., Botsaris, G.D. 2004. In Ionic Liquids as Green Solvents: Progress and Prospects Chemical Engineering Science. 59, 2841-2852.

22) El-Hachemi, Z., Crusats, J., Ribo, J.M., Veintemillas-Verdaguer, S. 2009. Cryst. Growth Des., 9, 4802-4806.

23) El-Hachemi, Z., Crusats, J., Ribo, J.M., McBride, J.M., Veintemillas-Verdaguer, S. Angew. 2011. Chem.-Int. Edit. 50, 2359-2363.

Chapter 7

Conclusions

The main aim of this thesis was to develop new procedures to systematically study crystal nucleation. Nucleation is one of the important phenomena in crystallisation as it initiates crystal formation in the case of a batch process or new generations of crystals in a running crystallisation processes. The rate of the nucleation dictates the evolution of subsequent crystallisation phenomena like crystal growth and agglomeration. Despite of its importance, nucleation still remains an inadequately understood phenomenon especially in the fundamental concepts.

In Chapter 2, spontaneous nucleation within the metastable zone was studied applying different cooling rates and stirrer layouts conditions. First the MSZW was determined and then induction time measurements were measured at isothermal conditions. Upon faster cooling rate the MSZ shows a larger width because nucleation is detected at lower temperatures. The induction time measurements show less variation and faster average when the investigated temperature is closer to the metastable limit. Increasing temperature the induction time becomes longer because supersaturation has been reduced. The combination of MSZW and induction time measurements ensure the determination of nucleation kinetic through the cumulative probability distribution method. According to the obtained results, a longer time spent at a relatively low supersaturation in absence of nucleation, increases the nucleation rate and decreases growth time measured at higher supersaturation. During an induction time measurement, before crystals can be detected, two different regimes can be identified: the temperature treatment period and the constant supersaturated condition. As nucleation can take place in both regimes, the sample preparation affects the kinetic data determined from induction time measurements. A deep knowledge of conditions for spontaneous nucleation offers the possibility to control crystal formation and provides a reliable method, which on the on hand results in data that can be applied to accurately determine crystal nucleation rates and on the other hand can be used to study secondary nucleation under well-defined conditions.

In Chapter 3, a comparison between spontaneous nucleation in 1 ml stirred solution and in 65 nl stagnant microfluidic droplets was conducted. The aim was to obtain experimental nucleation rates

from two different methods testing if the applied interfacial and hydrodynamic conditions affect the measurements. The obtained results indicate that the nucleation in the microfluidic droplets occurs purely through diffusion increasing the time for detection of crystals within the droplets.

Microfluidic droplets have much higher surface to volume-ratio and different interface than stirred vials, indicating that interfacial effects are likely to play important role for nucleation within microfluidic droplets. This study shows how the different methods can be used to characterize different mechanisms involved in the nucleation event.

In Chapter 4, a reproducible seeding procedure to measure secondary nucleation was developed on a 3 ml scale ensuring well-controlled conditions in absence of primary nucleation events. A single crystal is used to carefully study the secondary nucleation in an agitated environment. When the single crystal is added to the supersaturated solution, it grows until reaching a certain size to enable the promotion of secondary nucleation through collisions with the stirrer or through fluid shear. It was analysed how the seeded parent crystal size plays a role in secondary nucleation. A minimum crystal size is needed before secondary nuclei can be generated. For a small single crystal, it was observed that after the seeding moment, the time before secondary nuclei form is longer. The developed method defines at which conditions of supersaturation secondary nucleation is negligible, this defining a secondary nucleation threshold. The used method permits a parallel discrimination of primary and secondary nucleation through well-controlled conditions within the MSZW.

In Chapter 5, the secondary nucleation rate measurement method was applied at different volumes of crystallizers (V=100 ml and V=700 ml) and extended to multiple crystals seeding in order to develop a workflow for an industrial assessment of secondary nucleation. Secondary Nucleation Supersaturation Thresholds were systematically determined providing successful results and improving the control of this crucial step of crystallization understanding at which level of supersaturation secondary nucleation is negligible. This novel seeding procedure can be

incorporated in industrial workflow procedures enabling rapid development of industrial crystallisation processes.

In Chapter 6, the developed workflow for secondary nucleation assessment was applied to study the chiral outcomes of $NaBrO_3$ and $NaClO_3$ crystallization after single crystal seeding in supersaturated solutions. Studies of self-seeding ($NaBrO_3$ single crystal in $NaBrO_3$ supersaturated solution and $NaClO_3$ single crystal in $NaClO_3$ supersaturated solution) and foreign seeding ($NaBrO_3$ single crystal in $NaClO_3$ supersaturated solution and $NaClO_3$ single crystal in $NaBrO_3$ supersaturated solution) lead to different possible crystallization scenarios when a supersaturation is seeded. When the self-seeding is carried out, a standard secondary nucleation is triggered and a high crystal purity is achieved. When the foreign seeding is applied, different scenarios are realized and the formed suspension has the same configuration but the opposite chirality in respect the parent crystal seeded.

The research presented in this thesis has led to advancements in understanding, characterization and monitoring of nucleation. Meticoulous and accurate studies were conducted for both primary and secondary nucleation providing different approaches to determine nucleation kinetic under well controlled conditions. A detailed worflow has been chracterized and applied for understanding and quantifying of crystallisation phenomena at laboratory and industrial scales. Now, all the steps to measure primary and secondary nucleation rates and secondary nucleation thresholds are chronologically defined. All the obtained reuslts will facilitate understanding of crystallisation processes, efficient and comprehensive route for process development and scale-up and appropriate process control strategy to address existing challenges.

7.1. Recommendations

Nucleation events within the MSZW under well-controlled conditions are influenced by the supersaturation history of the used solution, volume, solution interface and hydrodynamics (Chapter 2 and 3). All these parameters affect the determination of nucleation kinetic information. The used approach in this thesis is based on the main assumptions that nucleation is a stochastic event that

can be described by the Poisson distribution and a single nucleus mechanism is active. An accurate determination of nucleation kinetics requires a large sample of independent equivalent nucleation events under equal conditions. It is necessary to assess the reliability of the calculated nucleation rate defininying the interval of uncertainty for probability distribution of induction times in order to design experiments and process data yielding optimum estimation of nucleation rates.

The novel method for seeding to assess secondary nucleation showed its reliability and reproducibility using different compounds, applications and crystallisers (Chapter 4, 5 and 6). In principle, nucleation takes place before detection, as the nuclei are small and have to grow to be detected. Therefore, the detection largerly depends on the resolution of the used technique and the researcher needs to be careful and it would be useful to compare nucleation kinetics using different tools to validate the measurements. For instance, induction time measurements can be detected using simultaneously FBRM and turbidity probes. Then, knowing the resolution power of the used techniques, the measured induction times can be compared and validated.

The results presented in this thesis will enable achievement of consistent product quality by facilitating understanding and assessment of nucleation for more efficient process design, process development, and process control for cooling batch crystallisation. It would be very usefull for the crystallisation community if the proposed systematic approach for fundamental nucleation studies can be extended to continuous crystallisers and different types of crystallisation such as anti-solvent crystallisation.

This thesis describes two well-developed methods: the induction time distribution approach for nucleation rate determination and the seeding procedure for secondary nucleation rate and secondary nucleation threshold determination.

Now, future studies on crystal nucleation can use the developed knowledge of this work to define a research plan to study heterogenous particles, self-association in solution selecting suitable compound such as chiral, co-crystal, organic salts, metal organic framework (MOFs) and proteins.

Furthermore, the method to decouple primary and secondary nucleation events has been described

and it be can used to develop a systematic approach to study secondary nucleation mechanisms providing a fundamental understanding on attrition and fluid shear.

Acknowledgments

First of all, I would like to thank my two supervisors: Prof Jan Sefcik and Prof Joop ter Horst. It was very challenging to work with both of them at the same time. I learned how to compromise between different approaches in front of the same problems. I think this will be very useful for my future works because from now on, I will always think in double way ensuring the possibility of chosing between alternatives.

Then, I would like to thank the Doctoral Training Centre in continuous Manufacturing and Crystallisation (Grant Ref: EP/K503289/1) and the EPSRC Centre for innovation Manufacturing in Continuous Manufacturing and Crystallisation (Grant Ref EP/I033459/1) to finance my PhD. Furthermore, a special thank to COST Actions European Cooperation in Science and Technology for funding the short scientific mission (Grant Ref: COST-STSM-CM1402-34171). This grant allowed me to spend two beautiful months at CINAM in Marseille. The collaboration in Stèphane Veesler group produced enough results, which are conteined in Chapter 3.

A very warm thank to Dr René Steendam. Chapter 6 of this thesis existes because we collaborated using our expertieses in chiral purity determination and secondary nucleation rate measurements. He was a very good partner and I enjoyed a lot the experience of collaboration.

Thanks to Stephanie, Raaz, Francesca, Flavio and Giacomo to be my family in UK and to make me feel part of something. Thanks to my family, and in particular to my dad, for supporting all my decisions. Finally, thank to all my friends: Matteo, Adriana, Federica, Martina, Giovanni, Manuela, Bianca, Chiara to be with me day by day despite the geographic distance. The last but not the least, thank Giuseppe to support all my madness for the entire duration of my PhD.